Numerical Modelling of Slab Detachment with a Visco-Plastic composite Rheology

Bram Hillebrand
Department of Earth Sciences
Faculty of Geosciences
Utrecht University
Utrecht, The Netherlands

August 30, 2010

supervised by:
Drs. T. Geenen
Dr A.P. van den Berg
Prof. Dr. W. Spakman

Abstract

In this thesis we investigate slab detachment models with a visco-plastic composite rheology. In this visco-plastic composite rheology the low temperature high pressure plastic flow law Peierls creep replaces the commonly used yield mechanism as a stress limiter in order to keep stresses below the experimentally determined rock strength. We investigated the role of Peierls creep on slab detachment. We create a slab detachment model as it is commonly envisioned with a narrow shallow deformation zone in the slab just below the lithosphere due to Peierls creep and a mantle which is weakened around the slab due to dislocation creep. To achieve this we varied the flow law parameters activation volume and activation energy for all three deformation mechanisms (diffusion, dislocation and Peierls creep) out of which the visco-plastic composite rheology is comprised. We also investigated temperature and depth constraints to Peierls creep. Any constraints to Peierls creep leads to high stress levels in the models of 1 - 1.5 GPa while without constraints to Peierls creep maximum stresses are about 350 MPa. When there are no constraints to the occurrence of Peierls creep it generally creates a low viscosity zone around and beneath the slab unless dislocation creep weakens the mantle around the slab enough. By only adjusting activation- volume and energy for dislocation and Peierls creep we did not find an ideal model with the above described narrow deformation zone and weakening of the mantle due to dislocation creep. This could possibly be solved by a decoupling of the values of activation volume and energy for dislocation and Peierls creep therefore it might not be right to use the same values of activation volume and energy for dislocation and Peierls creep as several rheological studies suggest. A low viscosity zone due to Peierls creep at the base of the lithosphere always forms which is potentially important for surface deformation due to slab detachment.

Contents

Chapter 1

Introduction

Slab detachment or slab break-off is a geological process in which part of a subducted slab detaches and sinks further into the mantle. The hypothesis of the existence of detached parts of slabs resulted from the observation of gaps in hypo-central distributions [14]. Further indication comes from tomographic studies in the Mediterranean-Carpathian region [25], [26] and beneath Kamchatka [20] to name a few. Slab detachment is thought to explain several geological observations at the surface. Slab detachment may, depending on the depth of its occurrence, result in several kilometers of uplift. [5] Gaps in a subducting slab could also explain differences in regional volcanism [6] [8] [10]. Slab detachment has also been proposed for regions such as the Anatolia-Aegean region [9] and Baja California-Central America [6] [10].

In a subduction and or slab detachment process several forces act on the slab. Some of these forces will contribute to the sinking or detaching of the slab while other forces will counteract sinking or detaching (for a more detailed description of all forces see Billen (2008)[4]). Due to our simplified model setup of a hanging slab (see section (2)) there remain two important force contributions in our model. The negative buoyancy of the slab itself due to its colder temperature compared to the surrounding mantle and the resisting force of the mantle in which the slab wants to sink. This latter force is called here mantle support. The more viscous the mantle surrounding the slab the stronger resistive this force will be.

There are only a few numerical models of slab detachment among which are models by Andrews and Billen (2009) [2] and Gerya et al (2004) [11]. Both these models show that slab detachment is possible under realistic circumstances. They show two different mechanisms for slab detachment. The first mechanism is slab detachment by thermal diffusion [2] [11], the second mechanism is that of yielding [2]. The yielding mechanism is absent in the models by Gerya et al (2004) because, according to Andrews and Billen (2009), they use a yield strength of 1GPa that they consider to high. Andrews and Billen (2009) also showed in their paper that slab detachment does not take place when only a Newtonian rheology is used for the mantle and yielding is the only weakening mechanism in the slab. A weakening mechanism (non-Newtonian rheology) is needed in the mantle, because otherwise the mantle support is too large and the necessary stresses to induce yielding are not generated.

To limit the stresses occurring in their models both Andrews and Billen (2009) and Gerya et al. (2004) make use of the yield strength mechanism. This yield strength method mimics plastic behaviour of rocks under low temperatures and high stresses. Both studies choose a maximum temperature at which this yield strength may still occur. We try to use a more realistic rheological law, low temperature plasticity (Peierls creep) [15] [18], to replace this yield strength method.

In this thesis we present slab detachment models with a composite rheology of diffusion, dislocation and Peierls creep (section 2.2). We quantify the influence of the uncertainties in the flow law parameters activation energy and volume on our models. Further on we investigate the occurrence of Peierls creep and compare with the occurrence of yield strength in other studies. We also describe the numerical methods needed to keep the calculations stable. The overall aim is to investigate the geodynamic setting of last-stage subduction (hanging slab) and to investigate under which circumstances (rheology) detachment occurs.

Chapter 2

Model Setup

2.1 Governing equations

In this thesis we model a thermally driven visco-plastic flow for an incompressible fluid. We use a Boussinesq approximation which states that density differences can be neglected except in the driving forces. The velocity field is calculated from the conservation of mass (equation (2.1)) and the Stokes equation describing conservation of momentum (equation (2.2)). The temperature field results from the conservation of energy (equation (2.3)). Definitions and values of parameters are given in table (2.1).

$$\bigtriangledown \cdot u = 0 \tag{2.1}$$

$$- \bigtriangledown p + \bigtriangledown \cdot \eta \left(\bigtriangledown u \right) = f \tag{2.2}$$

$$\rho c_p \left(\frac{\partial T}{\partial t} + u \bigtriangledown T \right) - div \left(k \bigtriangledown T \right) = 0 \tag{2.3}$$

In the Stokes equation (equation (2.2)) f is the driving force. We consider a purely thermally driven flow with f=RaT where Ra is the Rayleigh number (see table (2.1)). η is the viscosity which is visco-plastic in this thesis and dependent on temperature, pressure, strain rate and stress (for more detail see section (2.2)). Time dependence only enters the model by the conservation of energy (equation (2.3)).

2.2 Rheology

Rheology: Factors and limitations

The viscosity of the earths mantle is influenced by a range of different factors such as temperature, pressure, stress, strain rate, water content, grain size and composition. The influence of these factors is described by a combination of rheological laws such as diffusion creep, dislocation creep and Peierls creep. Temperature, strain rate and stress are considered to be the most important factors which control the viscosity. On a global scale, water content, composition and grain size are considered secondary effects. However locally they can lead to large variations in viscosity [4].

Rheological laws such as diffusion creep, dislocation creep and Peierls creep are constructed from theoretical models and fitted by experimental studies for which large extrapolations from laboratory- to geological conditions are needed. Despite these large extrapolations rheological laws are able to reproduce the average viscosity estimates for the oceanic mantle asthenosphere ($2 \ 10^{19} Pas$) based on geoid analysis [7] [12] and at larger depths a viscosity of $10^{21} Pas$ as derived from post-glacial rebound analysis [22].

Symbol	Meaning	Value used	Dimension
u	Velocity	-	ms^{-1}
p	Pressure	-	Pa
σ	Stress	-	Pa
Ra	Rayleigh number $\frac{\rho_0\alpha\triangle Tgh^3}{\kappa\eta_0}$	-	-
ρ_0	Reference density	4316	kgm^{-3}
α	Thermal expansion coefficient	$3\cdot10^{-5}$	K^{-1}
T	Temperature	-	K
T_m	Melting temperature	-	K
$\triangle T$	$T_{max}-T_0$ Maximum temperature difference	1700	K
T_0	Zero temperature	273	K
T_{max}	Maximum temperature	1973	K
g	Gravitational acceleration	9.81	ms^{-2}
h	Length scale	$700\cdot10^3$	m
κ	Thermal diffusivity	$1\cdot10^{-6}$	m^2s-1
η_0	Reference viscosity	$1\cdot10^{22}$	Pas
p_0	Reference pressure	$1\cdot10^5$	Pa
z	Depth	-	m
η	Viscosity	-	Pas
η_{dif}	Viscosity due to diffusion creep	-	Pas
η_{dis}	Viscosity due to dislocation creep	-	Pas
η_p	Viscosity due to Peierls creep	-	Pas
$\dot{\epsilon}$	Second invariant strain rate	-	s^{-1}
μ	Shear modulus	$80\cdot10^9$	Pa
b	Burgers vector	$0.5\cdot10^{-9}$	m
d	Grain size	$1\cdot10^{-3}$	m
R	Gas constant	8.314	$JK^{-1}m^{-3}$
A_{dif}	Diffusion creep prefactor	$5.3\cdot10^{15}$	s^{-1}
m	Grain Size exponent diffusion creep	2.5	-
A_{dis}	Dislocation creep prefactor	$2.0\cdot10^{18}$	s^{-1}
n	Stress exponent dislocation creep	3	-
A_p	Peierls creep prefactor	$5.7\cdot10^{10}$	s^{-1}
σ_p	Peierls stress	$2.4\cdot10^9$	Pa
q	Stress dependence of the Peierls mechanism	2	-
E_{dif}	Diffusion creep activation energy	-	$Jmol^{-1}$
E_{dis}	Dislocation creep activation energy	-	$Jmol^{-1}$
E_p	Peierls creep activation energy	-	$Jmol^{-1}$
V_{dif}	Diffusion creep activation volume	-	m^3mol^{-1}
V_{dis}	Dislocation creep activation volume	-	m^3mol^{-1}
V_p	Peierls creep activation volume	-	m^3mol^{-1}

Table 2.1: The variables and parameters used in this thesis

Although theoretically the relation between stress, strain rate and viscosity is well understood there are limited constraints on the viscosity of the earth's mantle. The water content and its variation however is much less constrained. Experimental studies do show that water content has a weakening effect on rheology. We consider models in which the temperature, strain rate and stress field change with time. Water content is only taken into account through the use of rheological parameters for wet olivine.

The variation of grain-size and its dependence on deformation is poorly constrained. Therefore in this thesis (as in most studies) grain-size is kept constant. Although the composition of the mantle is more complex, it is generally treated as if it solely consists of olivine as we have done in this thesis. We do not include any phase boundaries.

In this research a composite rheology is used which consists of diffusion creep, dislocation creep and Peierls creep. Roughly speaking differences in viscosity are due to temperature (diffusion creep) strain rate (dislocation creep) or stress (Peierls creep) although dislocation creep and Peierls creep are also dependent on temperature and all are also dependent on pressure. A composite viscosity is calculated using equation (2.4) and (2.5).

$$\frac{1}{\eta_{comp}} = \left(\frac{1}{\eta_{dif}} + \frac{1}{\eta_{dis}} + \frac{1}{\eta_p} \right) \tag{2.4}$$

Here dif, dis and p denote diffusion-, dislocation- and Peierls- viscosity respectively.

$$\eta = \frac{\sigma}{\dot{\epsilon}} \tag{2.5}$$

For reasons of numerical stability and accuracy we limit all viscosities between $10^{19} Pas$ and $10^{25} Pas$. The locations where viscosities reach these limits are in the cold parts of the lithosphere and the slab. Lithospheric pressure in the rheological laws is calculated using equation (2.6).

$$p = p_0 + \rho g z \tag{2.6}$$

Diffusion creep

Diffusion creep results from deformation through diffusive mass-transport along grain-boundaries (Cobble creep) and through the lattice (Nabarro-Herring creep) and increases linearly with stress (Newtonian rheology). This means that the associated viscosity is independent of strain-rate or stress, equation (2.8). Diffusion creep does however dependent on grain-size through a power-law relation with an exponent around 2.5. This value is the intermediate result of the power-law relation of Coble creep with grainsize (3) and Nabarro-Herring creep with grainsize (2). We keep grain size constant in our models. Therefore the only remaining variable in equation (2.8) are temperature and pressure. Equation (2.7) taken from Karato (1993) [17].

$$\dot{\epsilon} = A_{dif} \left(\frac{\sigma}{\mu} \right) \left(\frac{b}{d} \right)^m exp \left[-\frac{E_{dif} + pV_{dif}}{RT} \right] \tag{2.7}$$

Using equation (2.5), (2.7) and using B = A μ^{-1} $(b/d)^m$ we derive equation (2.8) describing the viscosity due to diffusion creep.

$$\eta_{dif} = B^{-1} exp \left[\frac{E_{dif} + pV_{dif}}{RT} \right] \tag{2.8}$$

For the meaning and values of all symbols we refer to table (2.1).

Dislocation creep

Dislocation creep results from deformation through the motion of crystalline dislocations within grains. The strain rate increases non-linearly with stress (Power-law rheology). Strain-rate dominates this rheology as can be seen from equation (2.10). Dislocation creep is independent of grain-size. From Karato (1993) [17] follows equation (2.9), using equation (2.5) and C = Aμ^{-n} we derive equation (2.10)

$$\dot{\epsilon} = A_{dis} \left(\frac{\sigma}{\mu} \right)^n exp \left[-\frac{E_{dis} + pV_{dis}}{RT} \right] \tag{2.9}$$

$$\eta_{dis} = C^{\frac{-1}{n}} \dot{\epsilon}^{\frac{1-n}{n}} exp \left[\frac{E_{dis} + pV_{dis}}{nRT} \right] \tag{2.10}$$

Peierls creep

Peierls creep is a mechanism which describes low-temperature high-pressure plastic flow. It depends exponentially on stress (exponential rheology). From the mechanisms we incorporate in this study it is the least understood. We use the definition by Kawazoe et al. (2009) [19]. This definition is given by equation (2.11).

$$\dot{\epsilon} = A_p exp \left[-\frac{E_p + pV_p}{RT} \left(1 - \frac{\sigma}{\sigma_p} \right)^2 \right] \tag{2.11}$$

Here σ_p denotes the Peierls stress. This equation does however not represent Peierls creep at low stresses. This is because strain rate will not dissapear with zero stress and thus, from equation (2.5), this will result in low viscosities at low to zero stresses independent of temperature. This problem is depicted in figure (2.1) and was described by Kameyama et al. (1999) [15].
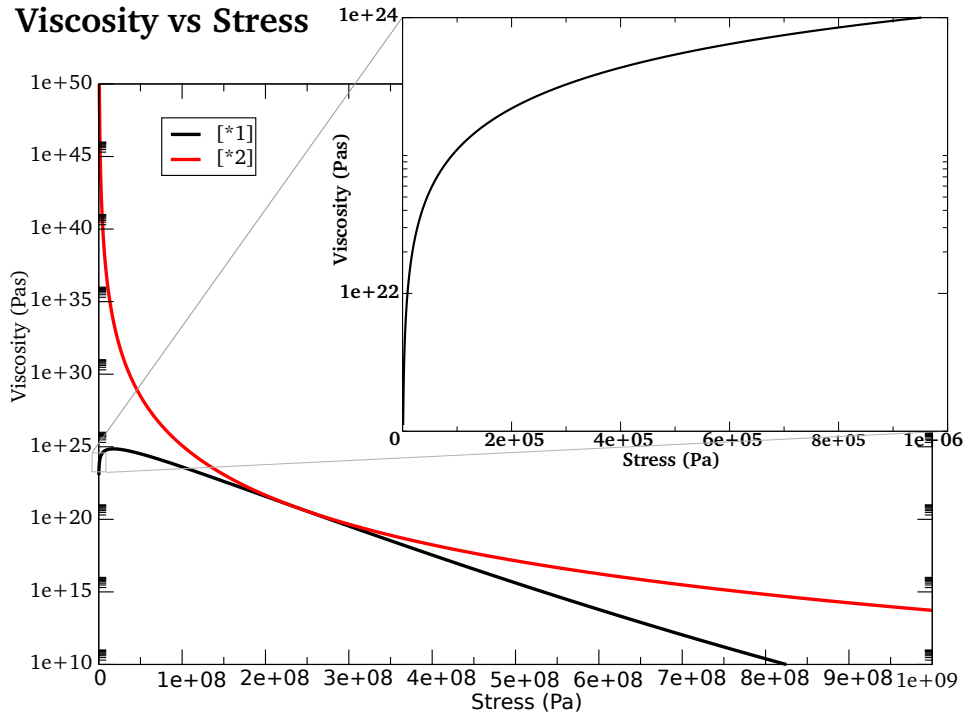

Figure 2.1: Figure showing the behaviour of equation (2.11) [*1] and (2.12) [*2]. Inset shows the behaviour towards zero stress. All calculations were done with T = 773K, p = 1.8·$10^9 Pa$ and $\gamma = 0.1$. For activation energy and volume we used the values of our reference model (model 1) which is described in detail in section (3).

Since Peierls creep should result in very high viscosities with low stress levels a first order Taylor expansion is used to stabilize the equation. This is shown in equation (2.12). This expansion is also used in Kameyama et al (1999)[15].

$$\dot{\epsilon} = A_p exp \left[-\frac{E_p + pV_p}{RT} (1-\gamma)^q \right] \left(\frac{\sigma}{\gamma \sigma_p} \right)^{S_{(T)}} \tag{2.12}$$

Here $S_{(T)}$ is given by equation (2.13)

$$S_{(T)} = \frac{E_p + pV_p}{RT} (1-\gamma)^{q-1} q\gamma \tag{2.13}$$

γ is an adjustable constant determined from the involved stress levels. For stress levels of the order of 100 MPa and Peierls stress being of the order of 1 GPa $\gamma = 0.1$. The effect of this Taylor expansion on viscosity with stress levels going to zero is shown in figure (2.1). Two things are important to note here, first that around the most important stresses (in the order of 100 - 400 MPa) the results for viscosity are the same for both formulations. Secondly, higher stresses result in a viscosity lower than $10^{19} Pas$ which effectively means that the large difference between the two formulations at high stresses do not matter because practically they fall outside the viscosity range that we allow in our models and both formulations would thus give a viscosity due to Peierls creep of $10^{19} Pas$ at these stress levels.

2.3   Model Geometry and Boundary conditions

The calculations are performed in a Cartesian model domain 2100 km wide and 700 km deep. The initial lithosphere and slab (which are purely distinguished from the mantle by there temperature) have an initial thickness of 105 km and 98 km respectively. The slab initially reaches to a depth of 525 km (see figure (2.2)). The temperature at the top boundary is kept at a constant temperature T_0. All other boundary conditions are natural homogeneous. For the Stokes equation the top surface has a no slip boundary condition, which means that all velocity components are set to zero, and the vertical boundaries have a free slip impermeable boundary condition. The bottom surface has a free outflow boundary condition.
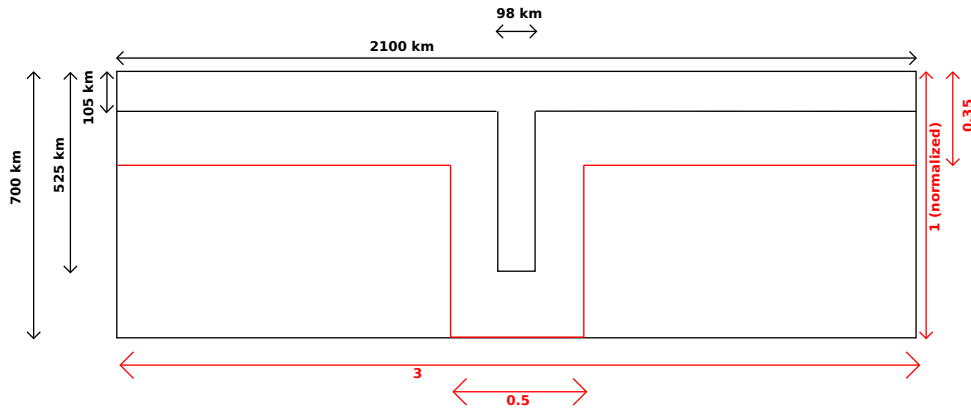

Figure 2.2: This figure shows the model setup. As explained in section 2.4 the distinction between slab and mantle is purely thermal. The red t-shaped box indicates where mesh refinement is applied

For the temperature calculations we use triangular elements with six points and for the stokes equation calculations we use triangular Taylor-Hood elements P2-P1. This means that we have triangular elements with 6 points. Pressure is approximated by linear basis function using the pressure values of only the three corner points of the triangle. Velocity is approximated by quadratic basis function using the values at all 6 nodal points. We use local mesh refinement resulting in a mesh resolution in and around the slab and lithosphere of about 20 km while in the the lower left and right corner it is about 80 km. The areas where mesh refinement is applied is given in figure (2.2). The number of elements approximate 6000 and the number of nodal points about 12000.

2.4 Model setup and Numerical methods

To solve the temperature and velocity fields we use the finite element method. The application was build with the general FE package SEPRAN. [24].

Initial conditions for temperature and viscosity

The temperature field used for our model runs is created by subjecting an initial temperature field (figure (2.3a)) to 5 Ma of thermal diffusion. This results in the temperature field shown in figure (2.3b). The initial temperature field is described by four temperatures (T_0, T_1, T_2 and T_3 (figure (2.3), table (2.2))) in the slab and a temperature function in the mantle (T_4 and T_{max} (figure (2.3)), table (2.2)). The temperature function in the mantle is constructed in such a way that it approaches the temperature distribution of figure 4.40 in the book by Schubert et. al. (2001) [1]. During the thermal diffusion the upper boundary of the model is kept at a constant temperature T_0.
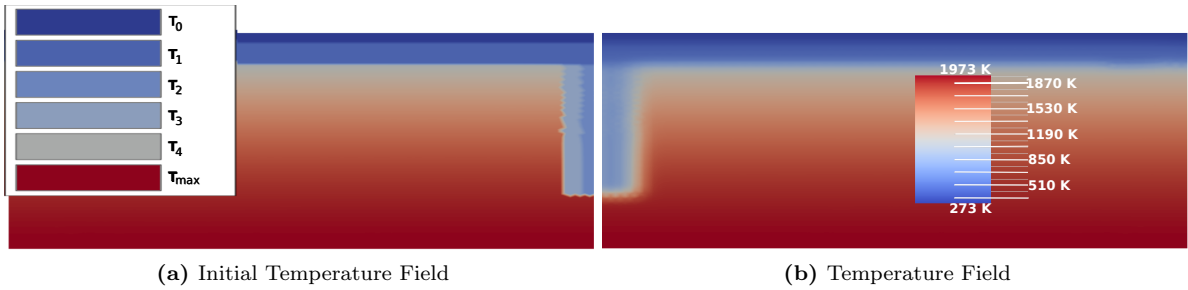

(a) Initial Temperature Field   **(b)** Temperature Field

Figure 2.3: The initial temperature field and the resulting temperature field used for our model runs. Both fields are symmetric along the y axis running through the middle of the slab. Therefore for 2.3a the left half and for 2.3b the right half is shown.

Symbol	Meaning	Value
T_0	Temperature at the top boundary	273 K
T_1	-	473 K
T_2	Inner Temperature of the slab	673 K
T_3	Outer Temperature of the slab	873 K
$T4$	Temperature just below the lithosphere	1073 K
T_{max}	Maximum temperature	1973 K

Table 2.2: Table with the temperatures used to create the initial temperature field

Our model setup has no prescribed velocities. To create initial velocity, stress and strain rate fields the velocity field during the first time step is calculated using an isoviscous rheology instead of the composite rheology which is used in all subsequent time-steps. This initial stress and velocity field is shown in figure (2.4).

Time

As mentioned (section (2.1)) time dependence is introduced into the model by the heat equation. For time integration we use the Crank-Nicholson method which is an implicit integration scheme. The integral is approximated with a trapezoidal integration rule. This time integration method is unconditionable stable and more accurate than other integration methods for example the backward Euler method. However if the timestep becomes to large (in relation with the spatial resolution) oscillations can occur in the solution. To prevent this we use the CFL condition to determine the timestep. This condition ensures that $\frac{u \cdot \triangle t}{\triangle x} \leq C$ where $\triangle x$ = an element size and, in our case, C = 0.25. To prevent any further oscillations in the solution we also make sure that each timestep is always between 0.75 and 1.01 times
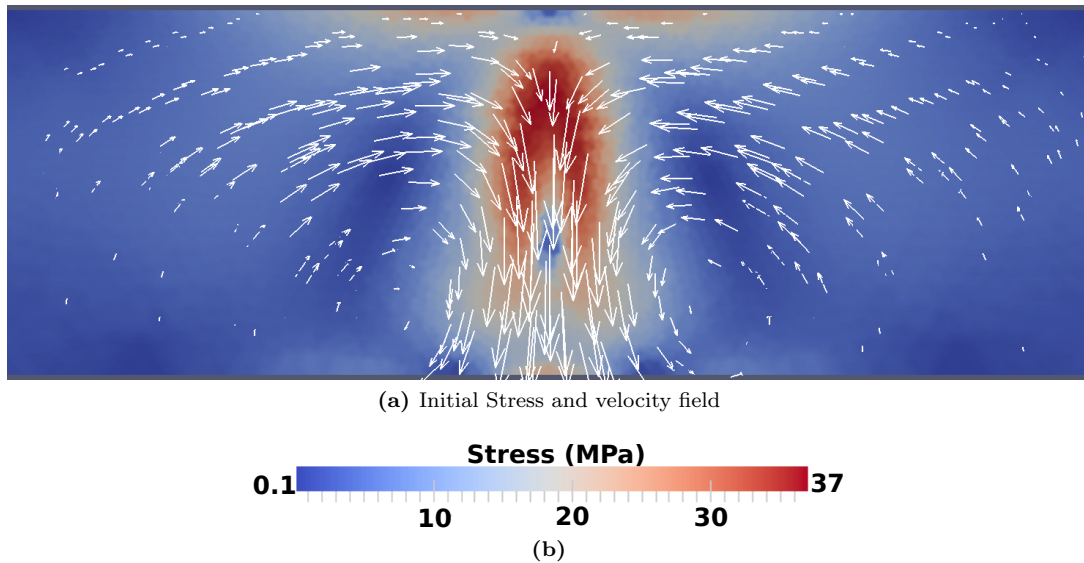
(a) Initial Stress and velocity field

Stress (MPa)

0.1 ▮▮▮▮▮▮▮▮▮▮▮▮▮▮▮▮▮▮▮▮▮ 37

10   20   30

(b)

Figure 2.4: This figure shows the stress field as a result of the first isoviscous step.

the preceding timestep. In practice this means for our models that the initial timestep (by default) is 1.5 years and it increases to a timestep of about 450 years.

Velocity field

After a new temperature field has been calculated we solve the velocity field. This velocity field is solved using a visco-plastic composite rheology (see section (2.2)). There is a non linear relation between viscosity, strain rate and stress and the viscosity field cannot be solved directly. Instead we use a bisection method. This method makes sure that the stress field which can be calculated with equation (2.5) is the same (allowing a small error of 0.01 percent) as the stress field used to calculate the viscosity field. This can take several iterations.

However in our models this results in a problem. If we include Peierls creep in the calculations of the viscosity during the bisection method, stresses seem to lower to values not large enough to activate Peierls creep and slab detachment never takes place. This is due to the sensitive relation between stress and viscosity for Peierls creep (see section (2.2), figure (2.1)). An 100 MPa increase in stress can result in, for relevant stress levels, about 3 to 4 orders of magnitude decrease in viscosity. This results in the negative feedback loop shown in figure (2.5).
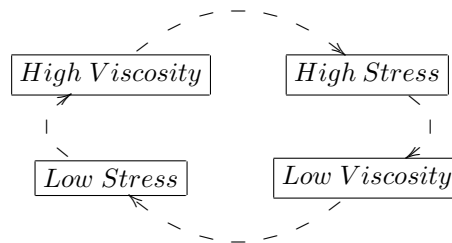

Figure 2.5: Schematic figure illustrating the negative feedback loop.

Because in our models we only allow 6 orders of difference in viscosity this results in the fact that Peierls creep acts as a bimodal process, it either deforms the slab plastically or it doesn't effect the slab at all. We therefore chose, like one would use the yield mechanism, to only include Peierls creep after the bisection method has solved the non-linearity between strain rate, stress and viscosity due to diffusion and dislocation creep. The resulting stress and strain rate field are used to compute the final visco-plastic viscosity field which now includes Peierls creep.

The viscosity field with which the velocity field is calculated is not the same as the viscosity field which is the result of this velocity field. The differences however are so small that we decided to solve the Stokes equation once each time step and compare this with a model in which we solved the Stokes equation twice each time step. This gave the same results as solving the stokes equation once each timestep. Since solving the Stokes equation takes up the major part of the computing time each timestep we chose to solve the Stokes equation only once each time step.

Stability

One important initial problem in our model is that, again due to the sensitivity of Peierls creep to stress, there appear large viscosity contrasts within one element (figure (2.7)). This gives a numerical problem which has as effect that Peierls creep 'eats' into the lithosphere and progressively weakens the entire lithosphere and slab (figure (2.6)). To avoid this problem viscosity, temperature and stress are averaged per element after they have been solved for each nodal point. This can still lead to elements which combine a high viscosity with a high strain rate to avoid this strain rate is calculated directly in the barycenter of each element instead of at each nodal point and averaging afterwards. By using these two averaging methods we prevent large viscosity contrasts within one element and more importantly there are no longer any elements which combine a high viscosity with a high strain rate and we thus prevent the 'eating' of Peierls creep into the lithosphere and slab.
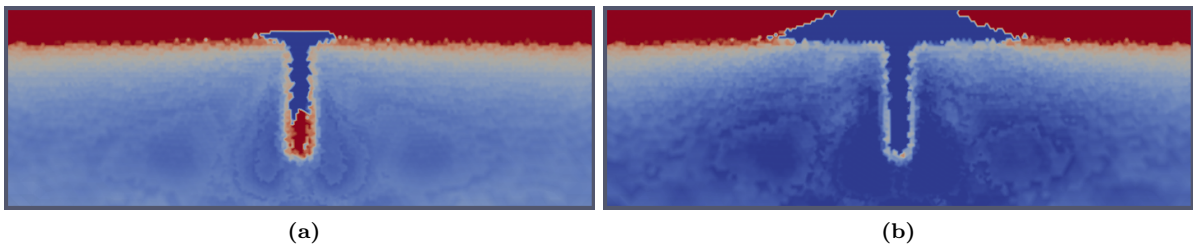

(a)   **(b)**

Figure 2.6: This figure shows the numerical problem when high viscosity contrasts occur over one element.
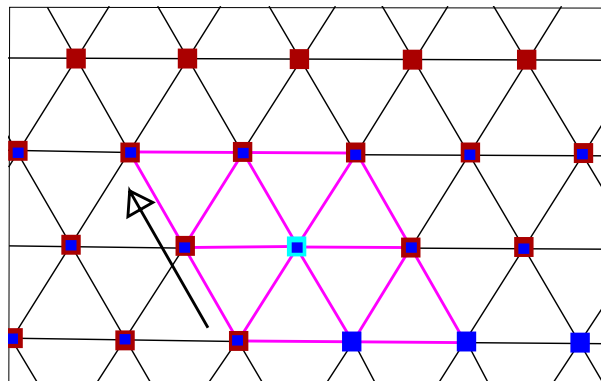

Figure 2.7: This figure illustrates the element growth. The pink lines indicate two elements. The large squares indicate the Viscosities calculated for that specific nodal point at t_1 and the smaller squares within them the viscosity at t_2. Where only one square is shown t_1 and t_2 have the same value for viscosity. A blue square indicates a viscosity of $10^{19} Pas$ and a red square $10^{25} Pas$. The light blue square indicates a intermediate viscosity. The figure illustrates how the low viscosity zone grows one element each timestep because within one element the viscosity contrast over the nodal points can be 6 orders of magnitude. The black arrow indicates the direction of the growth.

Chapter 3

Results

3.1 The influence of activation volume and energy

As mentioned in section (2.2) significant extrapolations from the laboratory conditions are needed to make rheological laws applicable to upper mantle conditions. It is therefore relevant to investigate the effect of uncertainties in the values for activation- volume and energy on viscosity under upper mantle conditions. In this section we investigate the sensitivity of our model for variations in activation volume and energy. For diffusion and dislocation creep we investigated upper mantle conditions, for peierls creep conditions that correspond to the upper part of the slab. Exact values for temperature, pressure and other parameters are given in the captions. The black boxes in figures (3.1, 3.2 and 3.3) indicate common values from the literature for wet olivine.

The influence on diffusion creep

In figure (3.1) the dependence of diffusion creep on activation- volume and energy is illustrated. The figure shows that diffusion creep is more sensitive to changes in activation energy than activation volume. It also shows that the choice of activation- volume and energy has a significant influence on the viscosity due to diffusion creep and thus potentially on the outcome of our models.
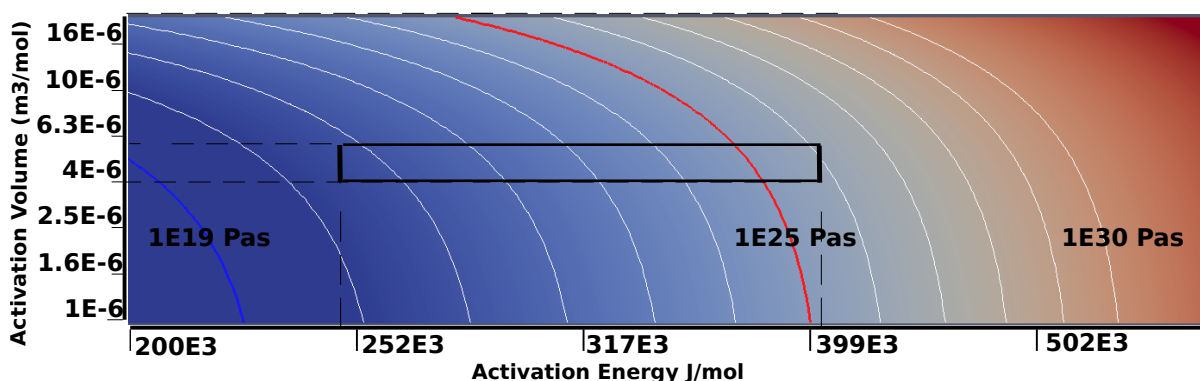

Figure 3.1: Figure illustrates the sensitivity of diffusion creep to activation volume and activation energy. The contour lines are lines for constant viscosity . The red line indicates the maximum viscosity of $10^{25}Pas$, the blue line indicates the minimum viscosity of $10^{19}Pas$. $p = 6 \cdot 10^9 Pa$ and T = 1500 K. The black box indicates common values from the literature.

The influence on dislocation creep

As shown by Andrews and Billen (2009) [2] dislocation creep is more important during slab detachment than diffusion creep in the area surrounding the descending slab. Figure (3.2) shows that the influence of uncertainties in activation- volume and energy is much smaller for dislocation creep compared to

diffusion creep. A doubling of the activation energy results in about 10 orders increase in viscosity due to diffusion creep and only about 4 orders for dislocation creep.
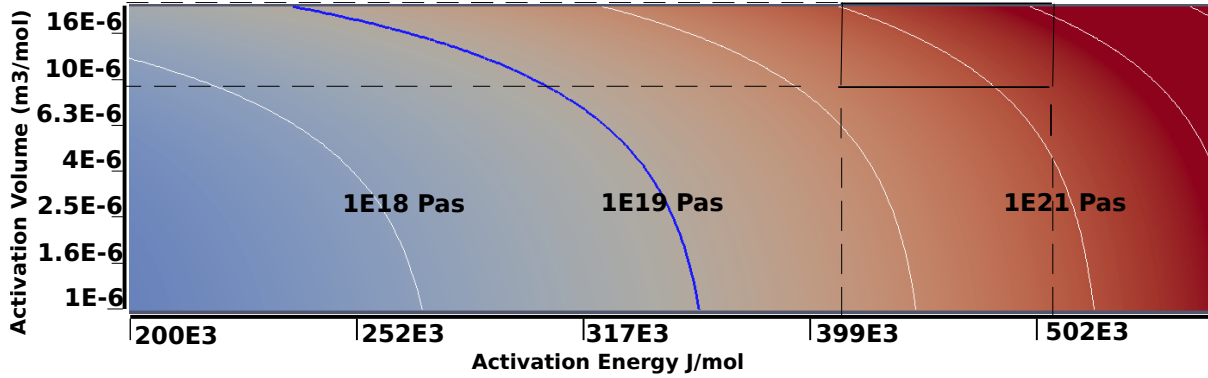

Figure 3.2: Figure illustrating the sensitivity of dislocation creep to activation volume and activation energy. Both scales are logarithmic. The contour lines are lines for constant viscosity . The red line indicates the maximum viscosity of $10^{25} Pas$, the blue line indicates the minimum viscosity of $10^{19} Pas$. p $= 6 \cdot 10^9 Pa$, T $= 1500$ K and $\dot{\epsilon} = 10^{-15} s^{-1}$. The black box indicates common values from the literature.

The influence on peierls creep

For peierls creep only a few experimental studies exist and constraints on the values for activation-volume and energy are therefore limited. Studies on galena [3], anhydrite [21] and marble [13] suggest that activation- volume and energy for dislocation and peierls creep are very similar. Therefore we choose the same activation- volume and energy for peierls creep and dislocation creep. this was also done by Katayama and Karato (2008) [18]. Figure (3.3) shows that the choice for activation- volume and energy for peierls creep has a very significant influence on viscosity and thus potentially on our models. We tested a large variation of activation- volumes and energies. The results are discussed in sections (3.3, 3.4 and 3.5). Another variable of Peierls creep, namely Peierls stress (σ_p , equation (2.12)), potentially has a significant influence on viscosity. However in contrast with activation- volume and energy, Peierls stress is well constraint.
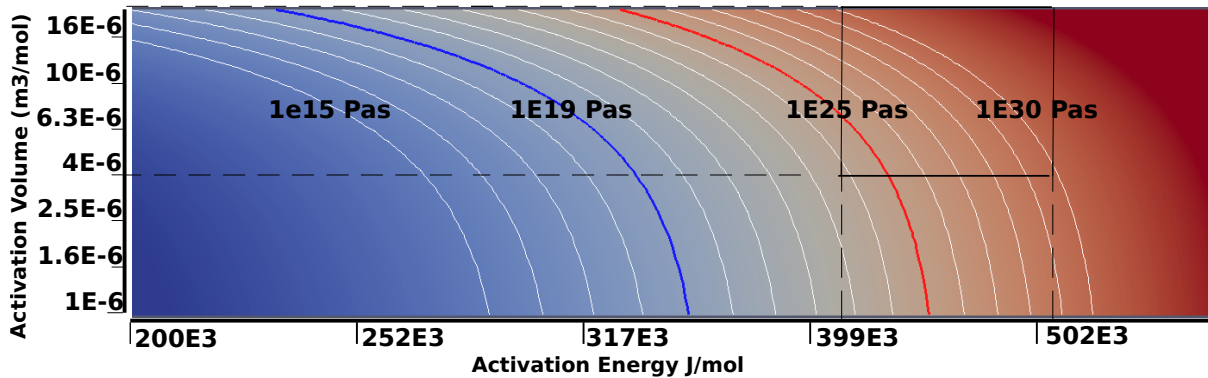

Figure 3.3: Figure illustrating the sensitivity of viscosity due to peierls creep to activation volume and activation energy. Both scales are logarithmic. The contour lines are lines for constant viscosity . The red line indicates the maximum viscosity of $10^{25} Pas$, the blue line indicates the minimum viscosity of $10^{19} Pas$. p $= 6 \cdot 10^9 Pa$, T $= 1500$ K, $\dot{\epsilon} = 10^{-15} s^{-1}$ and $\sigma = 500$ MPa. The black box indicates common values from the literature.

3.2 The Reference Model, model 1

Table (3.1) lists the parameter values for the different model runs we performed. To ensure we arrived at a model where slab detachment would take place we chose fairly low values for activation- volume and energy, even for wet olivine, for all three deformation mechanisms. Because, as explained in section (3.1) , activation- volume and energy for peierls creep are poorly constrained we chose to couple activation- volume and energy for dislocation and peierls creep in all models.

| Model | Diffusion | | Dislocation and Peierls | | Constraints to Peierls creep | Slab detach-ment |
	$E \frac{kJ}{mol}$	$V \frac{cm^3}{mol}$	$E \frac{kJ}{mol}$	$V \frac{cm^3}{mol}$		
1	240	5	423	10	no	yes
2	240	5	423	12	no	yes
3	240	5	423	14	no	yes
4	240	5	423	16	no	yes
5	240	5	423	18	no	yes
6	240	5	423	20	no	no
7	240	5	423	22	no	no
8	240	5	423	24	no	no
9	240	5	423	8	no	yes
10	240	4	423	10	no	yes
11	240	2	423	10	no	yes
12	240	5	450	10	no	yes
13	240	5	500	10	no	no
14	240	5	450	14	no	yes
15	240	5	450	16	no	no
16	240	5	423	10	$0.3 \cdot T_m$	no
17	240	5	423	10	$0.4 \cdot T_m$	no
18	240	5	423	10	$0.5 \cdot T_m$	yes
19	240	5	423	10	$0.5 \cdot T_m$ and $\leq 280km$	yes

Table 3.1: Table showing the values of activation- volume and energy for different model runs. All other parameters are kept constant.

Temperature field evolution

Figure (3.4) shows the evolution of the temperature field. Total model time is roughly 800 Kyr. In these 800 Kyr we observe the slab deforming, it increases in length and becomes thinner just below the lithosphere and just above the tip of the slab. The slab descends into the mantle but it seems to stay connected with the lithosphere by a small tail like feature and in that sense it does not comply with the classical cartoon like idea of slab detachment where a small deformation zone develops just below the lithosphere, where the slab detaches, but the rest of the slab stays roughly undeformed. When we look in more detail at figure (3.4) we observe that thinning of the slab first takes place just below the lithosphere and later on just above the tip of the slab. The upper thinning zone is also better developed. The tail with which the slab seems to stay connected with the lithosphere is potentially important for surface deformation studies where slab detachment takes place. This material could be either from the lithosphere and be dragged along with the slab, or be left behind by the deforming slab.

The detachment process

The slab and the lithosphere are only distinguished from the mantle by temperature (section (2.4) explains in more detail the initial temperature conditions of our models). There are two important temperature indicators namely T_3 (873 K) which is the initial outer temperature of the slab and T_4 (1073 K) which the initial temperature just below the lithosphere and therefore the coldest mantle temperature. The evolution of these isolines may provide a better understanding of the deformation of the slab. For our reference model we observe that detachment has taken place but that the top of the slab and the remnant of the slab at the base of the lithosphere stay very close together. The gap at the end is about 30 km (figure 3.5).
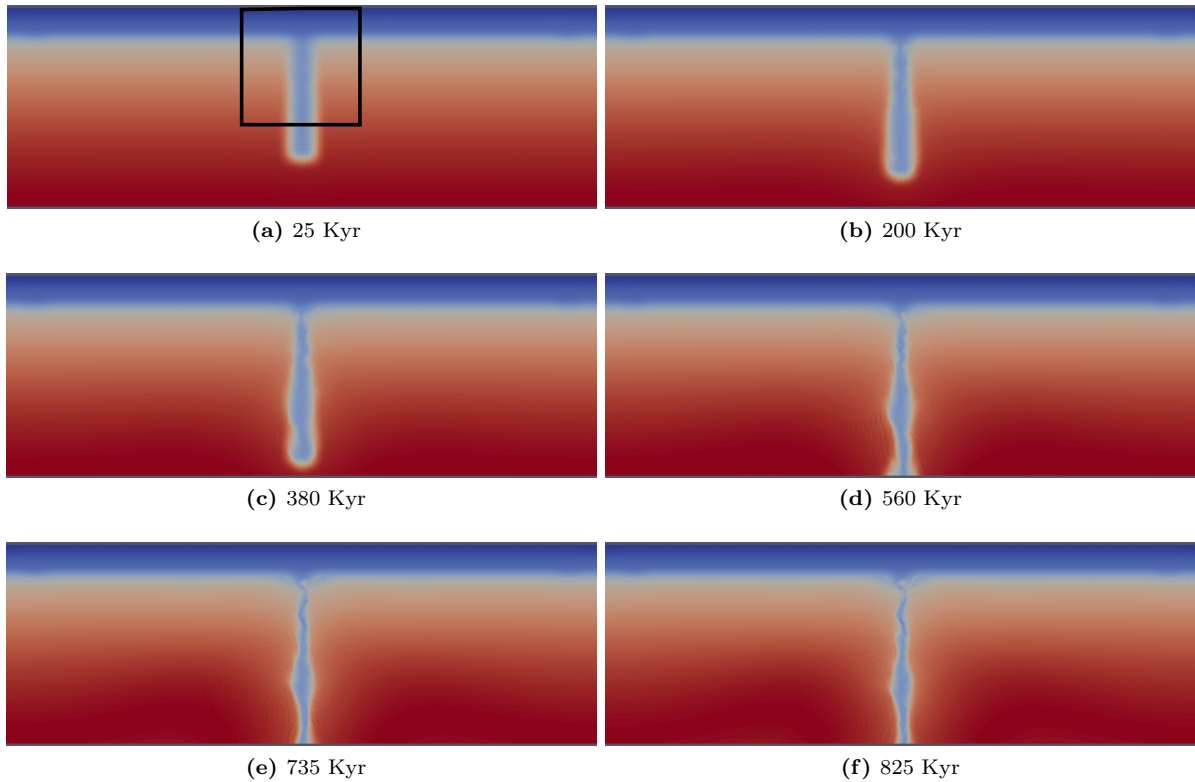
(a) 25 Kyr

(b) 200 Kyr

(c) 380 Kyr

(d) 560 Kyr

(e) 735 Kyr

(f) 825 Kyr

Figure 3.4: Temperature field, model 1. The black box in (a) indicates the area which is shown in more detail in figure (3.5)

Dominant deformation mechanism

Andrews and Billen (2009) [2] found two mechanisms by which slab detachment can occur, dislocation creep and yielding. Since we use Peierls creep to replace the yielding mechanism, detachment can either take place by dislocation- or Peierls creep. Figure (3.6) illustrates the dominant deformation mechanisms. The red area's which are labeled "Maximum Allowed Viscosity" indicate area's where all deformation mechanisms result in viscosities above 10^{25} Pas. These area's are therefore considered rigid and no or only small deformation takes place within them. We observe that, except for a few rigid blocks, in the entire slab deformation is dominated by Peierls creep. The figure also shows isotherms which illustrate that Peierls creep is dominant up to temperatures of 1473 K. This temperature is higher than the maximum temperature at which Andrews and Billen (2009) allow yielding (1073 K). However Katayama and Karato (2008) conducted experiments up to temperatures of 1373 K at which they still observed Peierls creep. Peierls creep could therefore very well be dominant at these temperatures. Dislocation creep is the dominant deformation mechanism in almost the entire mantle.

Velocity field evolution

Figure (3.7) shows plots of the magnitude of the velocity. Maximum velocities lie around 1 m/year and are mostly concentrated at the tip of the slab. At first the slab seems to move as one coherent block, indicated by the fact that a large block has the same velocity, but with time velocities near the tip become larger. Deformation of the slab is thus concentrated near the tip of the slab. From figure (3.5) we can make a rough estimate of the descending velocity of the top of the slab after detachment. For model 1 this velocity is about 7 cm/year.
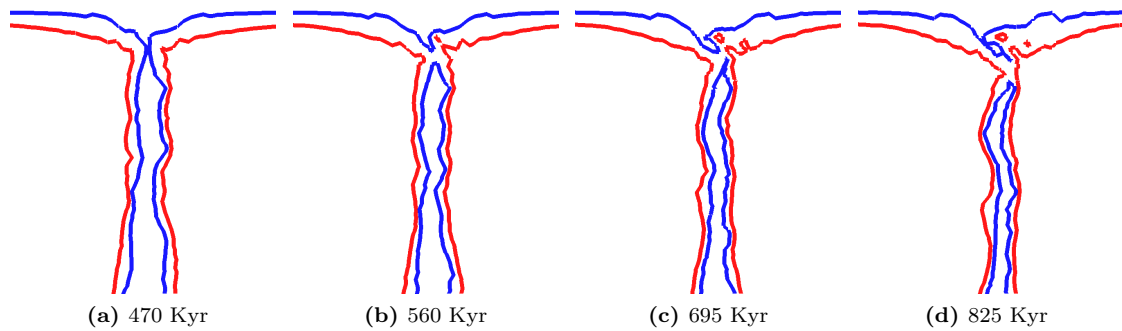
(a) 470 Kyr   **(b)** 560 Kyr   **(c)** 695 Kyr   **(d)** 825 Kyr

Figure 3.5: Temperature contours for 873 K (blue) and 1073 K (red) depicting the slab detachment in detail, model 1

Viscosity field evolution

In figure (3.8) we show the evolution of the viscosity field. If we compare figures (3.8b and 3.8d) with figures (3.6a and 3.6b) we observe that everywhere where Peierls creep is dominant, the viscosity falls below the allowed viscosity range. We observe the fragmentation of the rigid block into several smaller blocks. It also shows a low viscosity zone at the base of the lithosphere and around the slab.

3.3 The influence of activation volume for dislocation and Peierls creep

In the analysis of the reference model we observe deformation due to Peierls creep in almost the entire slab. The classical perception of slab detachment however is that deformation occurs in a narrow zone just below the lithosphere. We therefore want to try and limit the occurrence of Peierls creep to a smaller zone just below the lithosphere. To achieve this we increase the activation volume in models 2-8 because this makes both dislocation and Peierls creep more sensitive to pressure and may therefore limit Peierls creep to a more localized, shallower zone As a result of the coupling between Peierls and dislocation creep this will also have an influence on the occurrence of dislocation creep. To study the opposite effect we decrease the activation volume for Peierls and dislocation creep in model 9. All plots belonging to model 2-5 can be found in appendix A1-A4, plots belonging to model 9 can be found in appendix D1. Models 6, 7 and 8 do not lead to slab detachment.

Model 2, increased activation volume for dislocation and Peierls creep

In the temperature evolution of model 2 we observe that the upper thinning zone develops faster and more localized compared to model 1. When we study the corresponding viscosity plots and deformation mechanisms dominance plots clearly in the beginning the rigid block in the slab is larger and the area's where Peierls creep dominates are smaller. In the tip of the slab however we observe the area where Peierls creep dominates increase and the rigid blocks decrease in volume. Diffusion creep becomes the dominant deformation mechanism in the lower part of the mantle compared to model 2. In the velocity magnitude plot we observe that the slab seems to move as one coherent unit for a longer period compared to model 1. If we estimate the velocity at the top of the detached slab we find values of around 20 cm/year. The low viscosity zones below the lithosphere and around the slab still exist.

Model 3, increased activation volume for dislocation and Peierls creep

In the temperature evolution of model 3 we observe that the upper thinning zone is even more localized compared to model 1 and model 2. However the lower thinning zone shows the opposite trend and is not as well developed as in model 1 or 2. In the viscosity plots we observe that the low viscosity zone
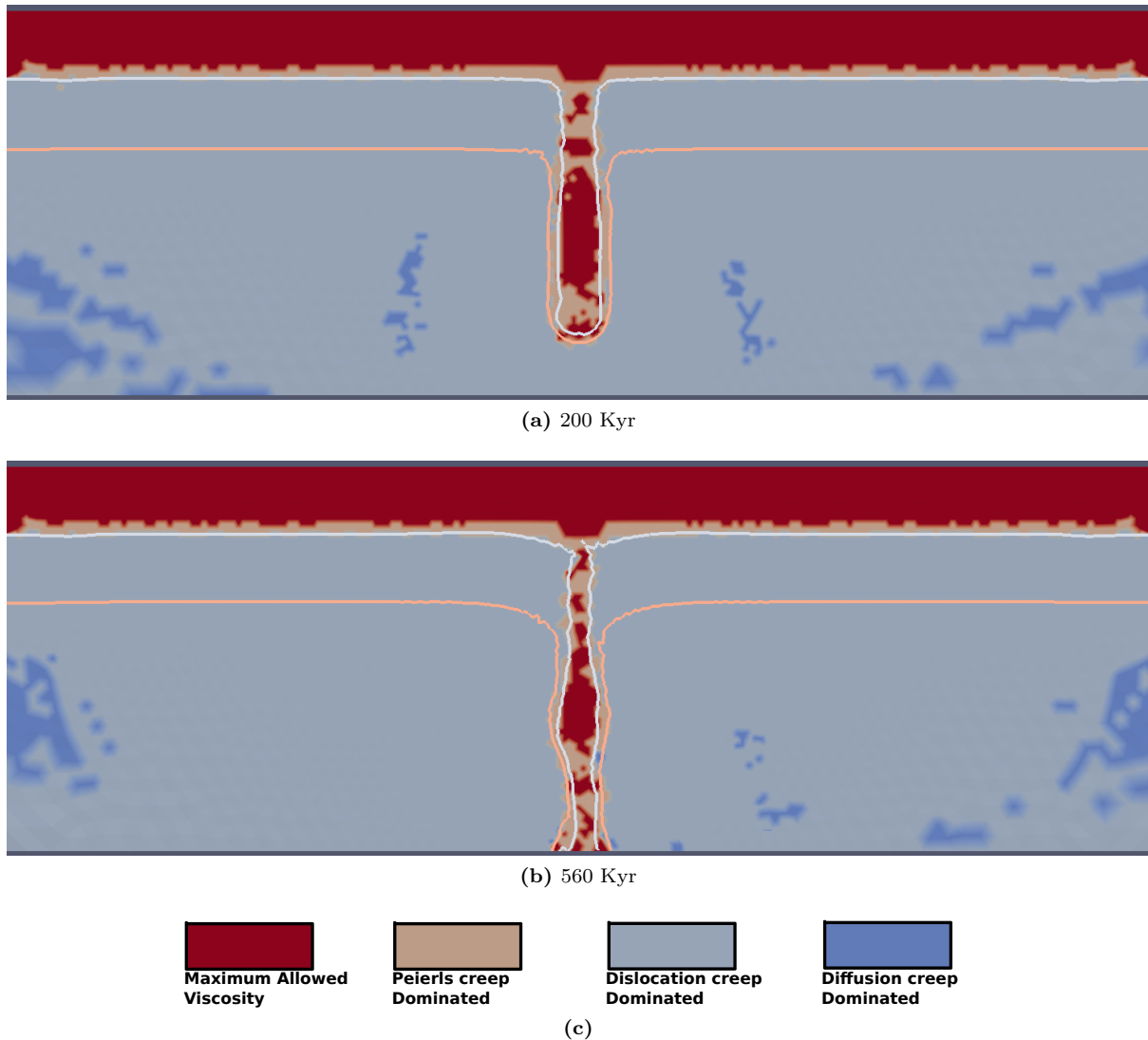
(a) 200 Kyr

(b) 560 Kyr

| Maximum Allowed Viscosity | Peierls creep Dominated | Dislocation creep Dominated | Diffusion creep Dominated |

(c)

Figure 3.6: These plots denote whether diffusion-, dislocation- or Peierls creep dominates rheology in model 1. Isotherms are also plotted and from top till bottom they denote 1073 K and 1473 K.

in and around the tip of the slab increases. In the deformation mechanism dominance plots we observe that this low viscosity zone is due to Peierls creep. We also observe that diffusion creep has replaced dislocation creep, compared to model 1, as the dominant deformation mechanism in a larger part of the lower mantle. The velocity at the top of the detached slab increased to about 30 cm/year. A difference between model 3 with models 1 and 2 is the dominance of Peierls creep near the tip of the slab where the temperature is above 1473 K.

Model 4, increased activation volume for dislocation and Peierls creep

In the temperature field evolution of model 4 we observe that the upper thinning zone is localized especially in the beginning of the model run. The lower thinning zone seems better developed compared to model 3 and thus breaks the trend we observed in our previous experiments (models 1-3). This is also observed both in the viscosity and deformation mechanism dominance plot. The area where Peierls creep is dominant at temperatures higher than 1473 K has increased. The area where diffusion creep has replaced dislocation creep as the dominant deformation mechanism in the mantle has also increased compared to models 1,2 and 3. The low viscosity zone at the base of the lithosphere extends less far laterally from the subduction location compared to models 1-3. The velocity at the top of the detached slab increases to about 60 cm/year. There is a low viscosity zone around the slab due to Peierls creep.
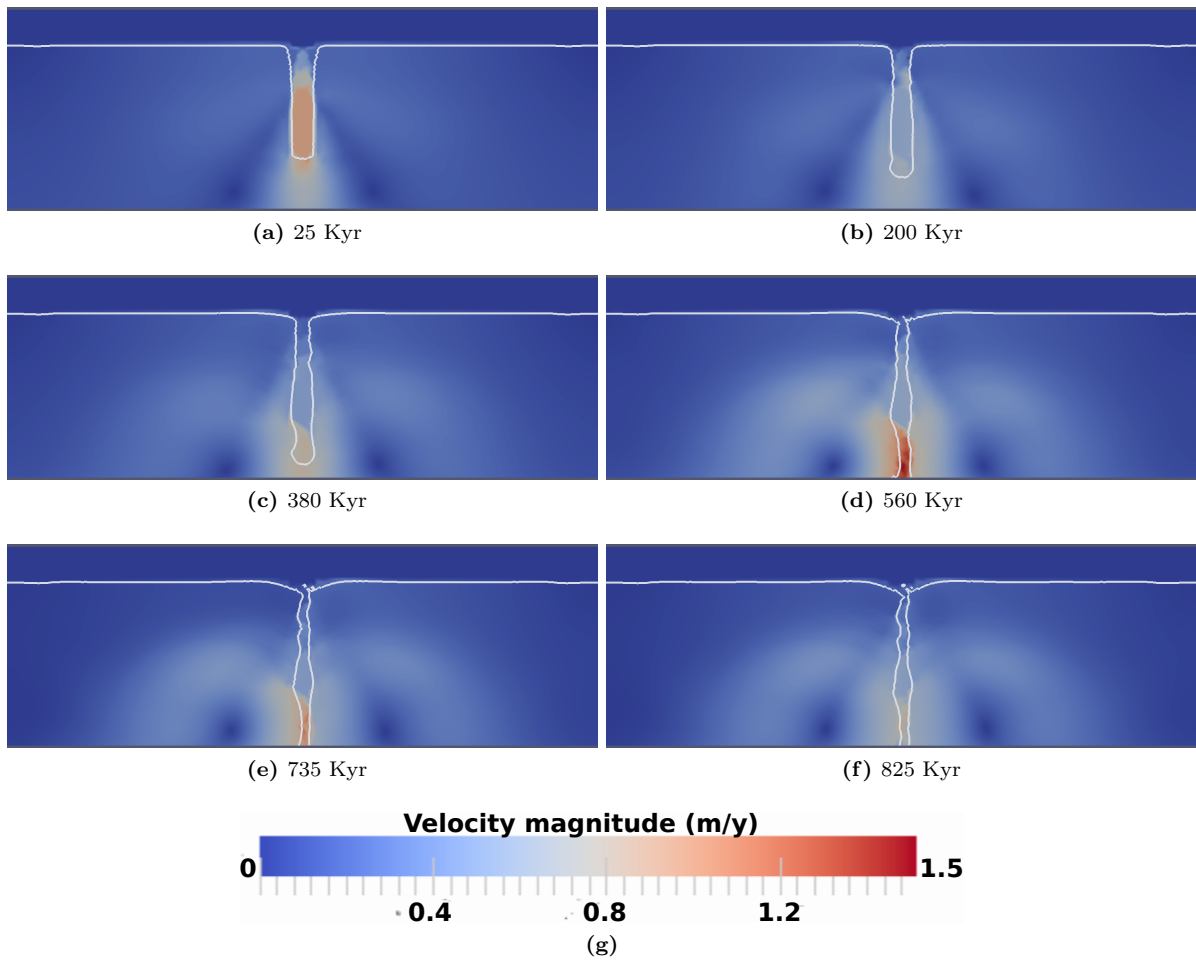
(a) 25 Kyr

(b) 200 Kyr

(c) 380 Kyr

(d) 560 Kyr

(e) 735 Kyr

(f) 825 Kyr

Velocity magnitude (m/y)

0   0.4   0.8   1.2   1.5

(g)

Figure 3.7: Velocity magnitude, model 1. White line is the 1073 K isotherm.

Model 5, increased activation volume for dislocation and Peierls creep

In the temperature field evolution of model 5 the localized thinning zone in the top of the slab is not as narrow as in model 4. In the viscosity and deformation mechanism dominance plots however we can observe that the deformation zone is still very localized. Again the low viscosity zones due to Peierls creep at temperatures higher than 1473 K have increased and the dominance of dislocation creep in the mantle decreased even further compared to models 1, 2, 3 and 4. An important observation is that although initially the slab hangs vertically in the mantle and the model is perfectly symmetric along an axis running from top to bottom through the middle of the slab, with time the slab develops a small dip from right to left. The low viscosity zone at the base of the lithosphere is initially smaller than in models 1-4 and dissapears with time. This feature is, in contrast with models 1-4, also not symmetric. Velocity at the top of the detached slab increased again to about 70 cm/year.
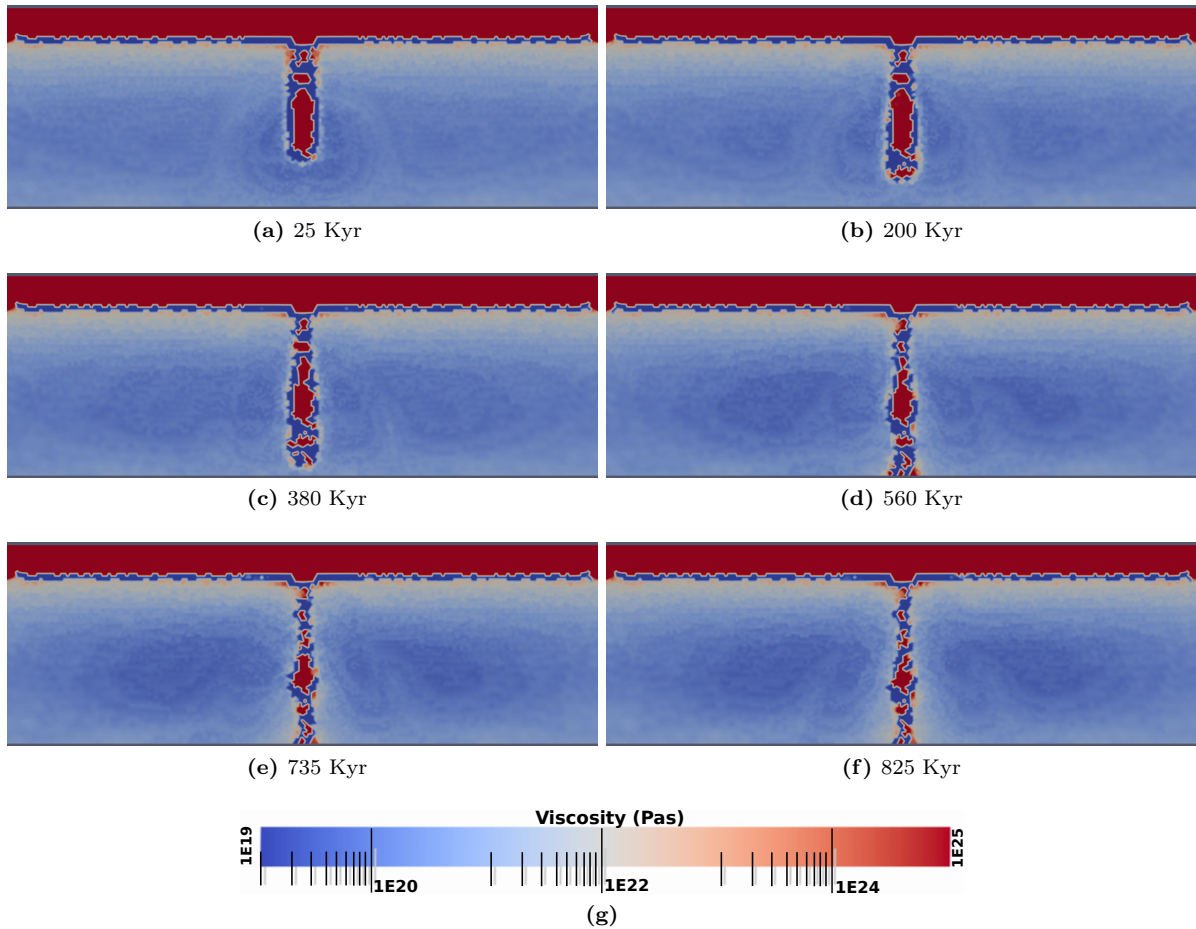
(a) 25 Kyr

(b) 200 Kyr

(c) 380 Kyr

(d) 560 Kyr

(e) 735 Kyr

(f) 825 Kyr

Viscosity (Pas)

(g)

Figure 3.8: Viscosity field, model 1

Models 6-8, increased activation volume for dislocation and Peierls creep, no slab detachment

Models 6, 7, and 8 all do not lead to slab detachment. The slab and lithosphere stay undeformed. There is a bit of movement of the mantle around the tip of the slab. This however does not lead to any detectable change within the 800000 years of our model run. The entire slab and lithosphere are rigid blocks. All deformation in the mantle is dominated by diffusion creep. Only at the top of the slab (just below the lithosphere) in the corners there are small area's where Peierls creep is dominant. This however does not cut through the entire slab and therefore the slab will not move. In model 6, 7 and 8 the activation volume for Peierls creep has become to high and Peierls creep is no longer active at stresses around 250 - 300 MPa, the maximum stresses in these models.

Model 11, decreased activation volume for dislocation and Peierls creep

When we investigate the temperature evolution of model 9 we observe that the upper deformation zone is larger in size compared to model 1. Also the deformation zone just above the tip of the slab has dissapeared. This can be seen from the viscosity and deformation mechanism dominance plots where we observe that the rigid block continues to the bottom of the slab. We observe that the entire mantle is now dominated by dislocation creep. The velocity plots show large velocities in the mantle as well as in the slab. The velocity at the top of the detached slab is roughly 1 m/year. The low viscosity zone at the base of the lithosphere still exists but the low viscosity zone around the slab has dissapeared for the lower part of the slab.

Summary

To summarize, increasing the activation volume for dislocation and Peierls creep does indeed lead to a more localized deformation zone just below the lithosphere. This is not the case for the deformation zone just above the tip of the slab which increases in size. Dislocation creep becomes less dominant at larger depths with increasing activation volume and more dominant with decreasing activation volume. When dislocation creep is no longer the dominant deformation mechanism around the slab (as in model 1 and 2) Peierls creep seems to partly take over and is therefore in models 3-5 dominant at places with temperatures above 1473 K. The low viscosity zone at the base of the lithosphere dissapears with increasing activation volume. In general the descending velocity at the top of the detached slab increases with increasing activation volume, except when the entire mantle is already dominated by dislocation creep in that case a decrease in activation volume increases velocities. A decrease in activation volume removes the lower part of the low viscosity zone around the slab. Some of these observed trends are summarized in figure (3.9).
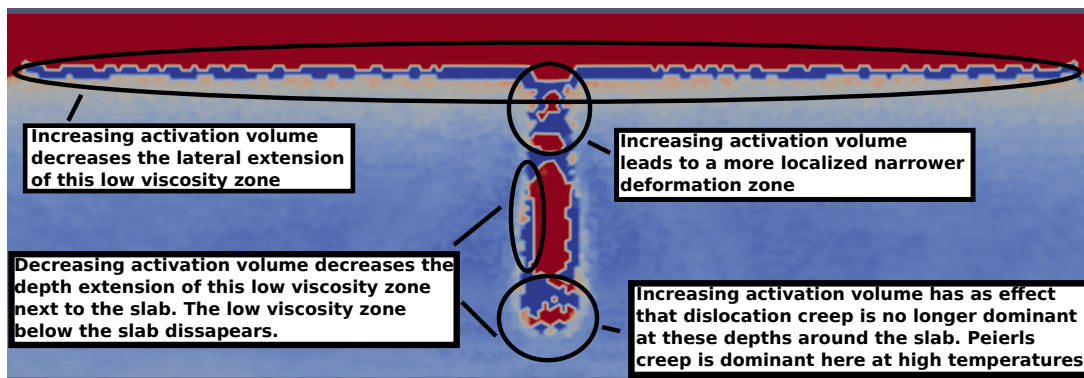
Figure 3.9: this figure summarizes a few trends we observe from models 1-5 and 9.

3.4   Decreased activation Volume for Diffusion creep

In the reference model we observed that almost the entire mantle is dominated by dislocation creep. To investigate the effect of dominant diffusion creep in the mantle we decreased the activation volume for diffusion creep in models 10 and 11 with respect to the reference model. All plots for model 10 and 11 are in appendix B1 and B2.

Model 10, decreased activation volume for diffusion creep

If we study the temperature field evolution for model 10 we see that deformation goes faster. The initial deformation zone just below the lithosphere is not significantly smaller or larger compared to model 1. Also the low viscosity zone at the base of the lithosphere has not changed. Just above the tip of the slab however the deformation zone is larger and the rigid blocks are smaller. The velocity is much higher in the mantle.

Model 11, decreased activation volume for diffusion creep

For model 11 the temperature field evolution shows an even faster deformation compared to model 1. The deformation zone just above the tip of the slab does not form anymore. There are however still two deformation zones. One just below the lithosphere and one better developed zone below the first one. As can be observed from the viscosity field plots as well as from figure (3.13) viscosity in the mantle only decreases from top to bottom till it reaches $10^{19}Pas$. It does not rise again and viscosities at a depth of 450 km are not lower than viscosities at 700 km depth which is the case for all other models.

Summary

To summarize, a decreased activation volume for diffusion creep results in faster deformation. Diffusion creep replaces dislocation creep as the dominant mechanism in the lower part of the mantle.

3.5 Increased activation energy for dislocation- and Peierls creep combined with an increased activation volume

In models 12 and 13 we increase the activation energy for dislocation and Peierls creep. This is done to reduce the low viscosity zone at the base of the lithosphere. In models 14 and 15 we again increase the activation volume for dislocation- and Peierls creep, but in this case model 12 is the "reference model". Models 13 and 15 do not show slab detachment. All plots for models 12 and 14 are in appendix C1 and C2.

Model 12, increased activation energy for dislocation and Peierls creep

The temperature field evolution of model 12 looks very similar to that of model 1. However the viscosity field does show a few differences. The number and size of the rigid blocks has decreased. Only in the first time snap shot the low viscosity zone at the base of the lithosphere has a smaller lateral extension. The velocity field looks rather similar. The velocity at the top of the detached slab has increased to 15 cm/year. Also the deformation mechanism dominance plots do not show much difference. The only difference is in the mantle where, in some places, diffusion creep has replaced dislocation creep as the dominant deformation mechanism.

Model 14, increased activation- volume and energy for dislocation and Peierls creep

If we compare model 14 to model 12 we observe that the deformation zone just below the lithosphere has become smaller in size. This can be seen from the temperature evolution but even more clearly in the viscosity plots. If we look at the velocity plots we see that the slab is moving more like a rigid block. We see that diffusion creep has replaced dislocation creep as the dominant deformation mechanism in a large part of the mantle. Peierls creep is dominant in places where temperatures exceed 1473 K. The velocity at the top of the detached slab has increased to 60 cm/year. The low viscosity zone at the base of the lithosphere seems to dissapear in the end. The low viscosity zone around the slab increases.

Summary

To summarize, there is not much difference between model 12 and model 1. Model 14 shows the same changes with respect to model 12 as models 2,3,4 and 5 with respect to model 1 (models 2,3,4 and 5 had increased activation volume for dislocation and Peierls creep with respect to model 1 just as model 14 has with respect to model 12).

3.6 Constraints to the occurrence of Peierls creep

Kameyama et al. (1999) [15] reported that although diffusion and dislocation creep are always active at high temperatures which they defined as $0.5T_m$ they are the only two deformation mechanisms. With Tm the melting temperature. At low temperatures, which they defined as $\leq 0.3T_m$, deformation could occur by Peierls creep. Katayama and Karato (2008) [18] reported a higher temperature of 1273 K at a stress of 100 MPa and a strain rate of $10^{-15}s^{-1}$, for the transition of Peierls creep to dislocation creep. Both studies thus report a maximum temperature at which Peierls creep is active which is lower than the 1473 K which is the maximum temperature at which Peierls creep is active in model 1.

Both previously discussed slab detachment models (by Andrews and Billen (2009) and Gerya et al. (2004)) used an upper temperature bound to limit the yield mechanism which is significantly lower than 1473 K. (Andrews and Billen (2009) used 1073 K, Gerya et al. (2004) 700 K). Although the yield mechanism is clearly not the same as Peierls creep it is meant to mimic its behaviour. Therefore it is relevant to investigate what happens in our models if we submitted Peierls creep to comparable temperature constraints.

Models 16, 17 and 18, temperature constraints for Peierls creep

To investigate the effect of a temperature cutoff for Peierls creep we created three model runs, namely Models 16, 17 and 18, where Peierls creep was only allowed up till a certain temperature. We chose to use a depth dependent maximum temperature rather than a fixed temperature and used the definition by Kameyama et al. (1999). To use different temperatures we used the following three definitions: for model 16 $0.3T_m$ (which means maximum allowed temperatures are between 651 K at the top of our model domain and 816 K at the bottom of our model domain), for model 17 $0.4T_m$ (868 K - 1088 K) and for model 18 $0.5T_m$ (1085 K - 1360 K). To calculate the melting temperature with depth we used the Simon equation (3.1) [23]. This function was also used by Karato et al. (2001) [16] for deformation of subducted slabs in the mantle transition zone. All other settings are the same as in model 1 (see table (3.1)).

$$P(GPa) = 2.44 \left(\frac{T(K)}{2171} \right)^{11.4} - 1 \tag{3.1}$$

Model 19, temperature and depth constraints for Peierls creep

In model 19 we added a depth constraint of 280 km on top of a temperature constraint of 0.5Tm for Peierls creep to investigate the need for the weakening effect of Peierls creep around the slab for slab detachment. From these four models only model 18 and 19 show slab detachment. The results are shown in appendix E1 and F1 respectively.

Effect of the temperature and depth constraints

Although there are differences between the temperature and viscosity field development of model 1 and model 18 the overall evolutions are very similar. If we investigate figure (3.10) we observe a viscosity field for model 17 at 25 Kyr. If we compare this with the viscosity fields at the same time of model 1 and 18 there are two clear differences. First, model 1 and 18 have a low viscosity zone (due to Peierls creep) around the slab this zone is absent in model 17. Second the viscosity contrast between the mantle and the parts of the slab which deform due to Peierls creep just below the lithosphere is higher for model 17 compared to model 1 and 18.
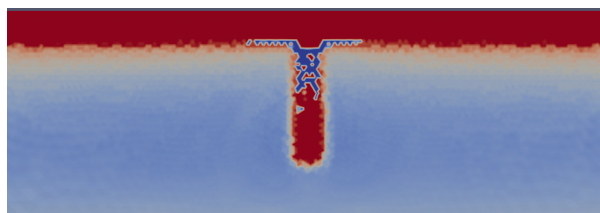

Figure 3.10: This figure shows the viscosity field of model 17 at 25 Kyr.

The depth constraint in model 19 (280 km) on top of the temperature constraint (the same as in model 18) has as effect that the low viscosity zone around the slab due to Peierls creep is prevented. Although slab detachment takes considerably more time (745 Kyr as opposed to 515 Kyr in model 18) it does take place without the weakening effect of Peierls creep around the slab.

When Peierls creep has temperature and or depth constraints it does not limit stresses everywhere. Stresses which still appear in models 18 and 19 lie around the 1 - 1.5 GPa which is high, definitely when compared to stresses which arise in models without any constraints (which are 300 - 350 MPa). These stresses are found around the slab (figure (3.11)).
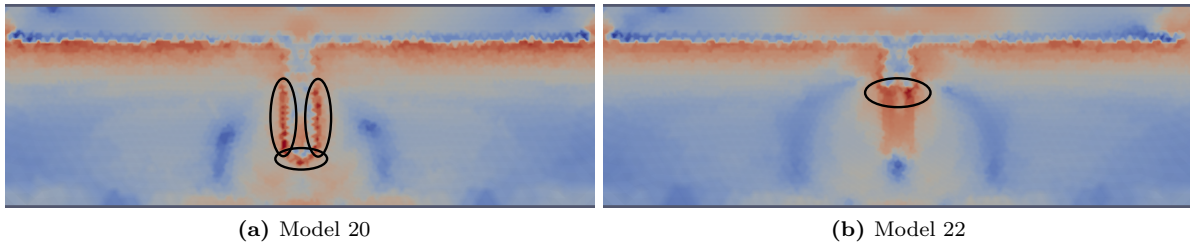

(a) Model 20   **(b)** Model 22

Figure 3.11: In the regions indicated by the ellipses in the two figures above stresses ultimately reach levels of 1 - 1.5 GPa

3.7 Viscosity profiles
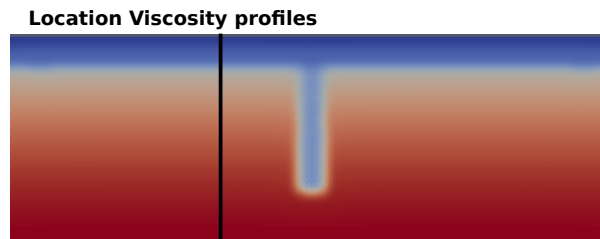
Figure 3.12: This figure shows the location of the viscosity profiles

Figures (3.13, 3.14) show the viscosity profiles for the different models at 300 km from the slab for the beginning of the model runs and half way during the model run respectively. We can identify from figure (3.13) the low viscosity zone at the base of the lithosphere in all models except for models 6, 7, 8 , 13 and 15 where no slab detachment takes place and model 5. However model 5 also shows a low viscosity zone at the base of the lithosphere (figure 3.14) . At around 450 km depth viscosities lie between $5 \cdot 10^{19}$ and $5 \cdot 10^{20}$ Pas in the beginning of the model runs and between $2 \cdot 10^{19}$ and $4 \cdot 10^{20}$ half way during the model runs. At 700 km depth viscosities lie between 10^{20} and $2 \cdot 10^{21}$ Pas. The results of most models are quite similar except for models 9, 10, and 11. In models 10 and 11 activation volume for diffusion creep is lower than in the other models and this weakens the mantle. In model 9, section (3.3), dislocation creep is weakening the mantle. We illustrate that with increasing activation volume for dislocation and Peierls creep the mantle on average becomes stronger (models 1-5). The lowering of activation volume for diffusion creep (models 10 and 11) leads to a weaker mantle.
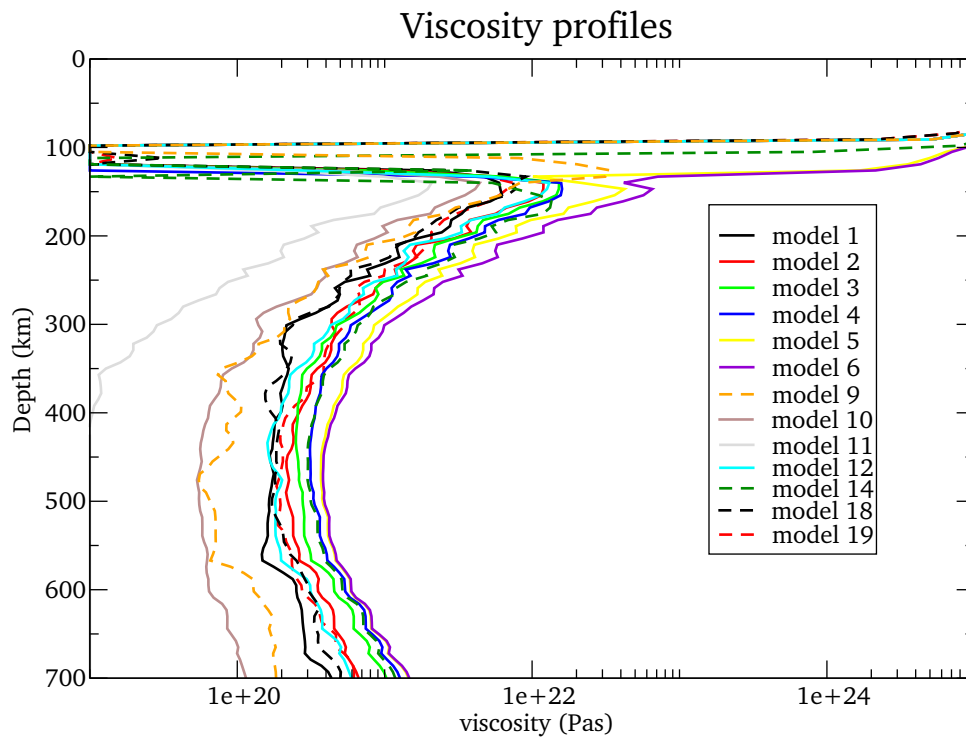
Figure 3.13: Models 7, 8, 13, 15, 16 and 17 are not shown since they give exactly the same result as model 6 in which also no slab detachment takes place.
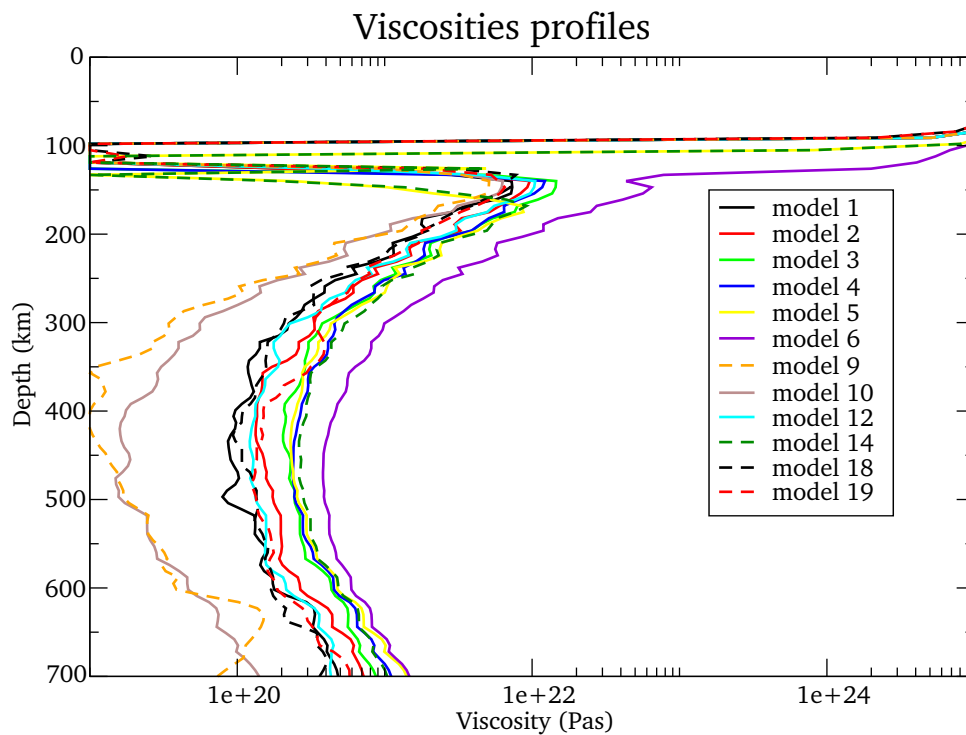

Figure 3.14: Same as figure (3.13) but about 400 Kyr into the model runs.

Chapter 4

Discussion

4.1   Sensitivity to Activation Energy and Activation Volume

Section (3.1) showed that the sensitivity of diffusion creep to activation energy and volume is significant. Models 1, 10 and 11 show that this can have an effect on the evolution, but not necessarily the outcome, all models show slab detachment due to Peierls creep. As can be expected a lowering of activation volume for diffusion creep leads to a weaker mantle. This weaker mantle leads to higher velocities in the mantle which leads to a weaker mantle due to dislocation creep around the slab.

For dislocation creep we observed that the effect of activation volume and energy is significantly less compared to diffusion creep. If we compare the results of models 1 and 9 (the only two models where dislocation creep is dominant in the entire mantle, figures (3.13 and 3.14)) we illustrate that a lower activation volume for dislocation creep leads to a lower viscosity. We observe that as the model evolves the effect becomes larger. Progressively the lower viscosity leads to a higher velocity which leads to a higher strain rate which leads to a lower viscosity due to dislocation creep. This effect is not as clear in models 2, 3, 4 and 5 (where we have increased activation volume for dislocation and Peierls creep) because in this case viscosity in the mantle is not entirely dominated by dislocation creep, but we do see that dislocation creep becomes progressively more dominant in the mantle with time.

For Peierls creep we observed that the influence of activation volume and energy is very large. In our models activation volumes of 20 cm^3 mol^{-1} and higher do not lead to slab detachment in combination with an activation energy of 423 kJ mol^{-1}. An activation energy of 500 kJ mol^{-1} or higher does not lead to slab detachment in combination with an activation volume of 10 cm^3 mol^{-1}. This is also shown in table (4.1) These results again show the sensitive behaviour of Peierls creep. An increase of 8 cm^3 mol^{-1} does not have a large influence (at least for Peierls creep) in models 1 to 5 while only an increase of an extra 2 cm^3 mol^{-1} (model 6) results in viscosities due to Peierls creep to go from the low end of our viscosity range (10^{19} Pas) to the high end of the viscosity range (10^{25} Pas) and no slab detachment takes place.

Occurrence of Slab Detachment

Activation Energy (kJ mol^{-1})	8	10	12	14	16	18	20	22	24
500	X	No	X	X	X	X	X	X	X
450	X	Yes	X	Yes	No	X	X	X	X
423	Yes	Yes	Yes	Yes	Yes	Yes	No	No	No

Activation Volume (cm^3 mol^{-1})

Table 4.1: Schematic figure showing which settings for activation volume and energy for dislocation and Peierls creep lead to slab detachment. Yes means slab detachment, no means no slab detachment and x means no model run with these setting was performed.

4.2 The Weakening of the mantle around the slab

Andrews and Billen (2009) [2] reported that a Newtonian only rheology (diffusion creep) in the mantle gave to much mantle support and slab detachment would not take place. They argued that a weakening mechanism needs to be present in the mantle. In their models the preferred weakening mechanism was dislocation creep. In our models weakening of the mantle is not always due to dislocation creep. For instance models 4 (appendix A3), 5 (appendix A4) and 14 (appendix C1) show only dislocation creep in the upper part of the mantle.

Almost all models show weakening around and below the slab due to Peierls creep. Notable exceptions are models 11 (appendix B1), 9 (appendix D1) and model 19 (appendix F1). In model 19 this is because below 280 km we do no longer allow Peierls creep to appear. In model 9 the mantle is weaker due to dislocation creep and part of the low viscosity zone around the slab dissapears.

All other models without constraints to Peierls creep show a zone around and below the slab which is weakened due to Peierls creep. In all these models Peierls creep is at least active at temperatures up to 1473K but sometimes even higher. Despite Peierls creep is described as a low temperature high pressure plasticity several different maximum temperatures have been reported at which it can be active. (see section 3.6) From models with three different temperature constraints (16, 17 and 18) only model 18, which allows Peierls creep up to temperatures of 1085 K at the top and 1360 K at the bottom of our model, results in slab detachment. Although the weakened zone around the slab is now slightly narrower it is still there. As reported in section (3.6) there are two differences between model 17 and 18. One is the extend of the weakened zone around the slab and second is the width of the area affected by Peierls creep in the slab just below the lithosphere in the slab which leads to a higher viscosity contrast and higher viscosities in model 17. Model 19, where Peierls creep is also not allowed below 280 km (see table (3.1) for details about the constraints), shows that the weakened zone around the slab due to Peierls creep is not needed for slab detachment. There is however still a weakening of the mantle by dislocation creep. This weakened zone does increase the velocity of slab detachment significantly.

Our models show that it is difficult to find settings which produce a model without a weak zone around the slab due to Peierls creep if no temperature or depth restrictions are imposed. However the weak zone around the slab due to Peierls creep is not needed for slab detachment.

4.3 The 'tail' connecting the detached slab to the lithosphere

In all models where slab detachment takes place the slab seems to stay connected by a cold temperature 'tail' with the lithosphere. The length and thickness of this tail varies per model. This tail can either be formed by material left behind by the descending slab or it could have been dragged along by the descending slab and originate from the lithosphere. This last option would result in a thinning of the lithosphere and could potentially be important for surface deformation.

If the material would come from the lithosphere this should lead to thinning of the lithosphere. However if we investigate figure (4.1) we observe that the temperature profiles next to the slab start to differ from each other at a depth of 150 to 200 km. No thinning of the lithosphere is visible in this figure. However at the base of the lithosphere, in almost every model, a low viscosity zone exists which can be easily deformed. Indeed in the velocity magnitude plots we do observe some movement in this zone. Therefore with the given information both options seem probable. It is therefore probably a combination of the two modes. If material from the lithosphere is dragged along this does not lead to any detectable thinning of the lithosphere in our models. Given the resolution of our mesh in this part of the model of about 20 km we cannot exclude lithospheric thinning smaller than our resolution.
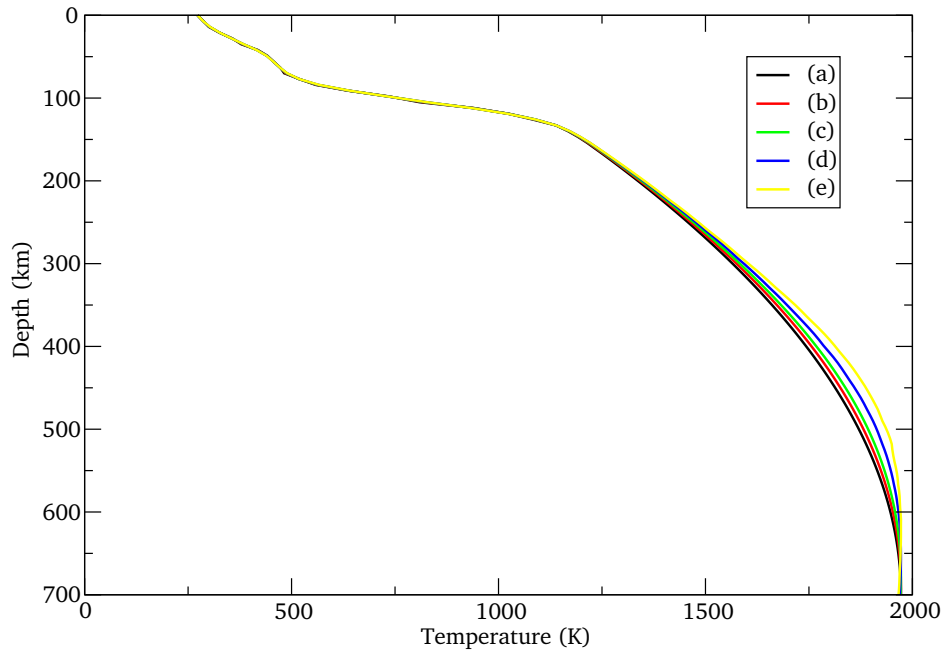
Figure 4.1: Temperature against depth about 300 km away from the slab for model 1. a, b, c, d and e stand for 0, 200 Kyr, 380 Kyr, 560 Kyr and 740 Kyr. f is the initial model

4.4   The velocity at the top of the detached slab

The velocities at the top of the slab for models 1, 2, 3, 4, 5, 9, 12, and 14 are summarized in figure (4.2). In section (3) we observed that models 1, 2, 3, 4 and 5 showed increasing descending velocity of the top of the detached slab with increasing activation volume for dislocation and Peierls creep. Model 9 however also shows increasing descending velocity of the top of the detached slab with decreased activation volume for dislocation and Peierls creep. These two results seen in contradiction with each other.

An important difference between models 1 and 9 and models 2, 3, 4 and 5 is that in model 1 and 9 deformation is dominated by dislocation creep in ,practically, the entire mantle. This is not the case for models 2, 3, 4 and 5 where deformation in the lower part of the mantle is dominated by diffusion creep. In these models deformation around the tip of the slab is dominated by Peierls creep. In model 9 the viscosity due to dislocation creep is lower (because of the lower activation volume) compared to model 1. This means that the mantle support in model 9 is lower than in model 1 and therefore the descending velocity is faster. In models 2, 3, 4 and 5 the increased activation volume for dislocation creep leads to an increased viscosity around the tip of the slab during the bisection method. This means that stresses are high enough for Peierls creep to be active. This creates a lower viscosity zone around the tip of the slab compared to models 1 and 9. Therefore the velocity of the top of the detached slab increases. With increasing activation volume this low viscosity zone seems to increase in size and may therefore explain the further increasing velocity in models 3, 4 and 5.

In section (3) we also found that a decreasing activation volume for diffusion creep leads to an increase in the velocity of the top of the detached slab. This is easier to explain. In model 10 but even more in model 11 deformation in the lower parts of the mantle is dominated by diffusion creep. In model 11 this even leads to viscosities below $10^{19}Pas$. Therefore the mantle support in models 10 and 11 is lower than in model 1 and the detached slab can descend faster.
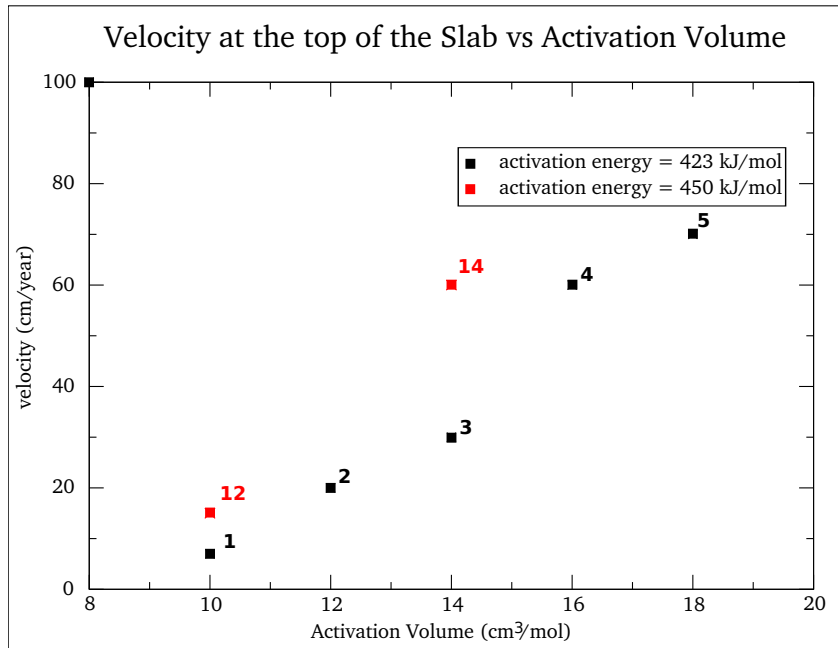
Figure 4.2: Figure showing the velocity at the top of the slab against the activation volume for dislocation and Peierls creep. The black squares are for an activation energy (for dislocation and Peierls creep) of 423 kJ/mol the red squares for a activation energy of 450 kJ/mol. The numbers near the squares correspond to model numbers.

To summarize, a faster descending detached slab is always due to more weakening of the mantle. This weakening can be in the entire domain (as in models 9, 10 and 11) or local (as in models 2, 3, 4 and 5). A weakening in the entire domain is due to either diffusion creep (models 10 and 11) or dislocation creep (model 9). Local weakening is due to Peierls creep.

4.5 Stress levels

Stress levels which are present in the models explain something about the stress limiting properties of Peierls creep. Although there are small differences, stress levels in the models where Peierls creep has no temperature and or depth restrictions are around 300 - 350 MPa. This is around the same stresses as Andrews and Billen (2009) use as yield stress (300 - 500 MPa). In the models where no slab detachment occurs (except for model 17 which has constraints on the occurrence of Peierls creep) maximum stresses are around 300 MPa.

For models 17 (no slab detachment) 18 and 19 (slab detachment) the stress levels are quite different. Because Peierls creep is limited in these models and cannot limit the stresses everywhere in the model stress levels reach values of around 1 - 1.5 GPa for models 18 and 19 and even 3.8 GPa for model 17 around and in the slab (figure (3.11)). These are stress levels which might not occur in the mantle or slab. They suggest that Peierls creep needs to be active at these locations to limit stresses here.

4.6 The ideal model

The classical cartoon like idea of slab detachment is that, just below the lithosphere, a narrow deformation zone forms and the slab detaches and sinks into the mantle. The sinking slab stays roughly undeformed. This narrow deformation zone would be due to Peierls creep and the descending of the slab would be facilitated by the weakening of the mantle around the slab by dislocation creep.

None of the models presented in this thesis meet all the above criteria. Most models have extended low viscosity zones due to Peierls creep around and beneath the slab. The two models which are most like the above described cartoon like idea of slab detachment are models 9 (appendix D1) and 19 (appendix F). Velocities in model 9 however are high, maximum velocities of 3 m/year and a descending velocity at the top of the slab of 1 m/year, and the 'tail' connecting the slab to the lithosphere is quite pronounced. The deformation zone is large. In model 19 velocities are acceptable, maximum velocities are around 0.6 m/year, the deformation zone is also limited due to the depth restriction for Peierls creep of 280 km. there is no detectable 'tail' connecting the slab to the lithosphere. However in model 19 stress levels reach values of about 1-1.5 GPa's just below 280km in the slab. Here Peierls creep can no longer act as a stress limiter.

None of the models result in a completely satisfying model run. Limiting Peierls creep with temperature and or depth restrictions leads to unrealistic high stress levels while no restrictions generally lead to models with a low viscosity zone due to Peierls creep around and beneath the slab. One solution could be the decoupling of activation volume and energy for dislocation creep and Peierls creep. Higher activation volume for Peierls creep may be able to reduce the size of the deformation zone just below the lithosphere in the slab (as in models 2, 3, 4 and 5) while a lower activation volume for dislocation creep may result in enough weakening of the mantle around the slab by dislocation creep and thus remove the low viscosity zone due to Peierls creep around and beneath the slab (as in model 9).

Chapter 5

Conclusions

In this thesis we modeled slab detachment using a viso-plastic rheology. This composite rheology exists of diffusion, dislocation and Peierls creep. Peierls creep is very sensitive to stress which leads to several problems in our calculations. One is that Peierls creep should be treated as a bimodal process and therefore excluded while solving the non-linearity between stress and viscosity, the other is that averaging methods are needed to prevent large viscosity contrasts within one element.

Using temperature and depth restrictions for Peierls creep does result in narrow deformation zones just below the lithosphere in the slab and it does remove the low viscosity zone around and beneath the slab but it also leads to unrealistic high stress levels (1-1.5 GPa's) around the slab and in the slab just beneath the depth restriction. To create models without the low viscosity zone due to Peierls creep around and beneath the slab without any restrictions to Peierls creep a decoupling between the values of activation volume and energy for dislocation and Peierls creep might be needed. If Peierls creep is not the weakening mechanism around the slab, dislocation creep takes over.

All models show a low viscosity zone at the base of the lithosphere due to Peierls creep. Although in our models no thinning of the lithosphere can be detected this could very well be due to our model resolution and this low viscosity zone could be important for surface deformation due to slab detachment.

Only when temperature restrictions to Peierls creep allow creep up to temperatures of 1085 K at the top of our model domain and 1360 K at the bottom of our domain $(0.5T_m)$ does slab detachment take place. Models with the restrictions $0.4T_m$ and $0.3T_m$, where the latter was suggested by Kameyama et. al. (1999) [15], do not lead to slab detachment.

Chapter 6

Acknowledgments

Bibliography

[1] *Mantle Convection in the Earth and Planets*. Cambridge University Press, 2001.

[2] E.R. Andrews and M.I. Billen. Rheologic controls on the dynamics of slab detachment. *Tectonophysics*, 2009.

[3] B.K. Atkinson. The temperature and strain-rate dependent mechanical behaviour of a polycrystalline galena ore. *Econ. Geol.*, 1976.

[4] M. Billen. Modeling the dynamics of subducting slabs. *Annu. Rev. Earth Planet. Sci.*, 2008.

[5] S.J.H. Buiter, R. Govers, and M.J.R. Wortel. Two-dimensional simulations of surface deformation caused by slab detachment. *Tectonophysics*, 2002.

[6] T. Calmus, A. Aguillón-Robles, R.C. Maury, H. Bellon, M. Benoit, J. Cotten, J. Bourgois, and F. Michaud. Spatial and temporal evolution of basalts and magnesian andesites ("bajaites") from baja california, mexico: the role of slab melts. *Lithos*, 2003.

[7] C.H. Craig and D. McKenzie. The existence of a thin low-viscosity layer beneath the lithosphere. *Earth and Planetary Science letters*, 1986.

[8] G. De Astis, P.D. Kempton, A. Peccerillo, and T.W. Wu. Trace element and isotopic variations from mt. vulture to campanian volcanoes: constraints for slab detachment and mantle inflow beneath southern italy. *Contrib Mineral Petrol*, 2006.

[9] C. Faccenna, O. Bellier, J. Martinod, C. piromallo, and V. Regard. Slab detachment beneath eastern anatolia: A possible cause for the formation of the north anatolian fault. *Earth and Planetary Science letters*, 2006.

[10] L. Ferrari. Slab detachment control on mafic volcanic pulse and mantle heterogeneity in central mexico. *Geology*, 2004.

[11] T.V. Gerya, D.A. Yuen, and W.V. Maresch. Thermomechanical modelling of slab detachment. *Earth and Planetary Science Letters*, 2004.

[12] B.H. Hager. Mantle viscosity: A comparison of models from post-glacial rebound and from the geoid, plate driving forces and advected heat flux. *Glacial Isostacy, Sea level and Mantle Rheology R Sabadini et al eds.*, 1991.

[13] H.C. Heard and C.B. Rayleigh. Steady-state flow in marble at 500 ℃to 800 ℃. *Geol. Soc. Am. Bull*, 1972.

[14] B. Isacks and P. Molnar. Mantle earthquake mechanisms and the sinking of the lithosphere. *Nature*, 1969.

[15] M. Kameyama, D.A. Yuen, and S-I. Karato. Thermal-mechanical effects of low temperature plasticity (the peiersl mechanism) on the deformation of a viscoelastic shear zone. *Earth and Planetary Science Letters*, 1999.

[16] S-I. Karato, M.R. Riedel, and D.A. Yuen. Rheological structure and deformation of subducted slabs in the mantle transition zone: implications for mantle circulation and deep earthquakes. *Physics of the Earth and Planetary Interiors*, 2001.

[17] S-I. Karato and P. Wu. Rheology of the upper mantle: A synthesis. *Science*, 1993.

[18] I. Katayama and S-I. Karato. Low-temperature, high-stress deformation of olivine under water-saturated conditions. *Physics of the Earth and Planetary Interiors*, 2008.

[19] T. Kawazoe, S-I. Karato, K. Otsuka, Z. Jing, and M. Mookherjee. Shear deformation of dry polycrystalline olivine under deep upper mantle conditions using a rotational drickamer apparatus (rda). *Physics of the Earth and Planetary interiors*, 2009.

[20] V. Levin, N. Shapiro, J. Park, and M. Ritzwoller. Seismic evidence for catastrophic slab loss beneath kamchatka. *Nature*, 2002.

[21] W.H. Muller and U. Briegel. The rheological behavior of polycrystalline anhydrite. *Eclogae Geol. Helv.*, 1978.

[22] W.R. Peltier. Global glacial isostacy and relative sea level: Implications for solid earth geophysics and climate sytem dynamics. *in Dynamics of the ice age Earth P. Wu (editor)*, 1998.

[23] D.C. Presnall and M.J. Walter. Melting of fosterite, mg_2sio_4, from 9.7 to 16.5 gpa. *Journal of Geophysical Research*, 1993.

[24] A. Segal and N.P. Praagman. The sepran package. technical report,. *http://dutita0.twi.tudelft.nl/sepran/sepran.html*, 2000.

[25] M.J.R. Wortel and W. Spakman. Structure and dynamics of subducted lithosphere in the mediterranean region. *Proc. Kon. Ned. Akad. v. Wetensch.*, 1992.

[26] M.J.R. Wortel and W. Spakman. Subduction and slab detachment in the mediterranean-carpathian region. *Science*, 2000.

Appendix A

Models 2 - 5

A.1   Appendix A1 (model 2)

(a) 25 Kyr

(b) 200 Kyr

(c) 380 Kyr

(d) 560 Kyr

(e) 735 Kyr

(f) 825 Kyr
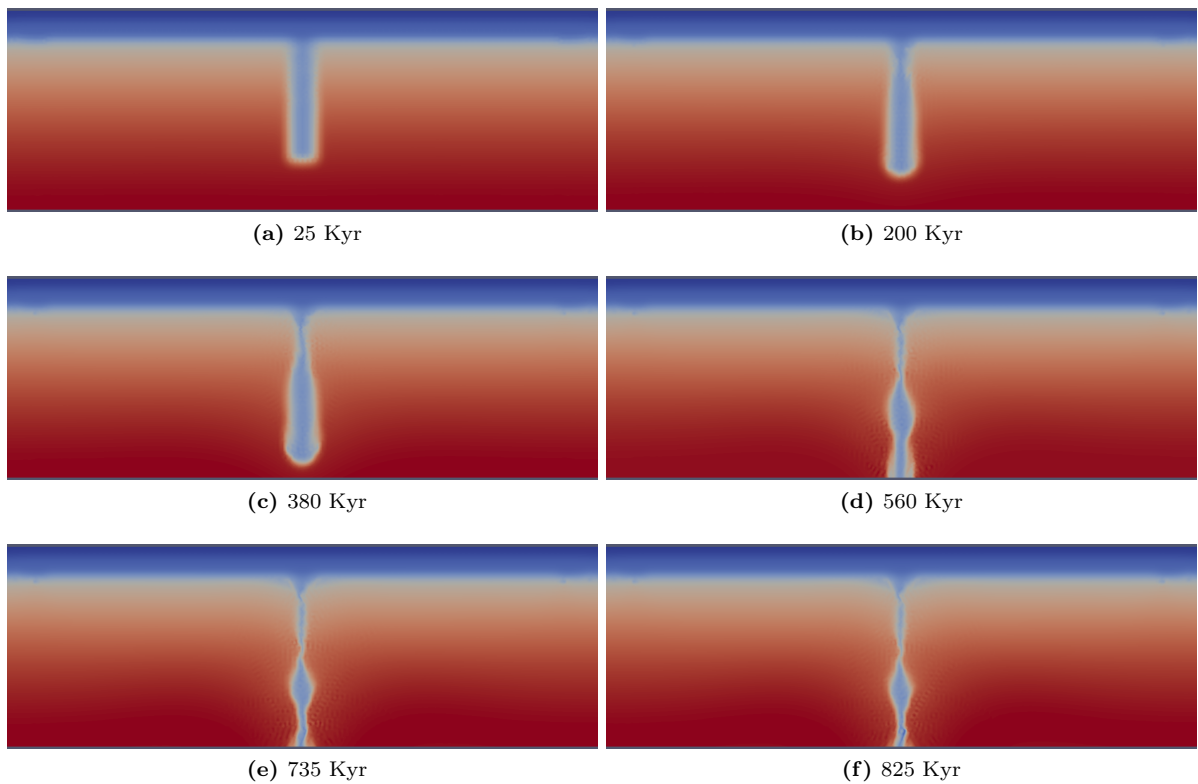
Figure A.1: Temperature field, model 2.

(a) 380 Kyr   **(b)** 600 Kyr   **(c)** 735 Kyr   **(d)** 825 Kyr
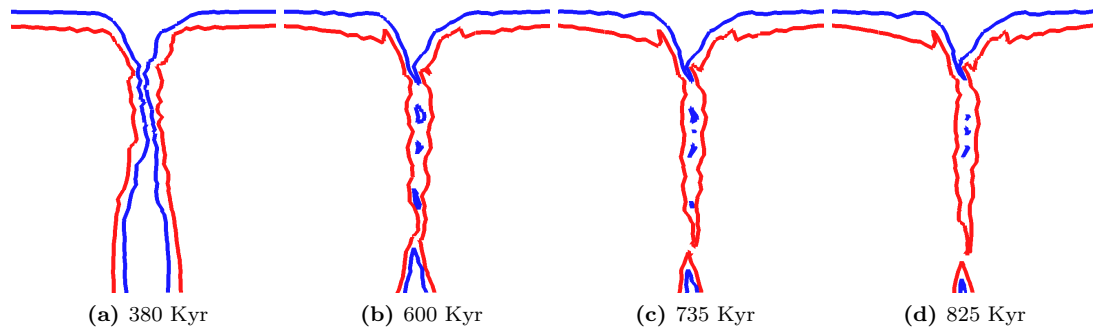
Figure A.2: Temperature contours for 873 K (blue) and 1073 K (red) depicting the slab detachment in detail, model 2
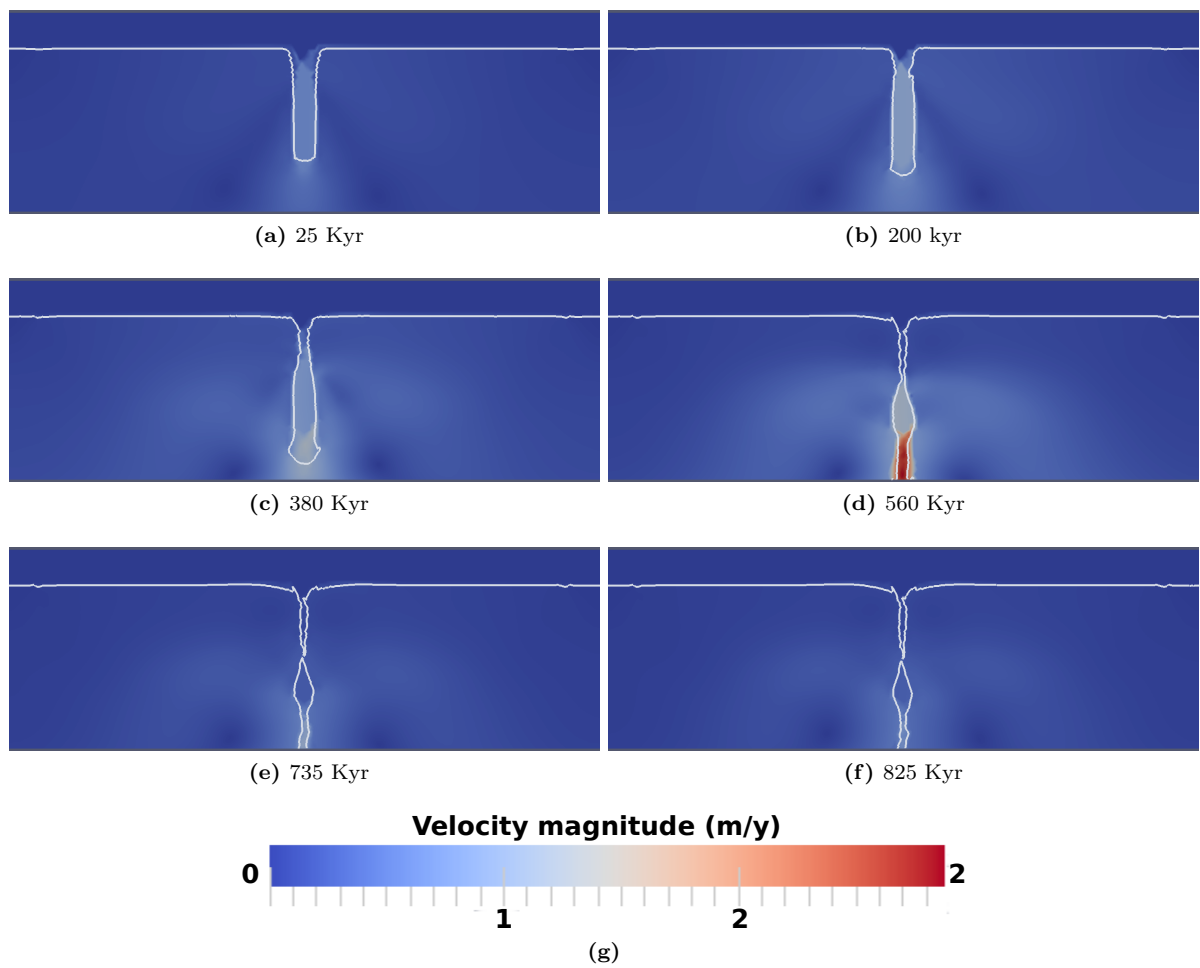

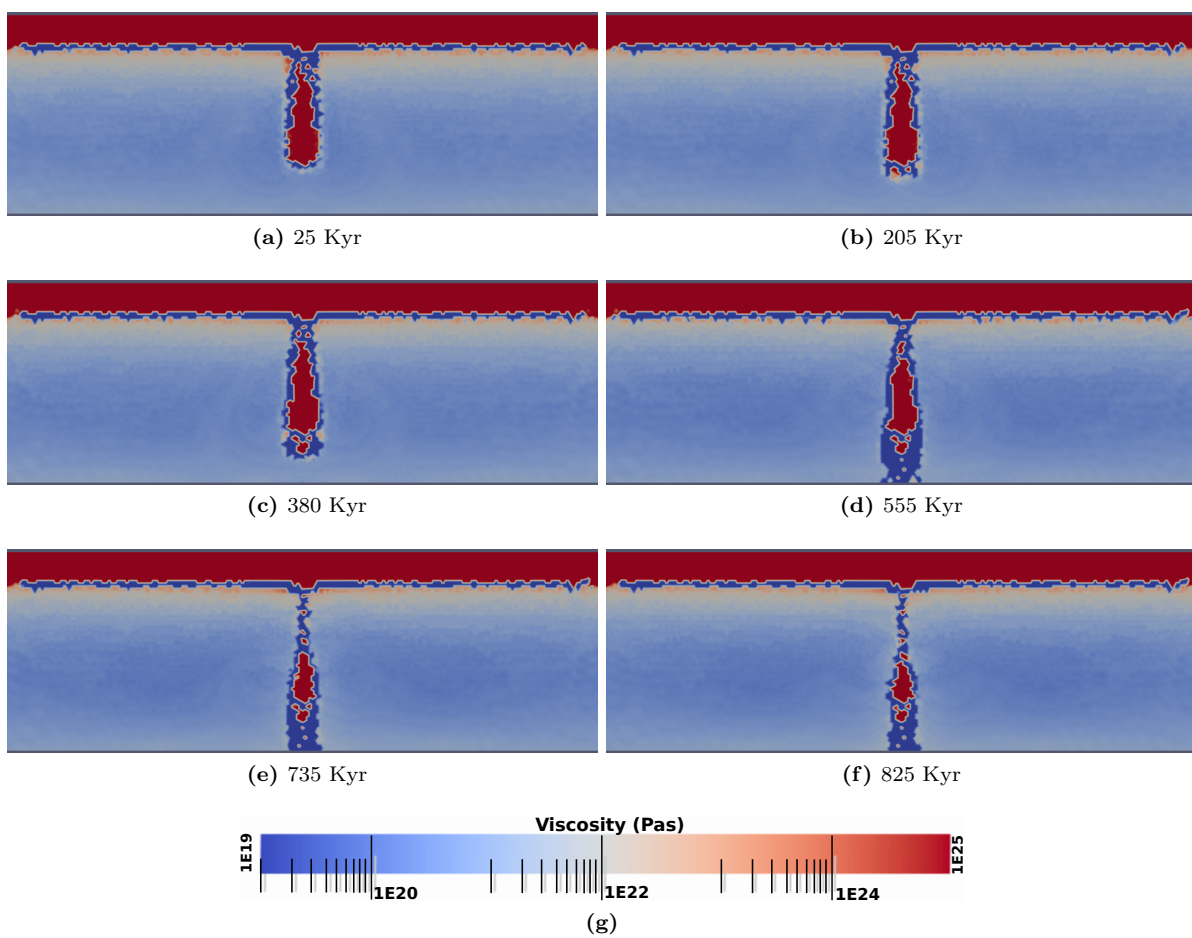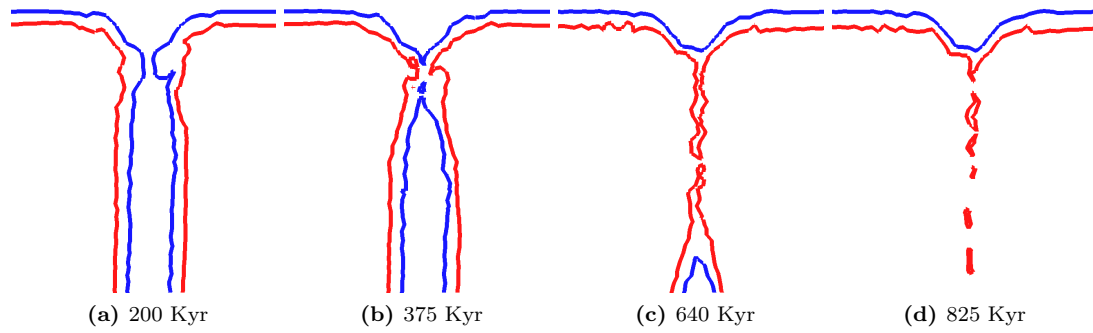**(a)** 25 Kyr   **(b)** 200 Kyr

(c) 380 Kyr   **(d)** 560 Kyr

(e) 735 Kyr   **(f)** 825 Kyr

(g)
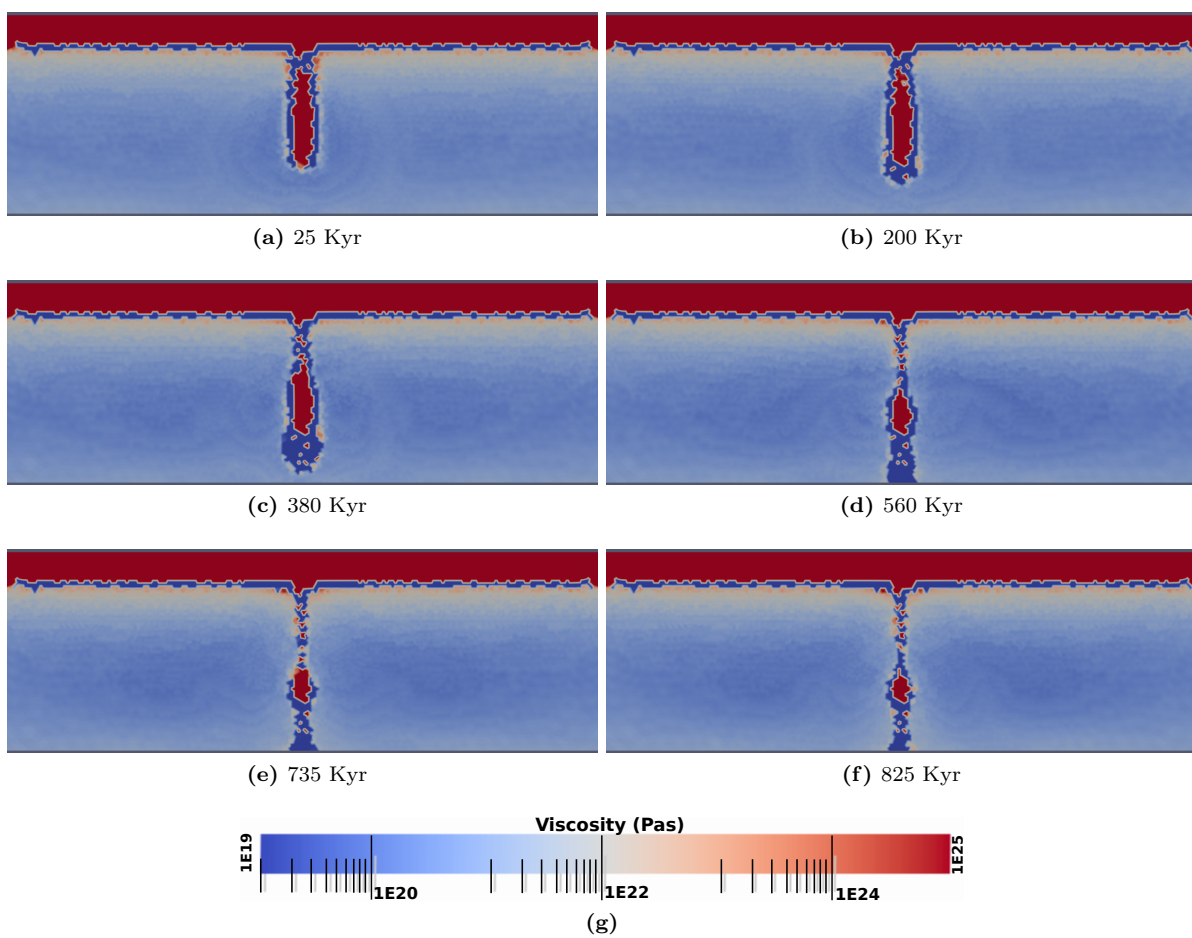
Figure A.3: Viscosity field, model 2

(a) 25 Kyr

(b) 200 kyr

(c) 380 Kyr

(d) 560 Kyr

(e) 735 Kyr

(f) 825 Kyr

Velocity magnitude (m/y)

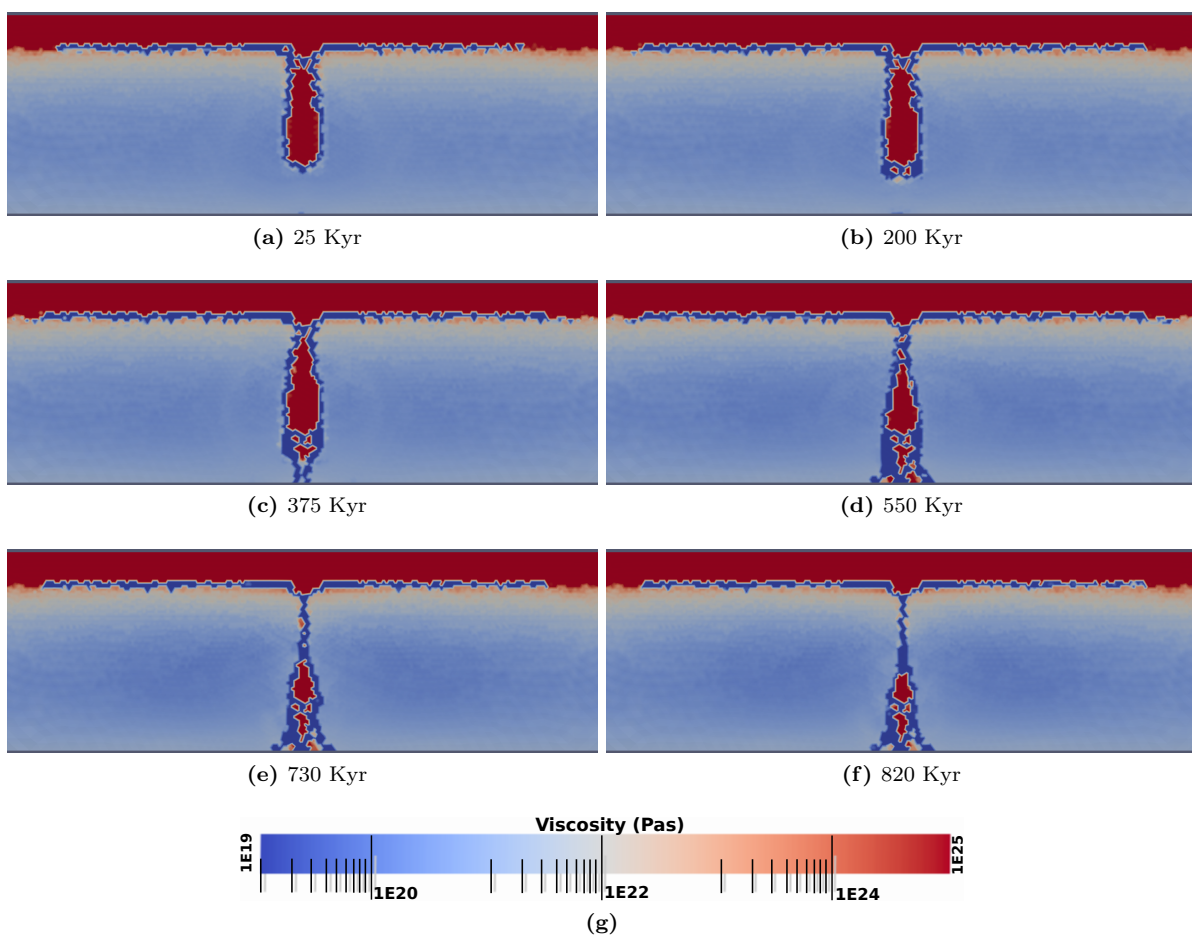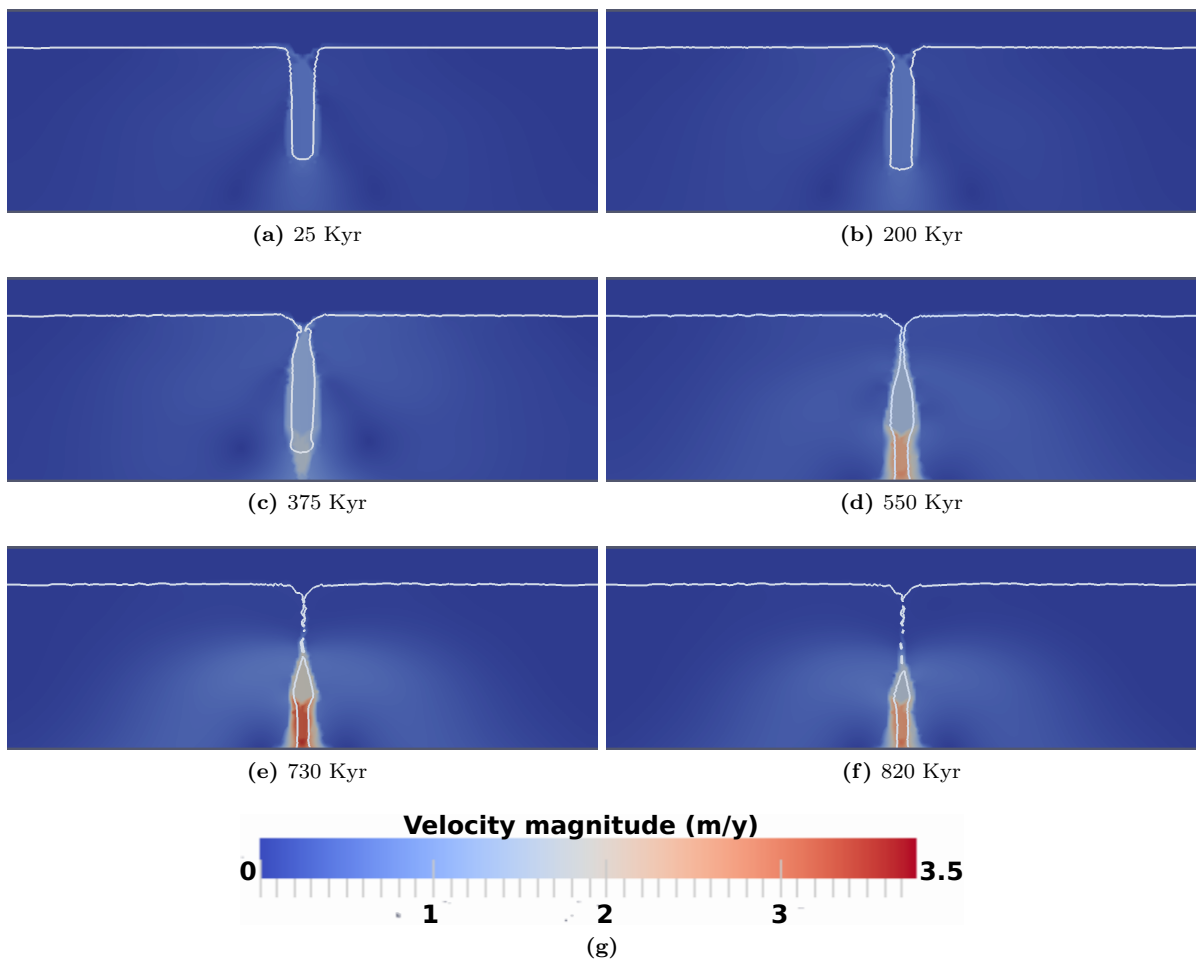0   2

1   2

(g)

Figure A.4: Velocity magnitude, model 2. White line is the 1073 K isotherm.

(a) 200 Kyr

(b) 560 Kyr

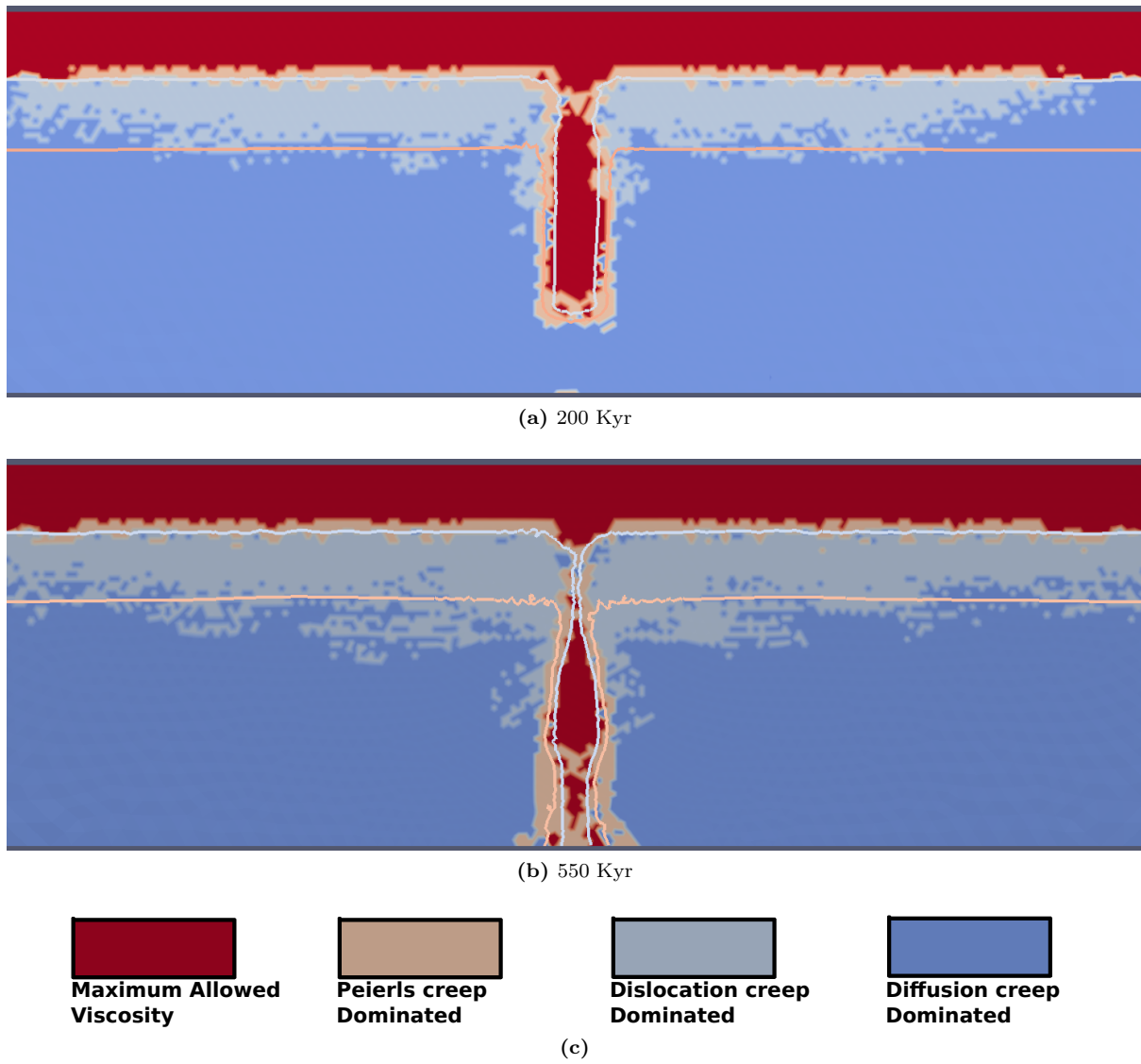| Maximum Allowed Viscosity | Peierls creep Dominated | Dislocation creep Dominated | Diffusion creep Dominated |

(c)
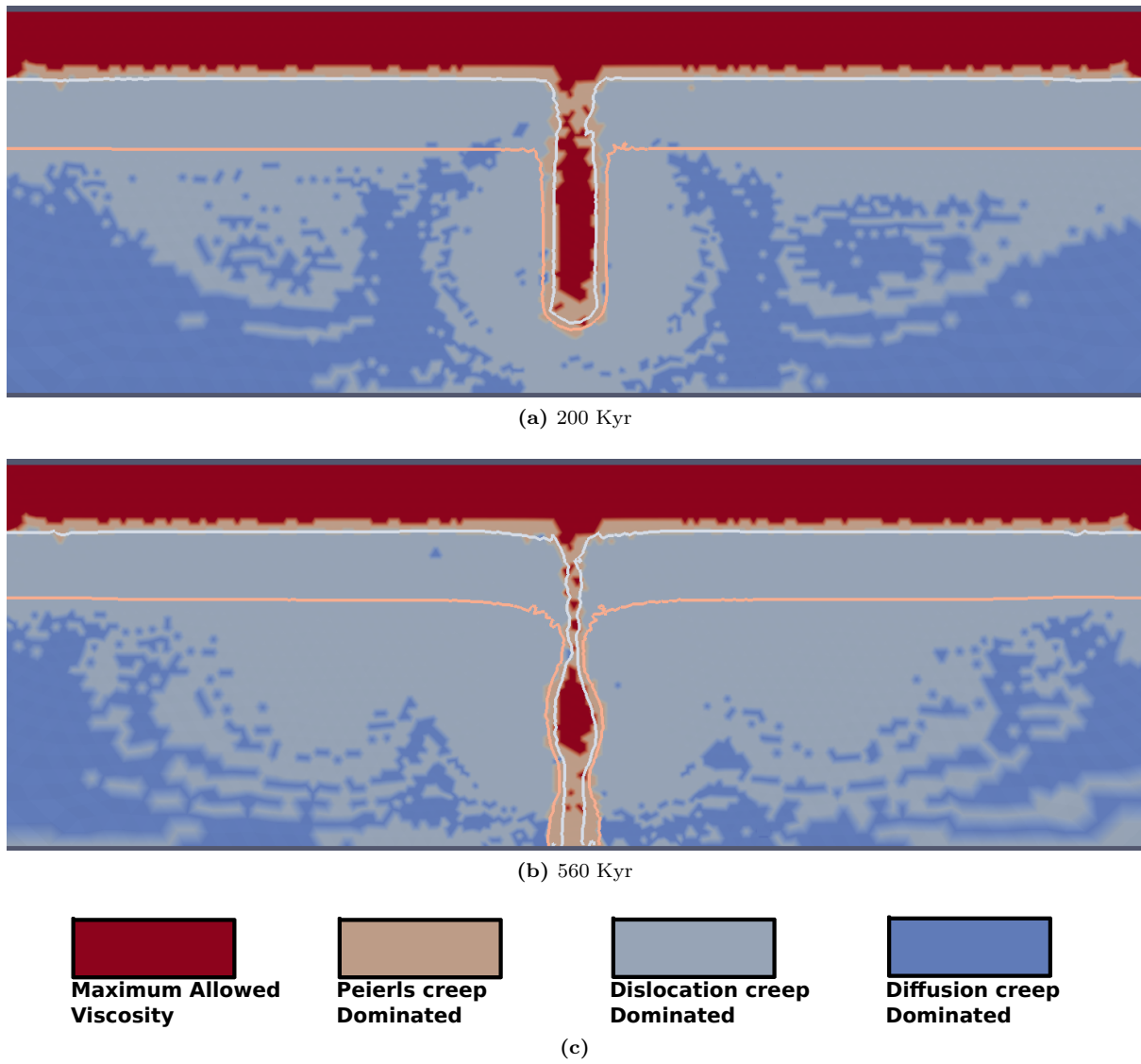
Figure A.5: These plots denote whether diffusion-, dislocation- or Peierls creep dominates rheology in model 2. Isotherms are also plotted for 1073 K and 1473 K.

A.2   Appendix A2 (Model 3)

(a) 25 Kyr

(b) 205 Kyr

(c) 380 Kyr

(d) 555 Kyr

(e) 735 Kyr

(f) 825 Kyr
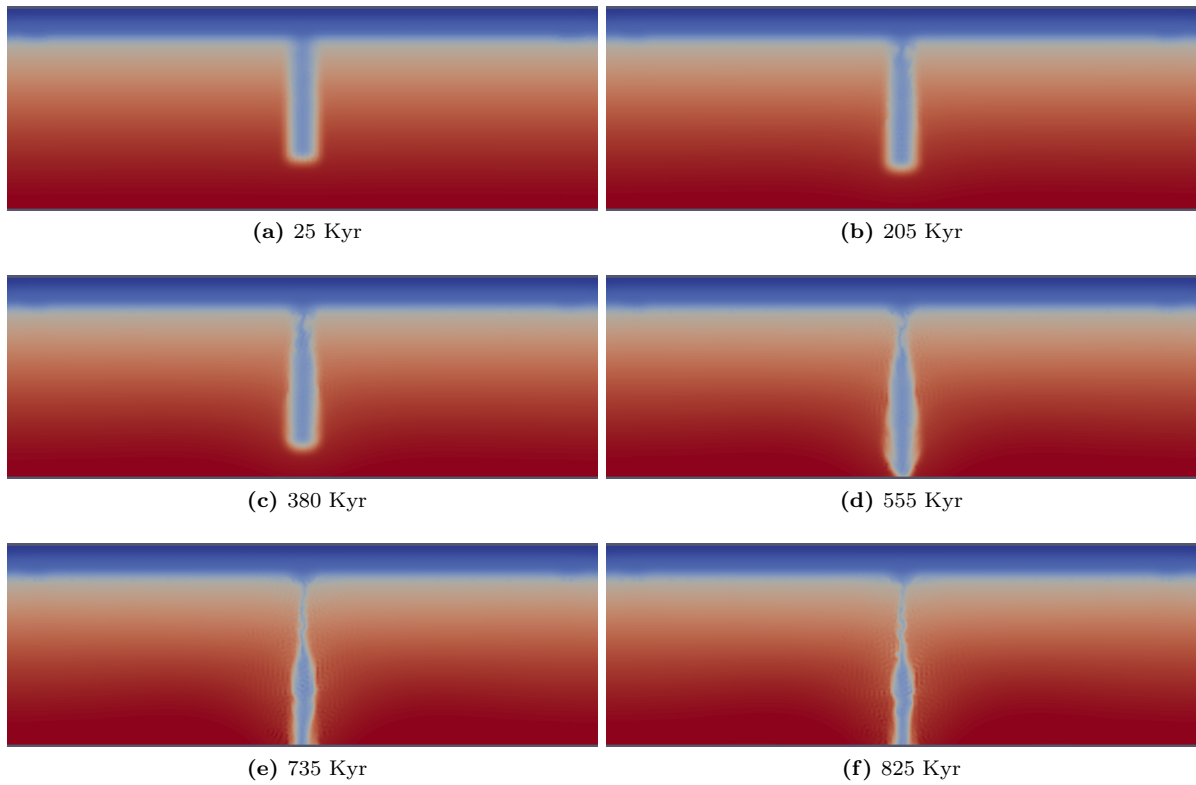
Figure A.6: Temperature field, model 3
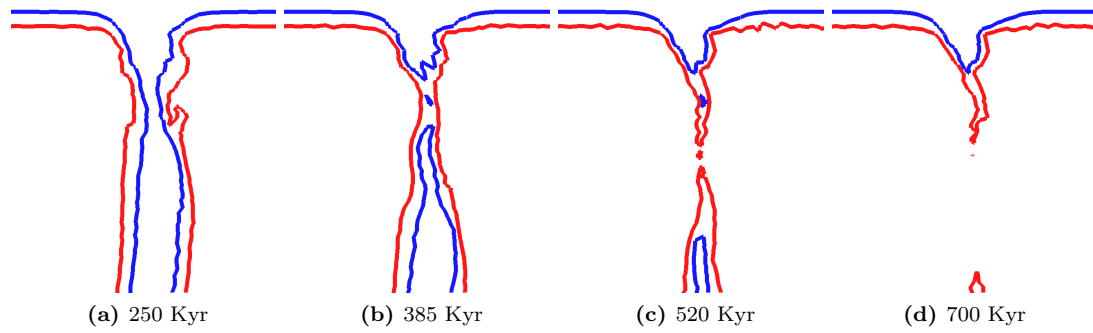
(a) 380 Kyr   **(b)** 515 Kyr   **(c)** 600 Kyr   **(d)** 825 Kyr
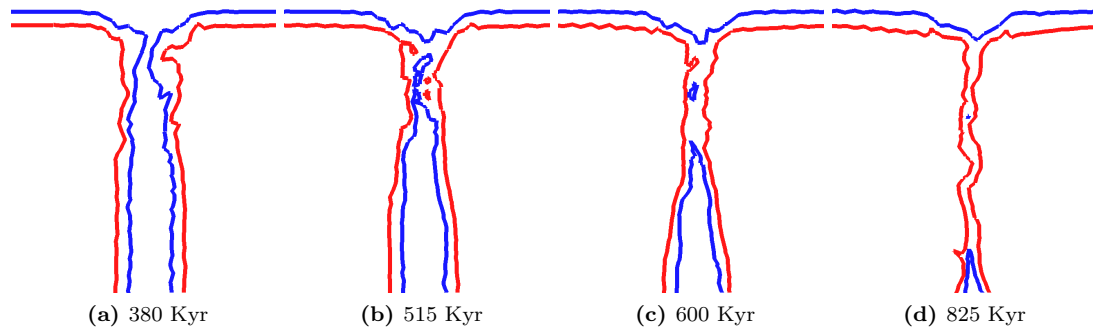
Figure A.7: Temperature contours for 873 K (blue) and 1073 K (red) depicting the slab detachment in detail, model 3

(a) 25 Kyr

(b) 205 Kyr
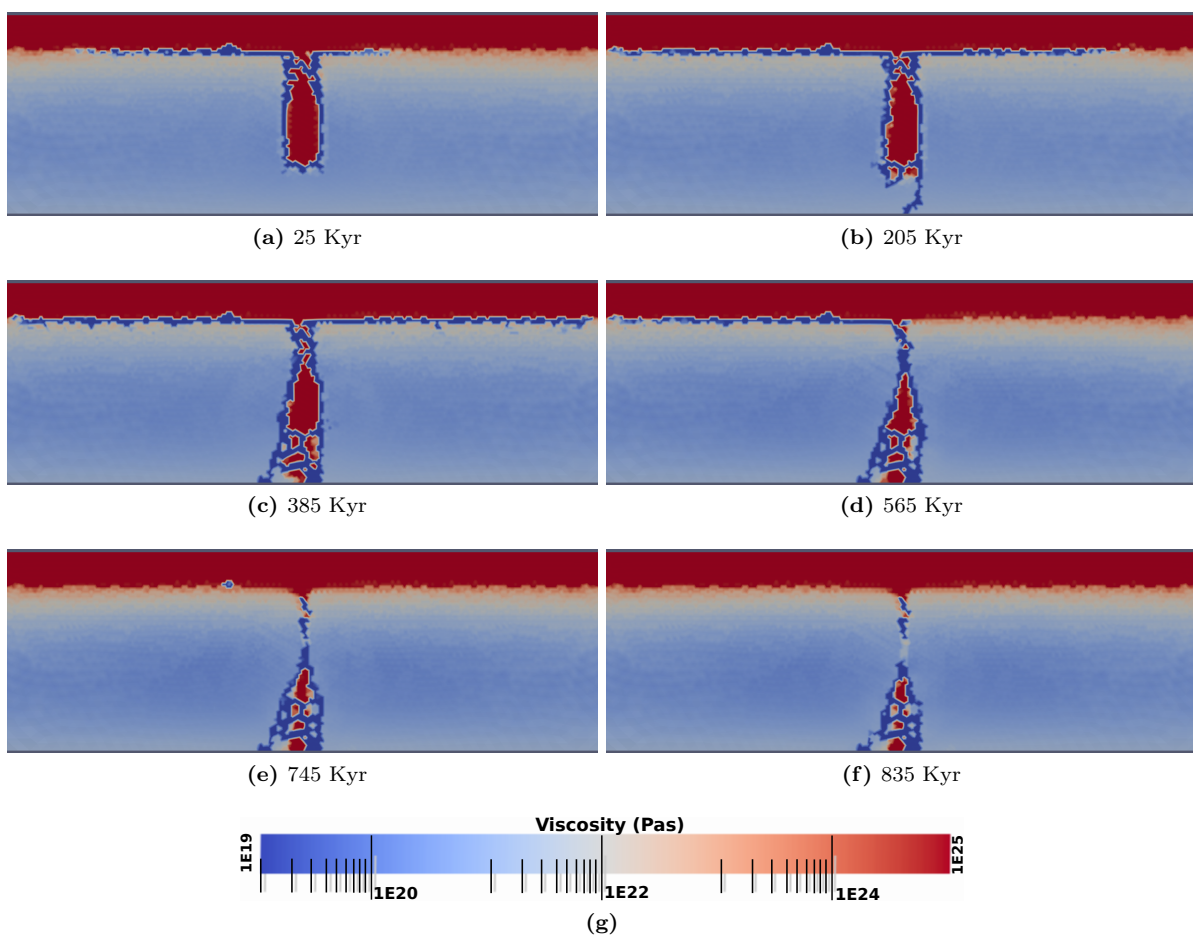
(c) 380 Kyr

(d) 555 Kyr

(e) 735 Kyr

(f) 825 Kyr

(g)

Figure A.8: Viscosity field, model 3

(a) 25 Kyr

(b) 205 Kyr

(c) 380 Kyr

(d) 555 Kyr

(e) 735 Kyr

(f) 825 Kyr

Velocity magnitude (m/y)

0   1   2   3   3.5

(g)
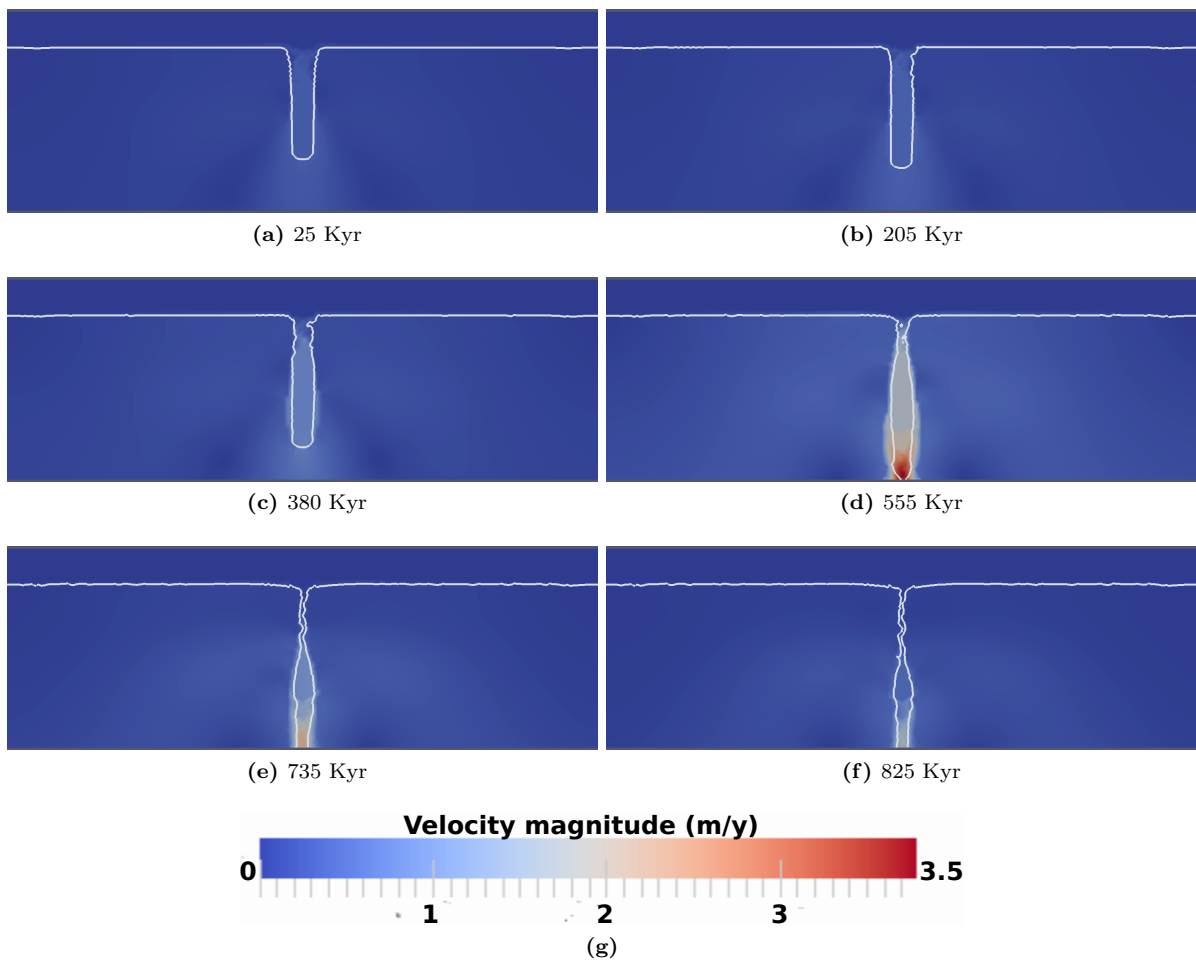
Figure A.9: Velocity magnitude, model 3. White line is the 1073 K isotherm.

(a) 205 Kyr

(b) 555 Kyr

| Maximum Allowed Viscosity | Peierls creep Dominated | Dislocation creep Dominated | Diffusion creep Dominated |

(c)
s
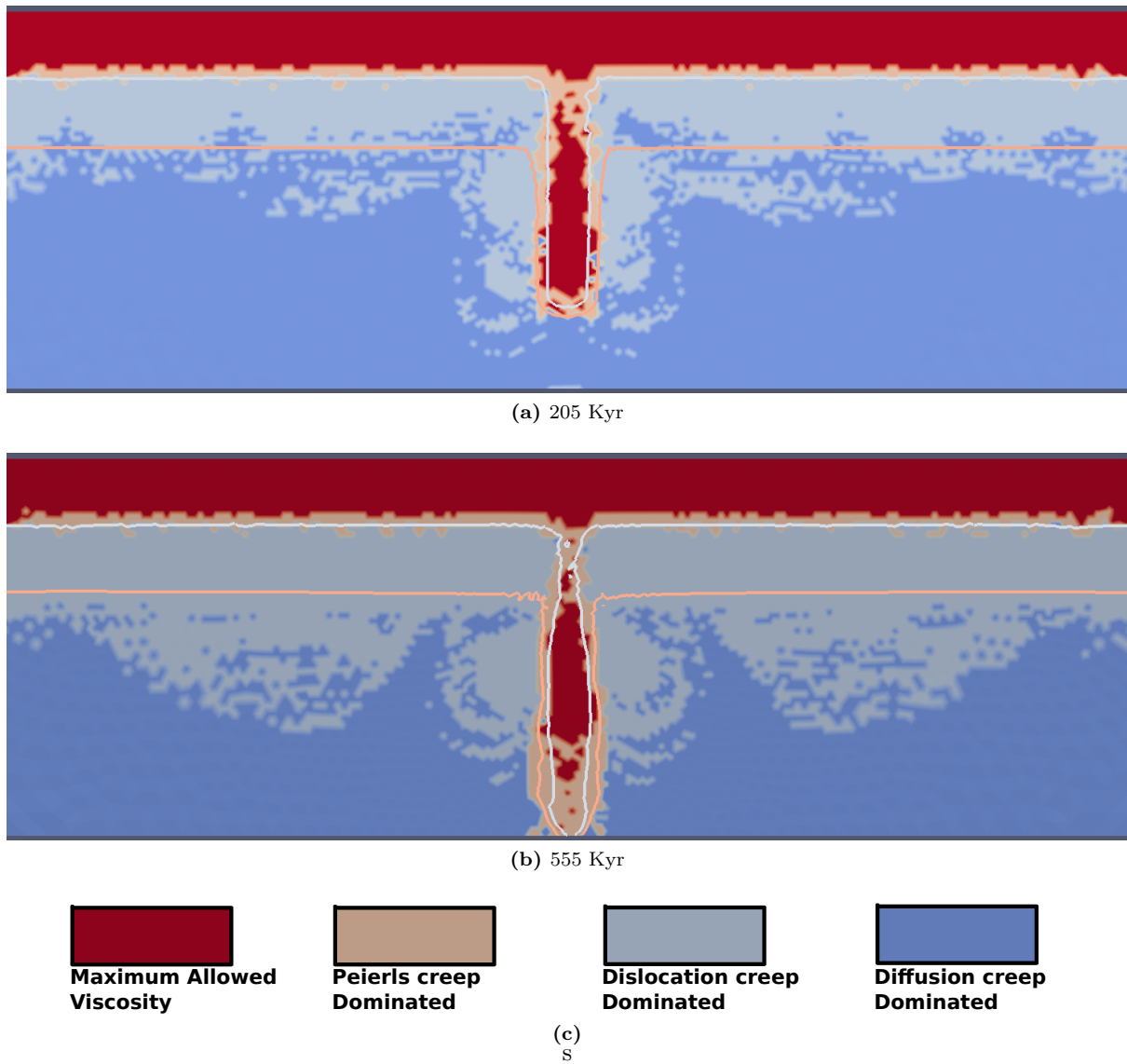
Figure A.10: These plots denote whether diffusion-, dislocation- or Peierls creep dominates rheology in model 3. Isotherms are also plotted for 1073 K and 1473 K.

A.3   Appendix A3 (Model 4)

(a) 25 Kyr

(b) 200 Kyr

(c) 375 Kyr

(d) 550 Kyr

(e) 730 Kyr

(f) 820 Kyr
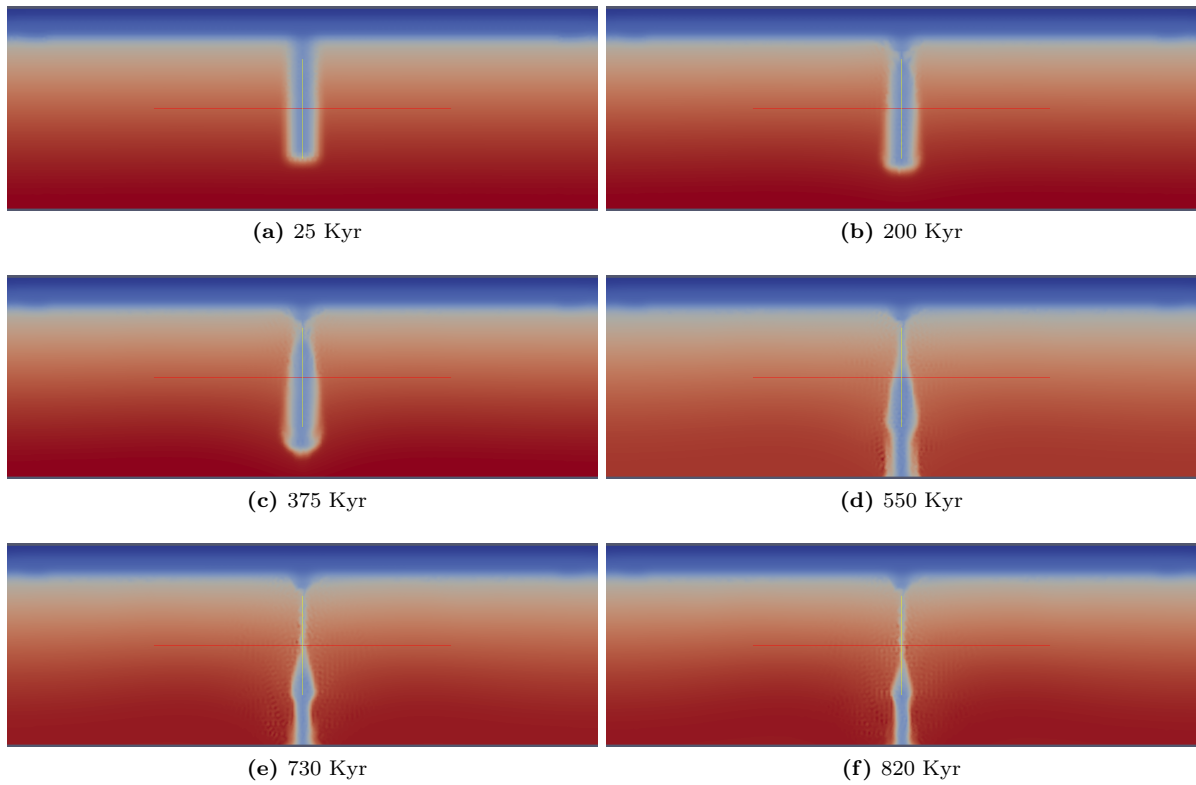
Figure A.11: Temperature field, model 4

(a) 200 Kyr   **(b)** 375 Kyr   **(c)** 640 Kyr   **(d)** 825 Kyr

Figure A.12: Temperature contours for 873 K (blue) and 1073 K (red) depicting the slab detachment in detail, model 4
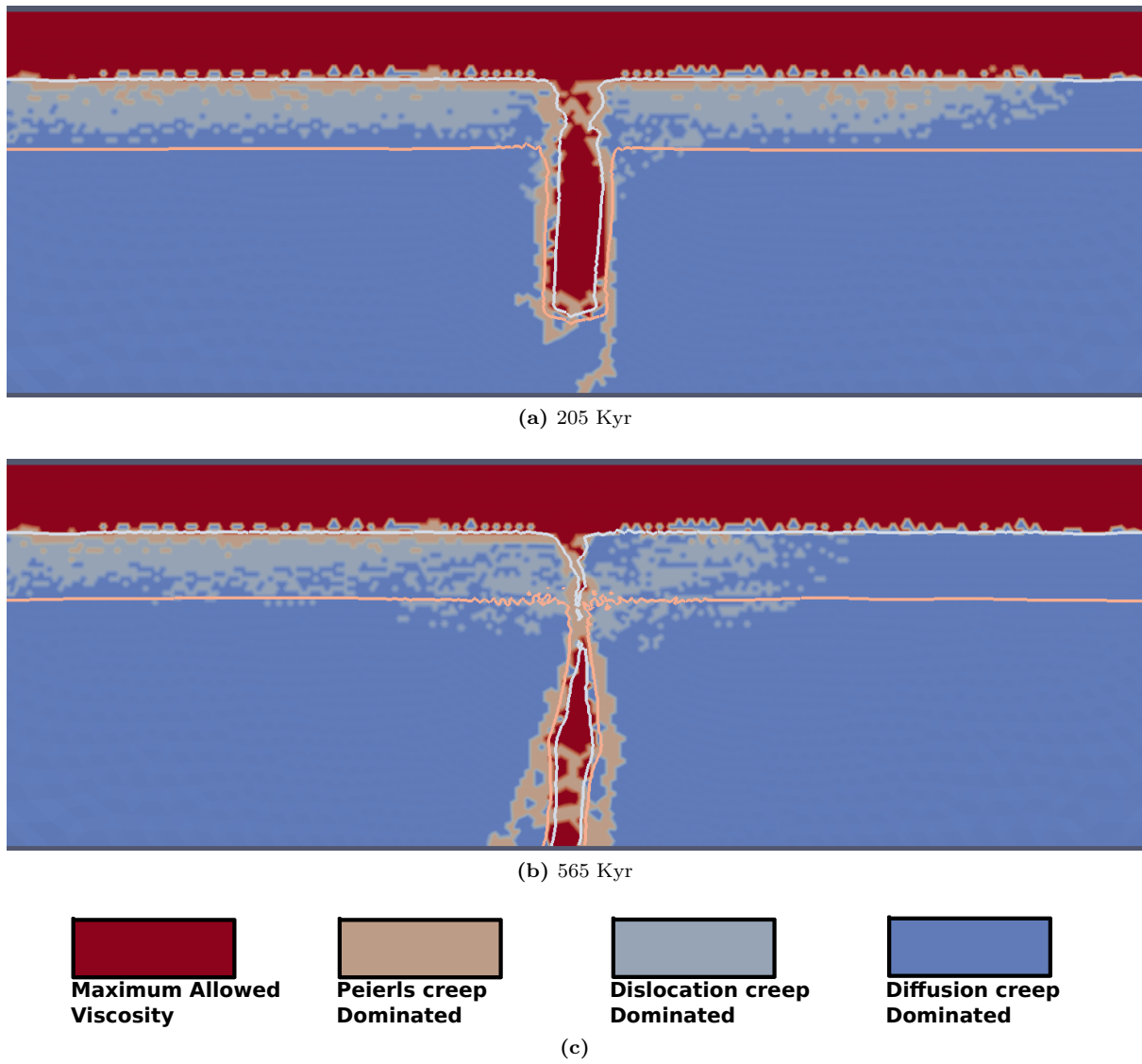

(a) 25 Kyr

(b) 200 Kyr

(c) 375 Kyr

(d) 550 Kyr

(e) 730 Kyr

(f) 820 Kyr

(g)

Figure A.13: Viscosity field, model 4

(a) 25 Kyr

(b) 200 Kyr

(c) 375 Kyr

(d) 550 Kyr

(e) 730 Kyr

(f) 820 Kyr

Velocity magnitude (m/y)

0   3.5
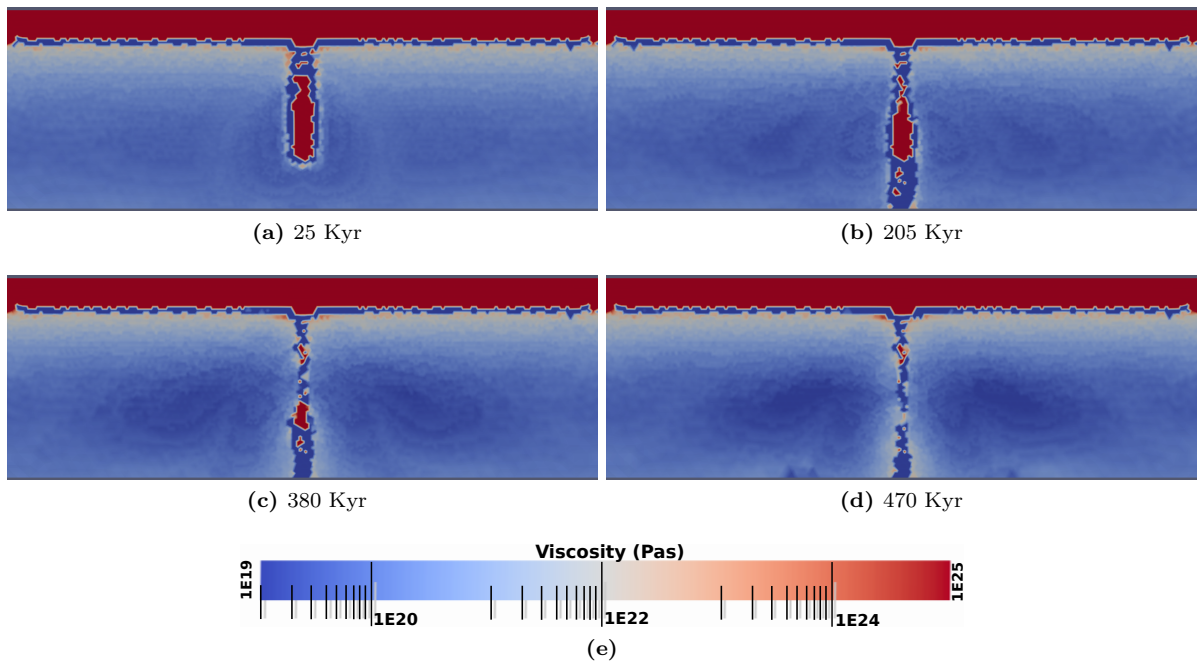
1   2   3

(g)

Figure A.14: Velocity magnitude, model 4. White line is the 1073 K isotherm.
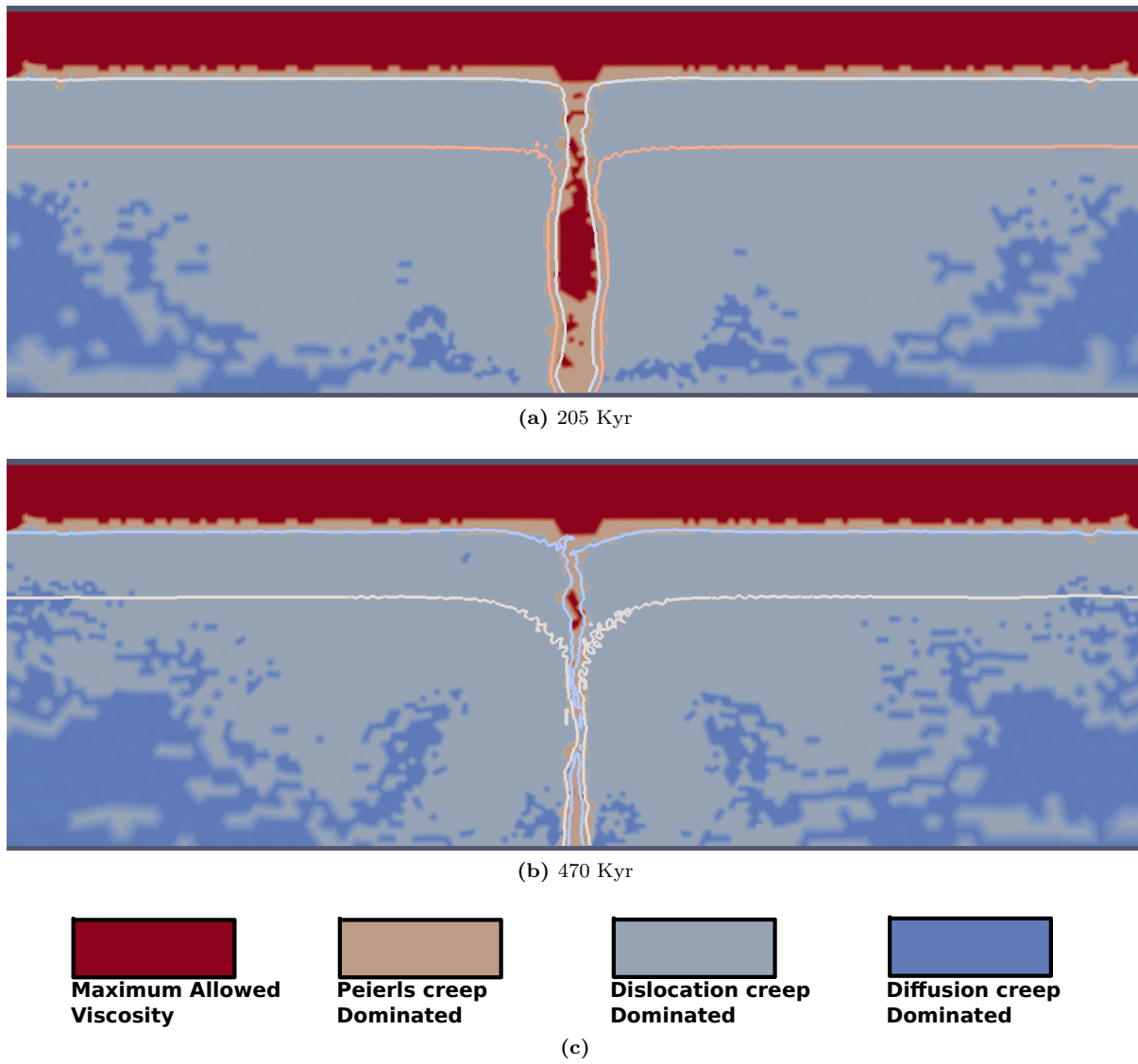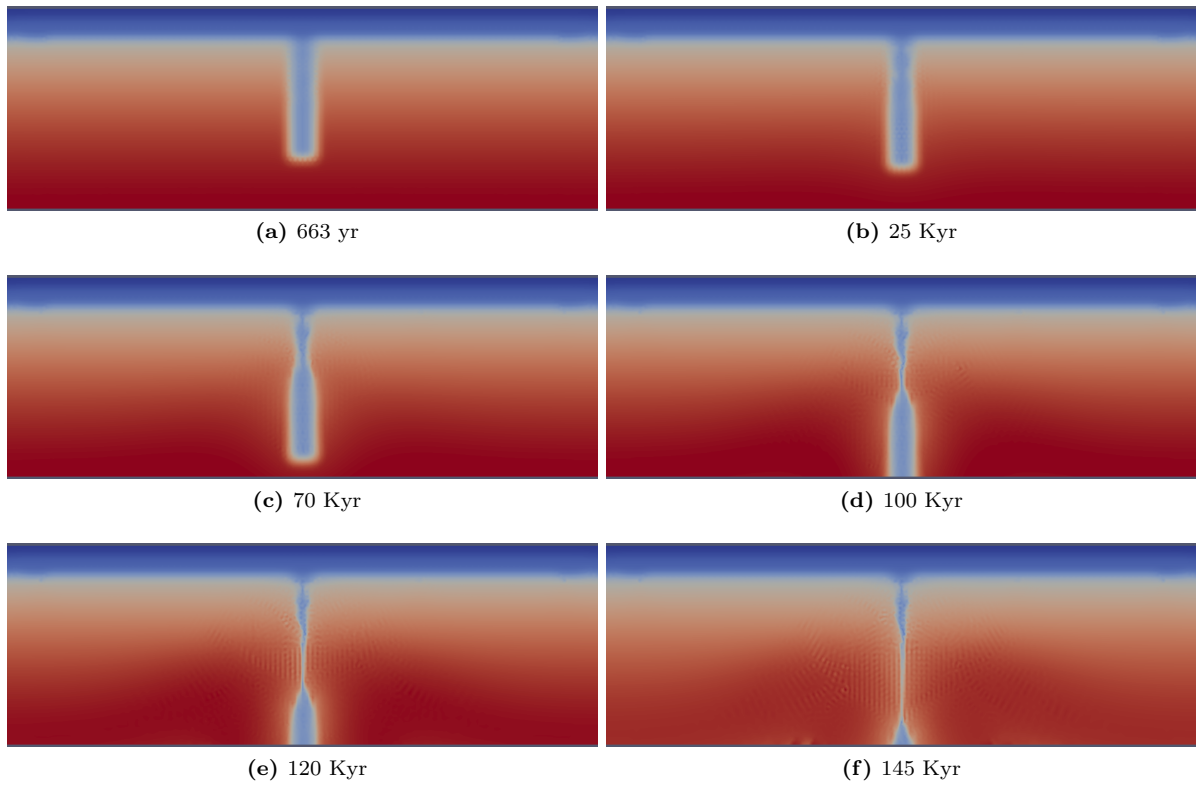
(a) 200 Kyr

(b) 550 Kyr

(c)

Figure A.15: These plots denote whether diffusion-, dislocation- or Peierls creep dominates rheology in model 4. Isotherms are also plotted for 1073 K and 1473 K.

A.4 Appendix A4 (Model 5)

(a) 25 Kyr

(b) 205 Kyr

(c) 385 Kyr

(d) 565 Kyr

(e) 745 Kyr

(f) 835 Kyr
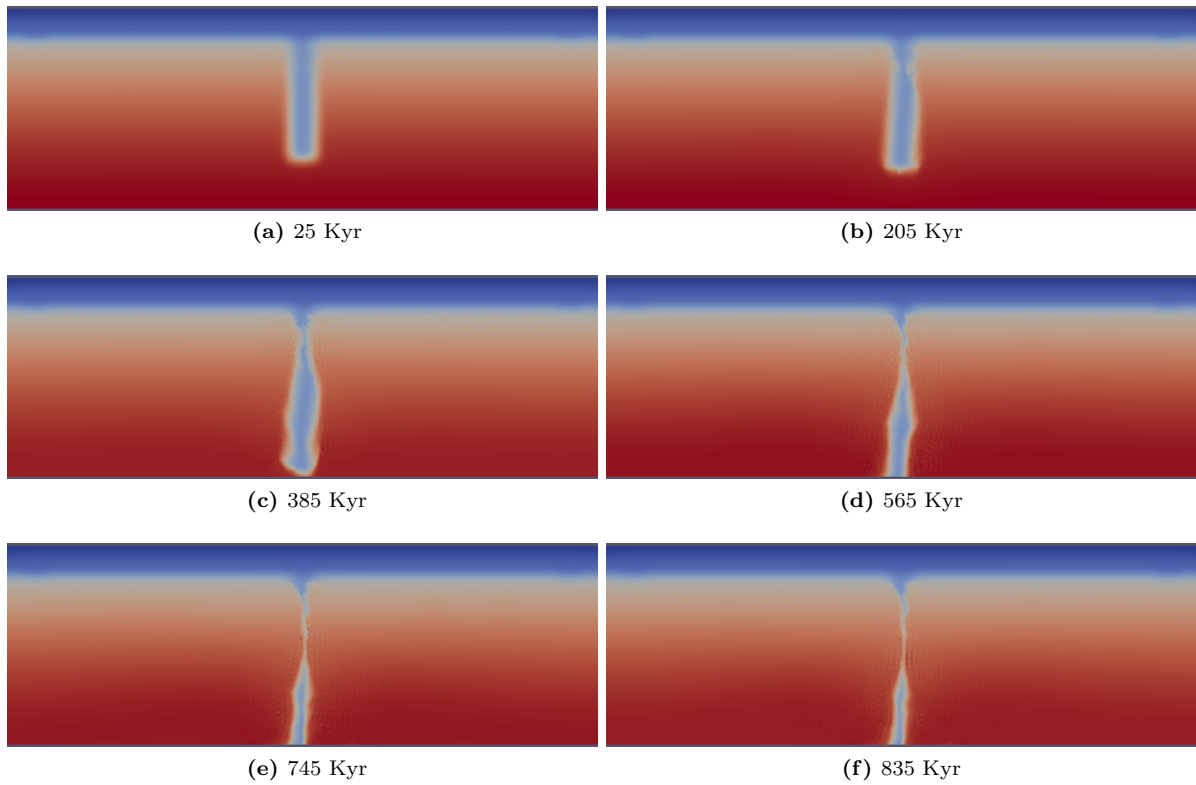
Figure A.16: Temperature field, model 5

(a) 250 Kyr   **(b)** 385 Kyr   **(c)** 520 Kyr   **(d)** 700 Kyr

Figure A.17: Temperature contours for 873 K (blue) and 1073 K (red) depicting the slab detachment in detail, model 5

(a) 25 Kyr

(b) 205 Kyr

(c) 385 Kyr

(d) 565 Kyr

(e) 745 Kyr

(f) 835 Kyr

(g)

Figure A.18: Viscosity field, model 5

(a) 25 Kyr

(b) 205 Kyr

(c) 385 Kyr

(d) 565 Kyr

(e) 745 Kyr

(f) 835 Kyr

Velocity magnitude (m/y)

0   3.3

1   2   3

(g)
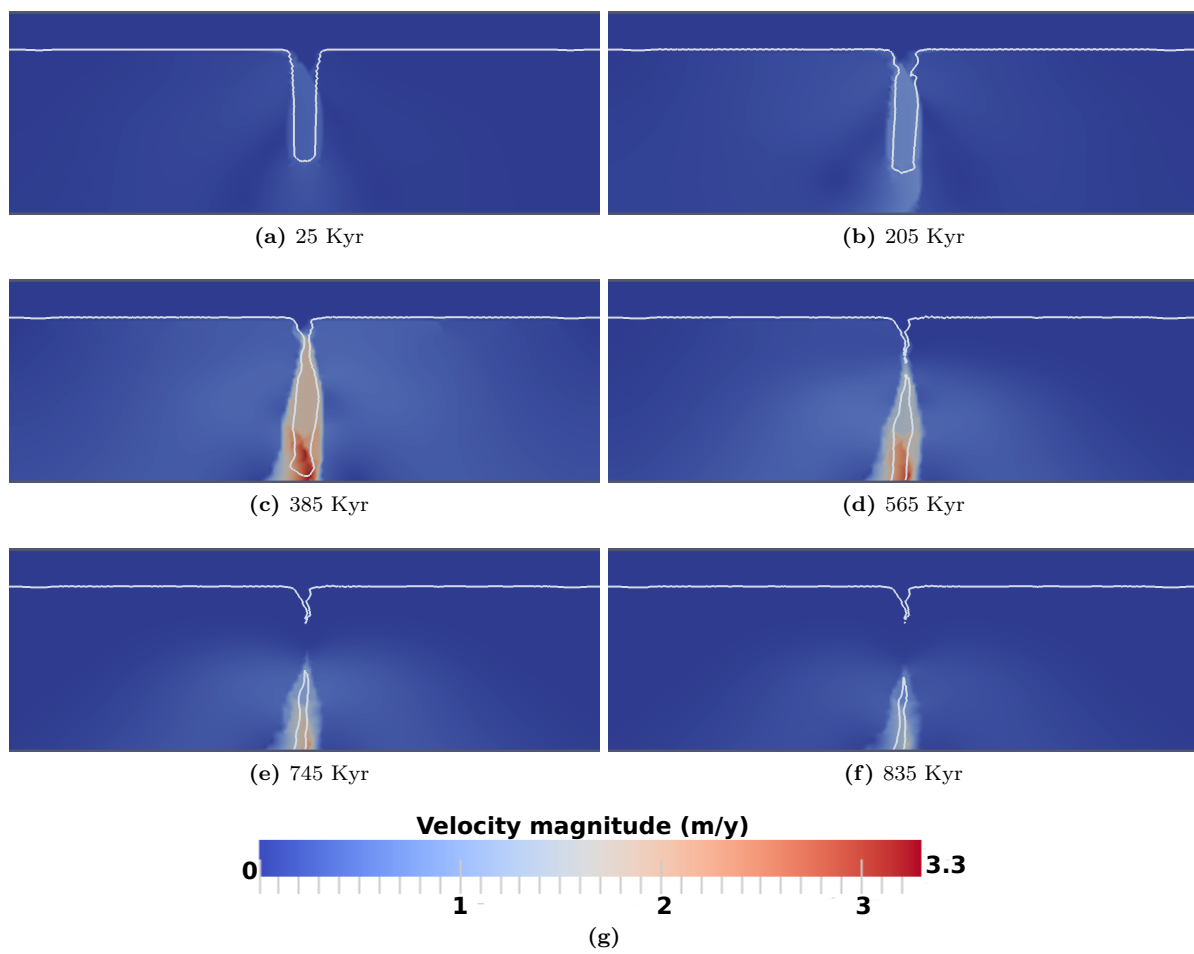
Figure A.19: Velocity magnitude, model 5. White line is the 1073 K isotherm.

(a) 205 Kyr

(b) 565 Kyr

Maximum Allowed Viscosity **Peierls creep Dominated** **Dislocation creep Dominated** **Diffusion creep Dominated**

(c)

Figure A.20: These plots denote whether diffusion-, dislocation- or Peierls creep dominates rheology in model 5. Isotherms are also plotted for 1073 K and 1473 K.

Appendix B

Models 10 and 11

B.1 Appendix B1 (Model 10)

(a) 25 Kyr

(b) 205 Kyr

(c) 380 Kyr

(d) 470 Kyr
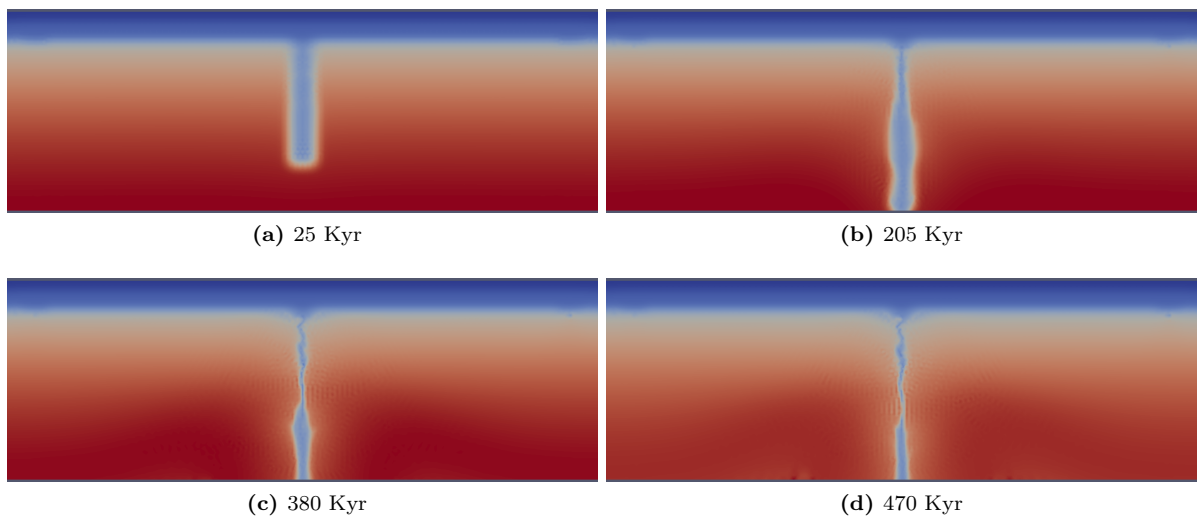
Figure B.1: Temperature field, model 10

(a) 248 Kyr

(b) 380 Kyr

(c) 560 Kyr

(d) 645 Kyr
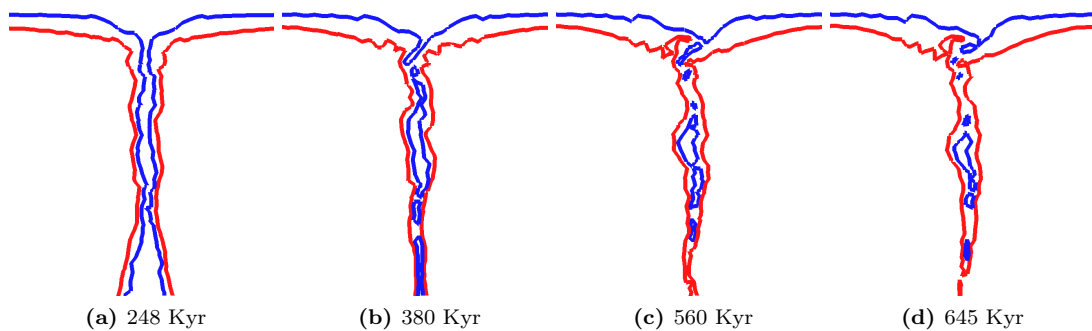
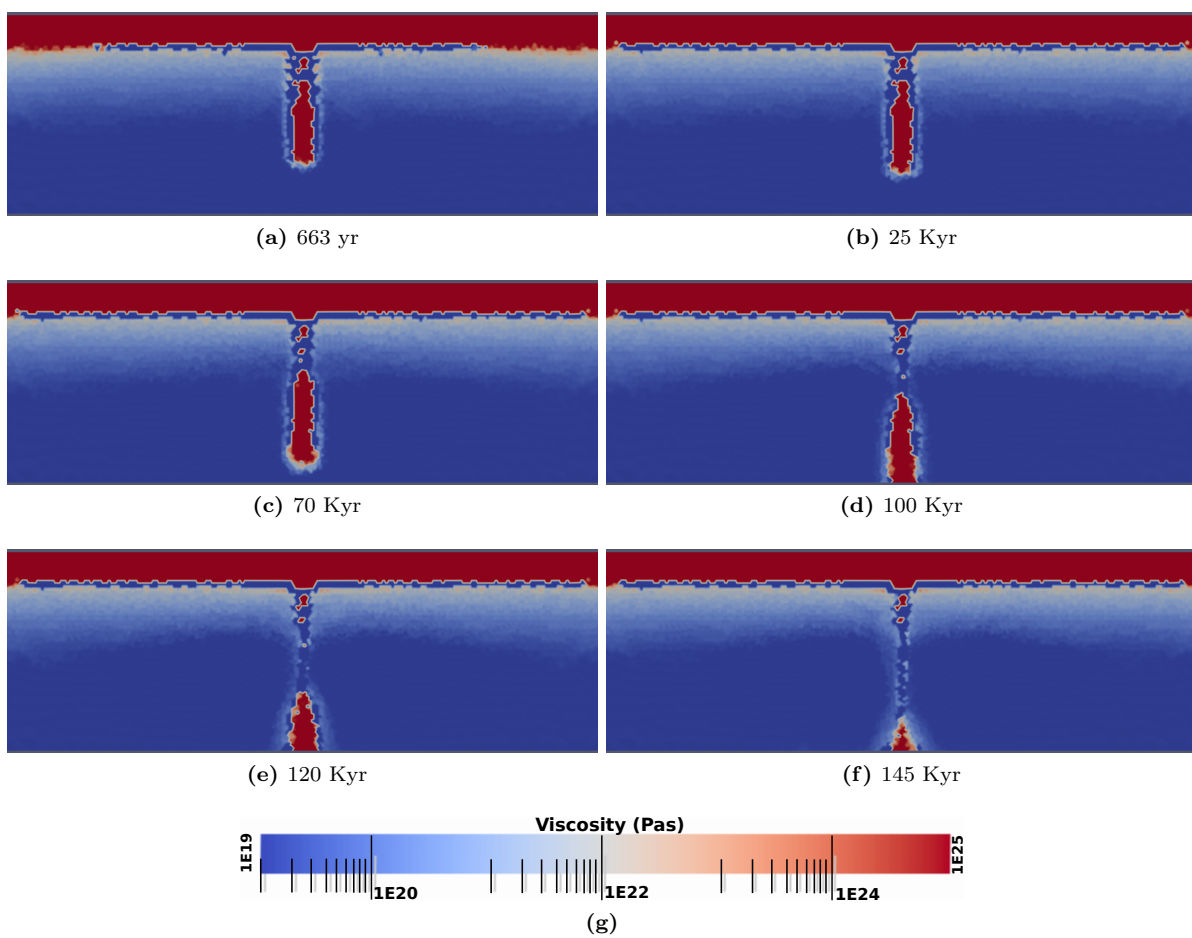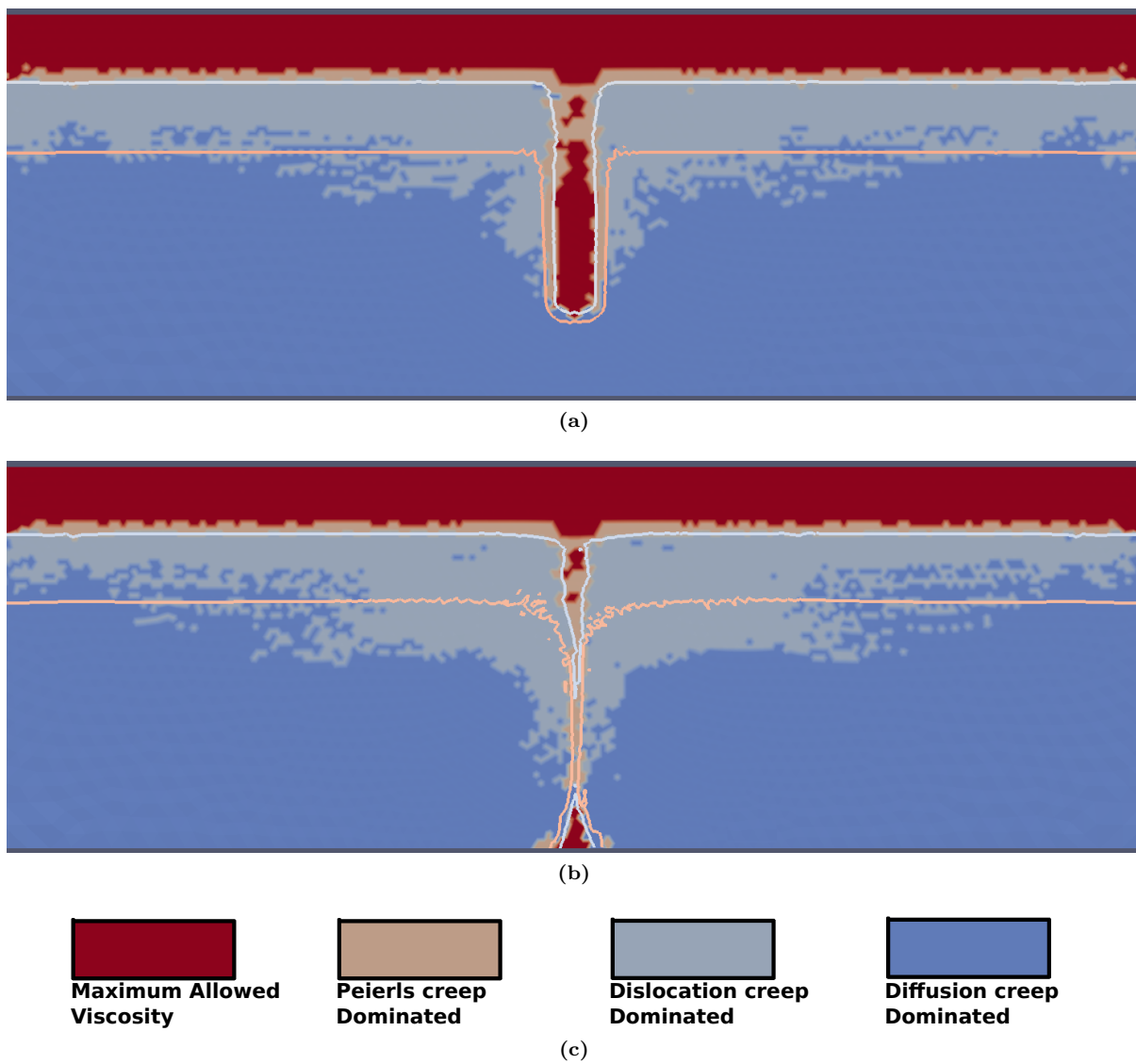**Figure B.2:** Temperature contours for 873 K (blue) and 1073 K (red) depicting the slab detachment in detail, model 10

(a) 25 Kyr

(b) 205 Kyr

(c) 380 Kyr

(d) 470 Kyr

(e)

Figure B.3: Viscosity field, model 10

(a) 25 Kyr

(b) 205 Kyr

(c) 380 Kyr

(d) 470 Kyr

Velocity magnitude (m/y)

0   1   2   3   3.5

(e)
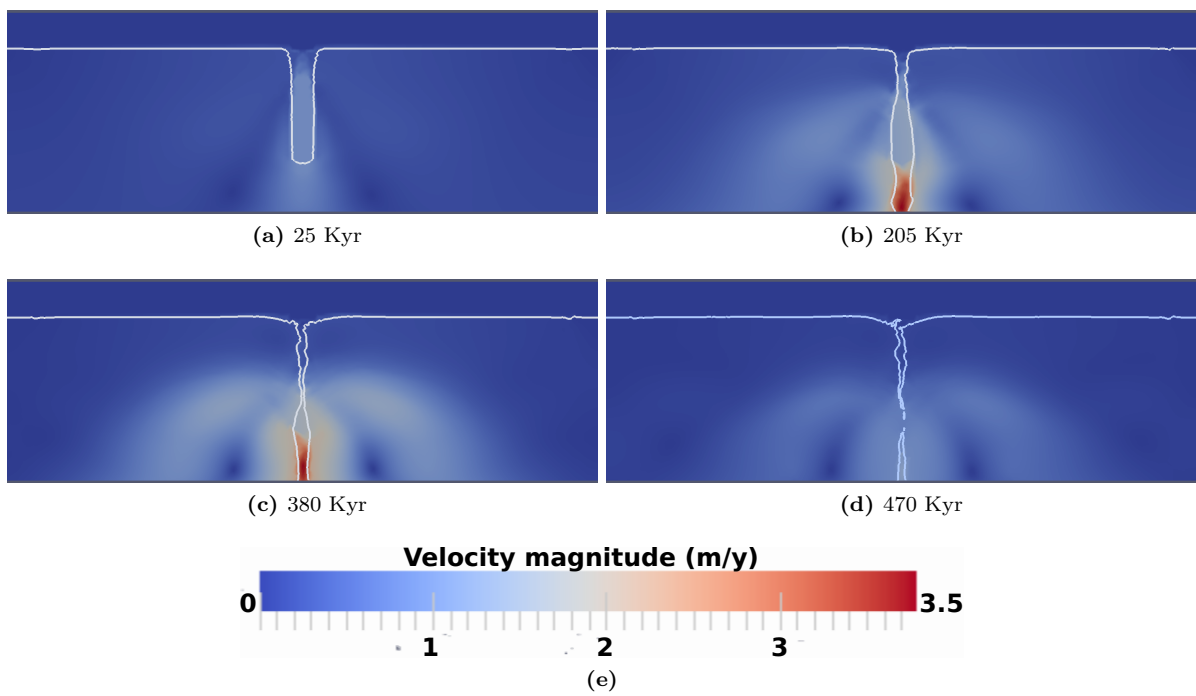
Figure B.4: Velocity magnitude, model 10. White line is the 1073 K isotherm.

(a) 205 Kyr

(b) 470 Kyr

| Maximum Allowed Viscosity | Peierls creep Dominated | Dislocation creep Dominated | Diffusion creep Dominated |

(c)

Figure B.5: These plots denote whether diffusion-, dislocation- or Peierls creep dominates rheology in model 10. Isotherms are also plotted for 1073 K and 1473 K.

B.2 Appendix B2 (Model 11)

(a) 663 yr

(b) 25 Kyr

(c) 70 Kyr

(d) 100 Kyr

(e) 120 Kyr

(f) 145 Kyr

Figure B.6: Temperature field, model 11

(a) 25 Kyr **(b)** 100 Kyr **(c)** 145 Kyr **(d)** 220 Kyr
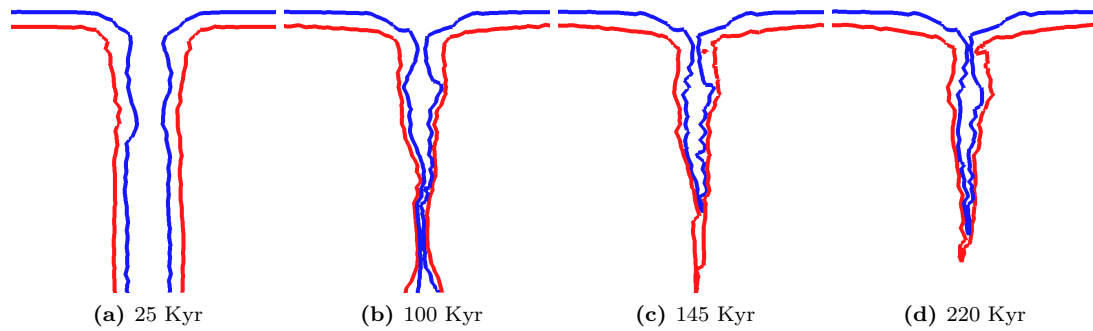
Figure B.7: Temperature contours for 873 K (blue) and 1073 K (red) depicting the slab detachment in detail, model 11

(a) 663 yr **(b)** 25 Kyr
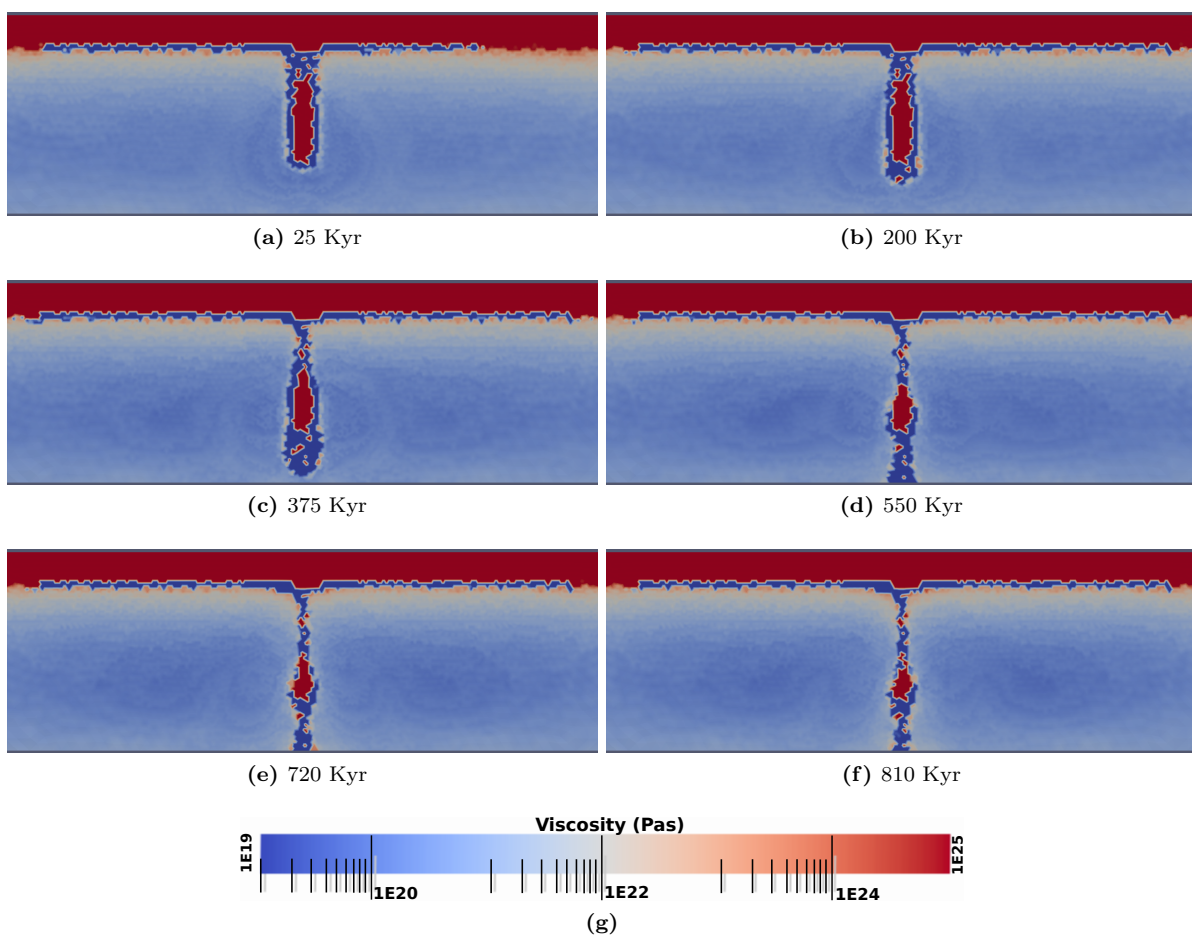
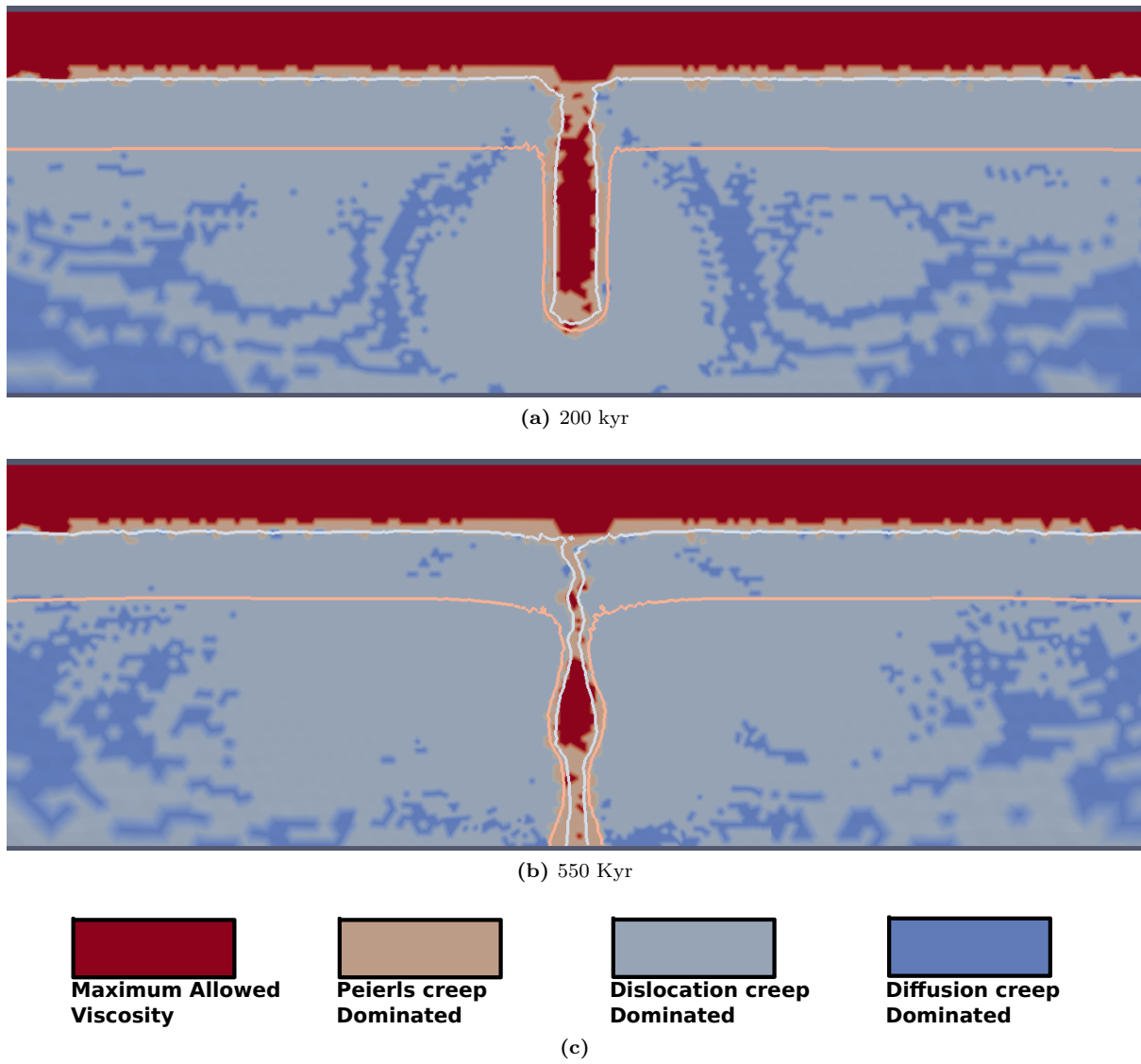**(c)** 70 Kyr **(d)** 100 Kyr

(e) 120 Kyr **(f)** 145 Kyr

(g)

Figure B.8: Viscosity field, model 11

(a) 25 Kyr   **(b)** 145 Kyr

(c)
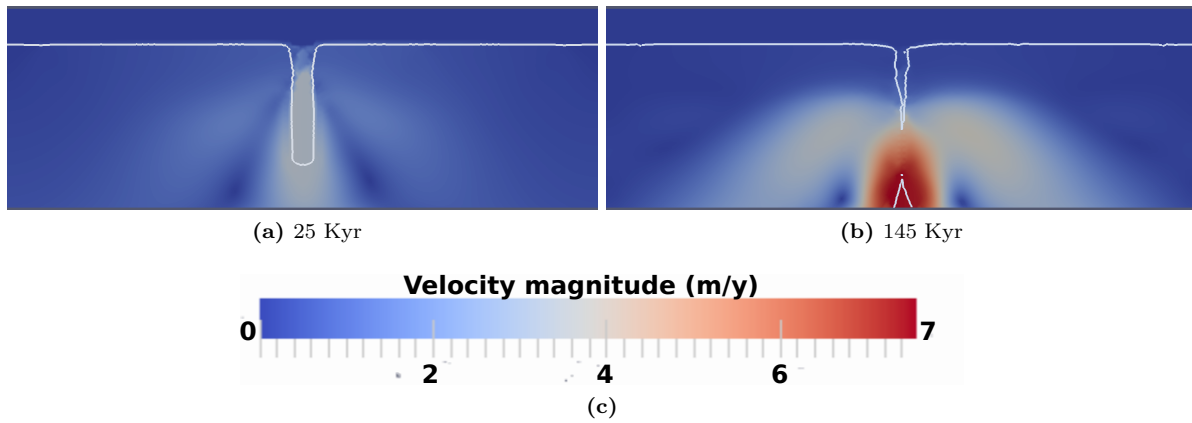
Figure B.9: Velocity magnitude, model 11. White line is the 1073 K isotherm.

(a)

(b)

Maximum Allowed Viscosity   **Peierls creep Dominated**   **Dislocation creep Dominated**   **Diffusion creep Dominated**

(c)

Figure B.10: These plots denote whether diffusion-, dislocation- or Peierls creep dominates rheology in model 11. Isotherms are also plottedfor 1073 K and 1473 K.

Appendix C

Models 12 and 14

C.1 Appendix C1 (Model 12)

(a) 25 Kyr

(b) 200 Kyr

(c) 375 Kyr

(d) 550 Kyr

(e) 720 Kyr

(f) 810 Kyr
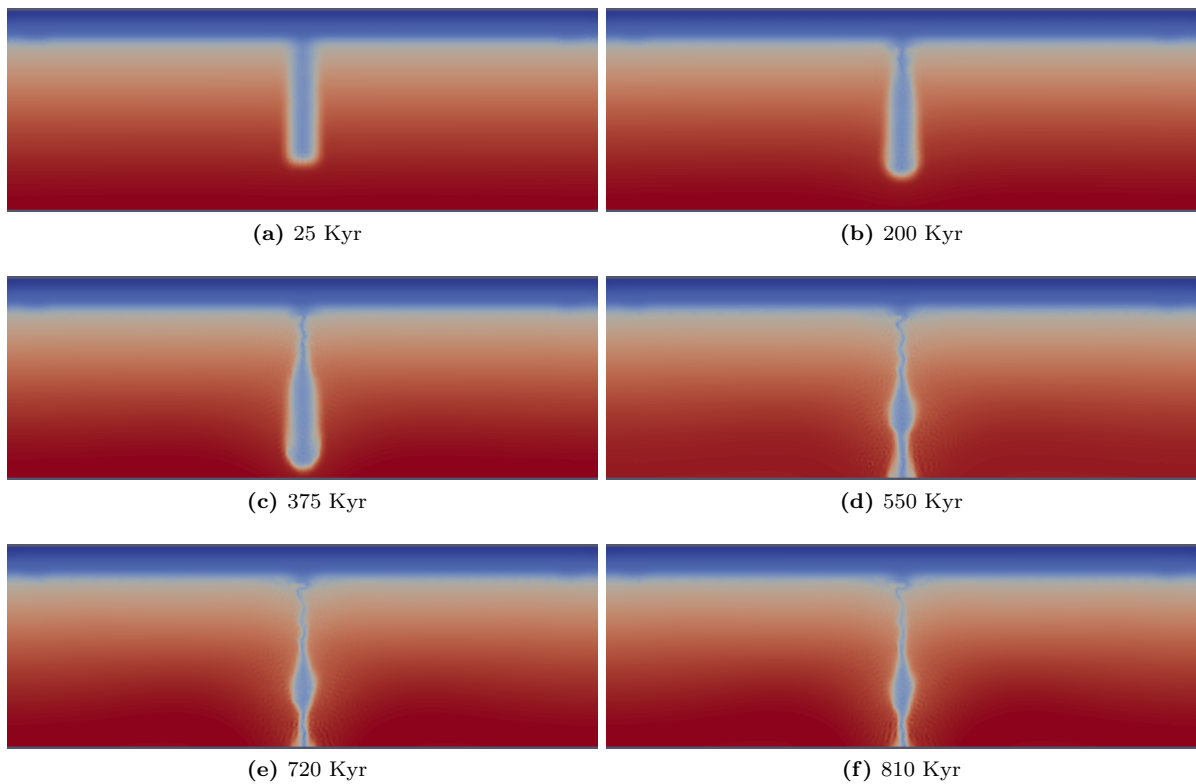
Figure C.1: Temperature field, model 12
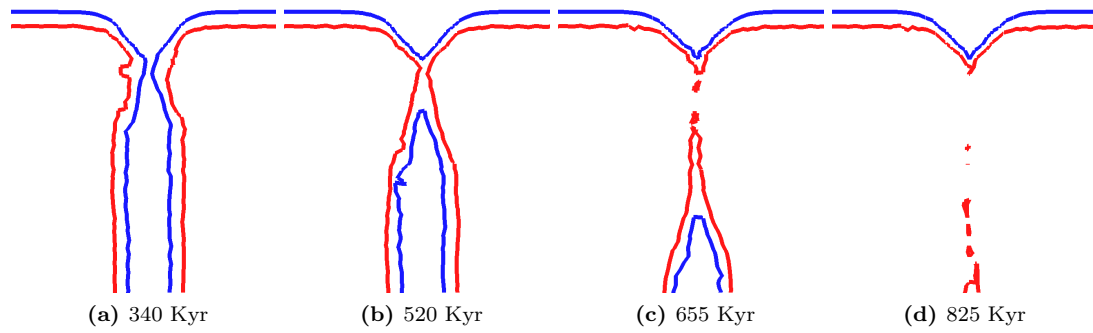
(a) 330 Kyr   **(b)** 460 Kyr   **(c)** 590 Kyr   **(d)** 810 Kyr
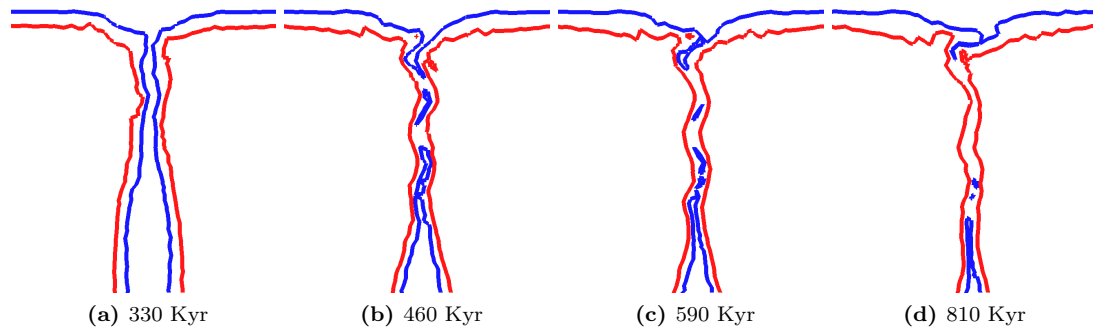
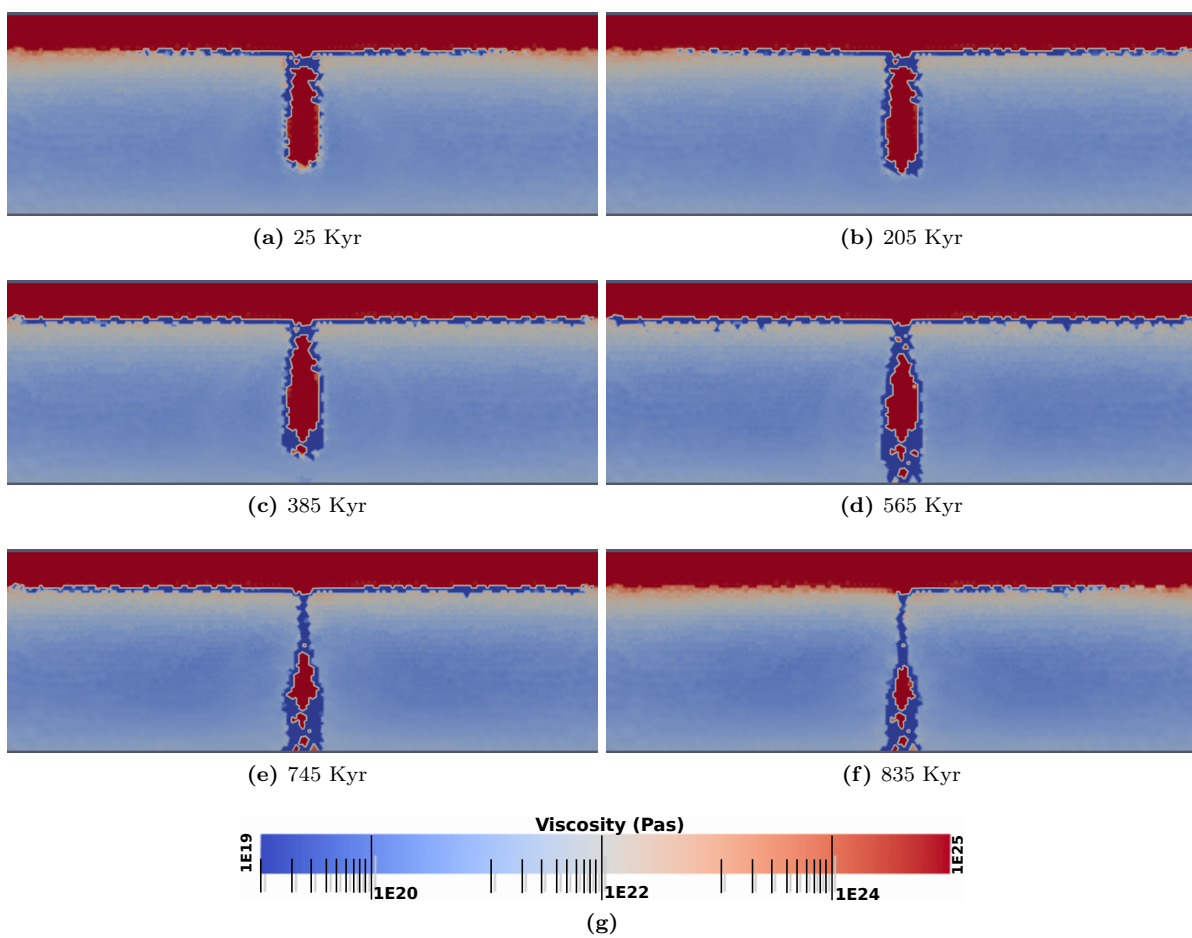**Figure C.2:** Temperature contours for 873 K (blue) and 1073 K (red) depicting the slab detachment in detail, model 12

(a) 25 Kyr   **(b)** 200 Kyr

(c) 375 Kyr   **(d)** 550 Kyr

(e) 720 Kyr   **(f)** 810 Kyr

(g)

Figure C.3: Viscosity field, model 12

(a) 25 Kyr

(b) 200 Kyr

(c) 375 Kyr

(d) 550 Kyr

(e) 720 Kyr

(f) 810 Kyr

Velocity magnitude (m/y)

0   0.4   0.8   1.2   1.5

(g)
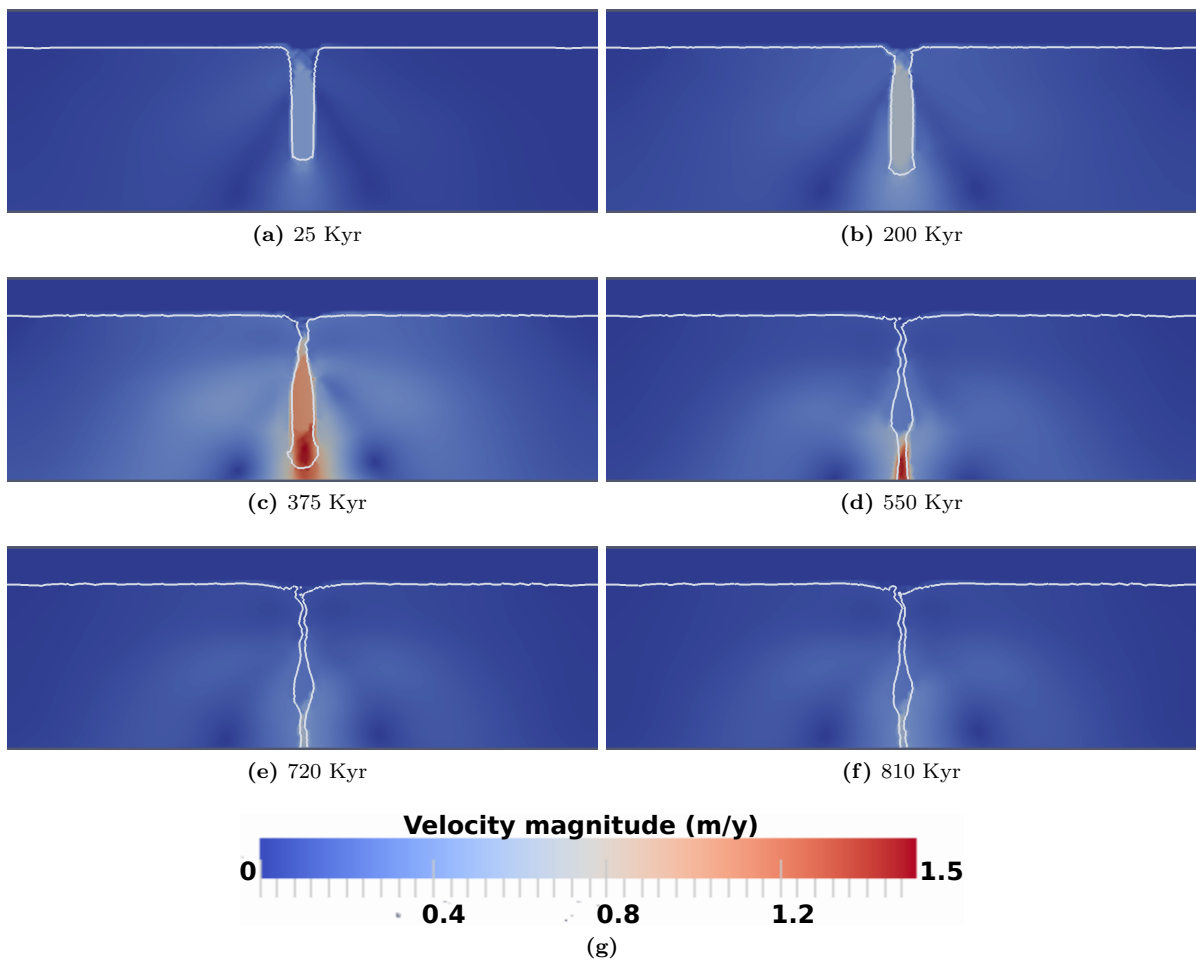
Figure C.4: Velocity magnitude, model 12. White line is the 1073 K isotherm.

(a) 200 kyr

(b) 550 Kyr

Maximum Allowed
Viscosity

Peierls creep
Dominated

Dislocation creep
Dominated

Diffusion creep
Dominated

(c)

Figure C.5: These plots denote whether diffusion-, dislocation- or Peierls creep dominates rheology in model 12. Isotherms are also plotted for 1073 K and 1473 K.

C.2 Appendix C2 (Model 14)

(a) 25 Kyr

(b) 205 Kyr

(c) 385 Kyr

(d) 565 Kyr

(e) 745 Kyr

(f) 835 Kyr
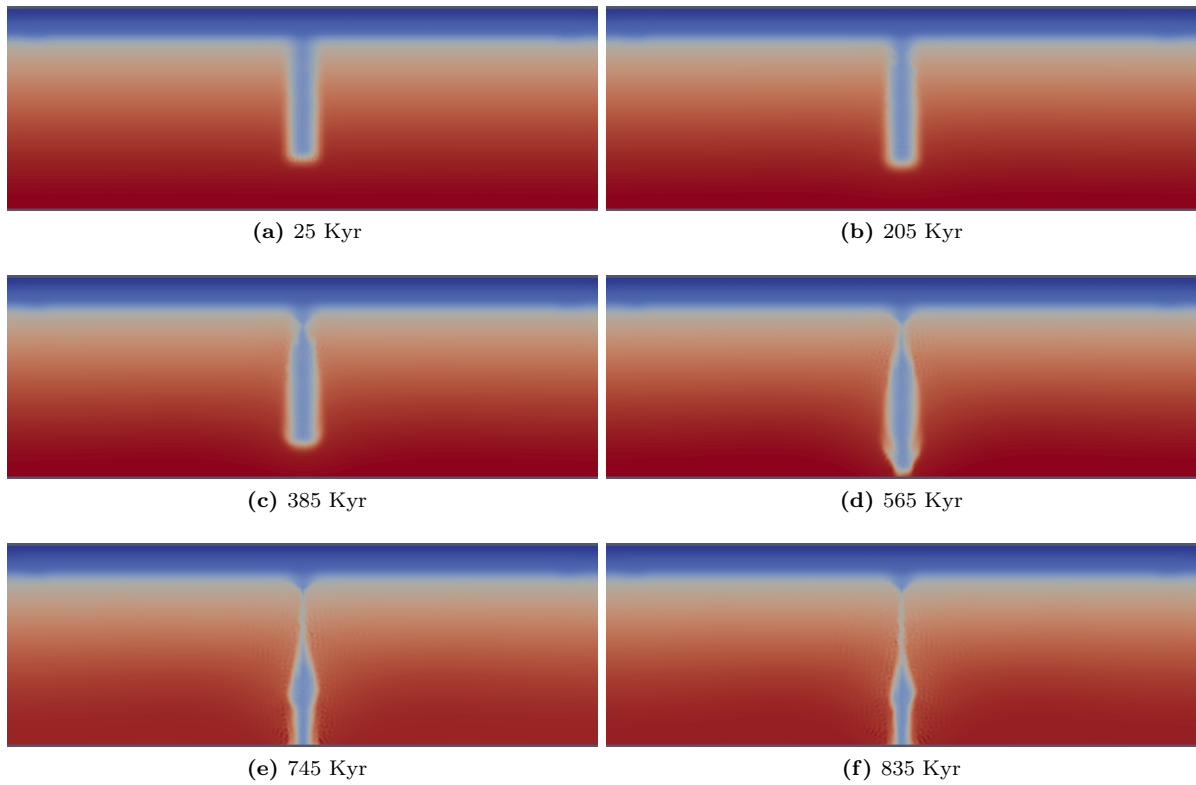
Figure C.6: Temperature field, model 14

(a) 340 Kyr   **(b)** 520 Kyr   **(c)** 655 Kyr   **(d)** 825 Kyr

Figure C.7: Temperature contours for 873 K (blue) and 1073 K (red) depicting the slab detachment in detail, model 14

(a) 25 Kyr   **(b)** 205 Kyr

(c) 385 Kyr   **(d)** 565 Kyr

(e) 745 Kyr   **(f)** 835 Kyr

Viscosity (Pas)

1E19   1E20   1E22   1E24   1E25

(g)

Figure C.8: Viscosity field, model 14

(a) 25 Kyr

(b) 205 Kyr

(c) 385 Kyr

(d) 565 Kyr

(e) 745 Kyr

(f) 835 Kyr

(g)
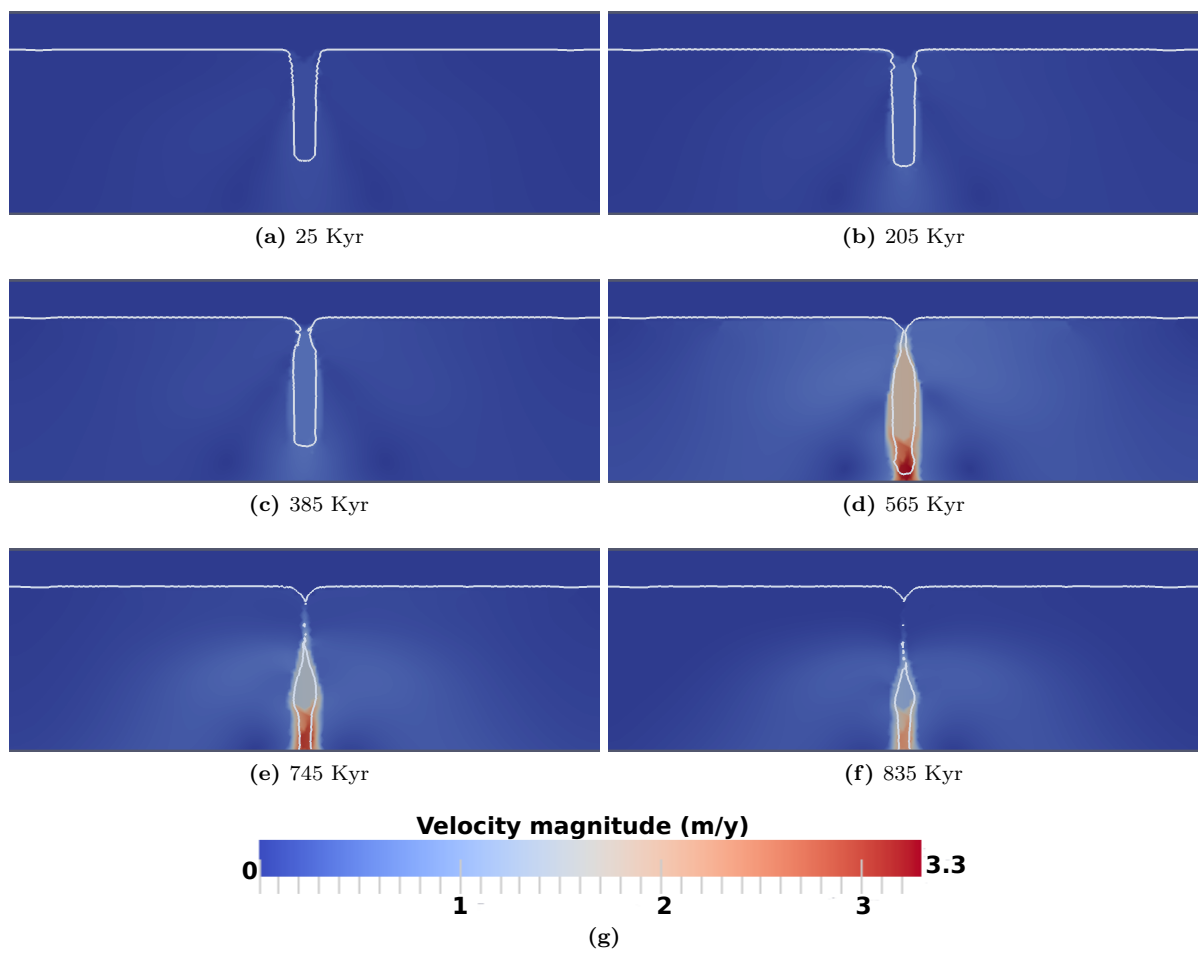
Figure C.9: Velocity magnitude, model 14. White line is the 1073 K isotherm.
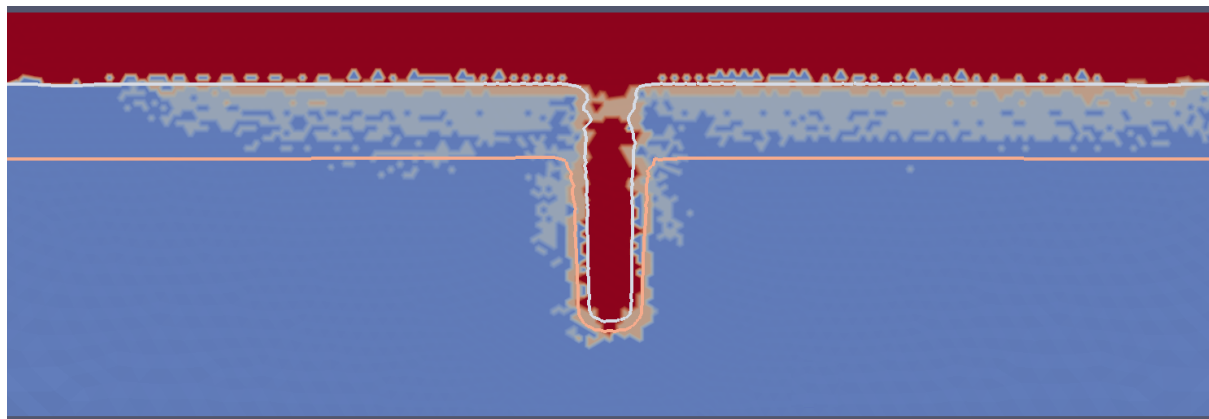
(a) 205 Kyr
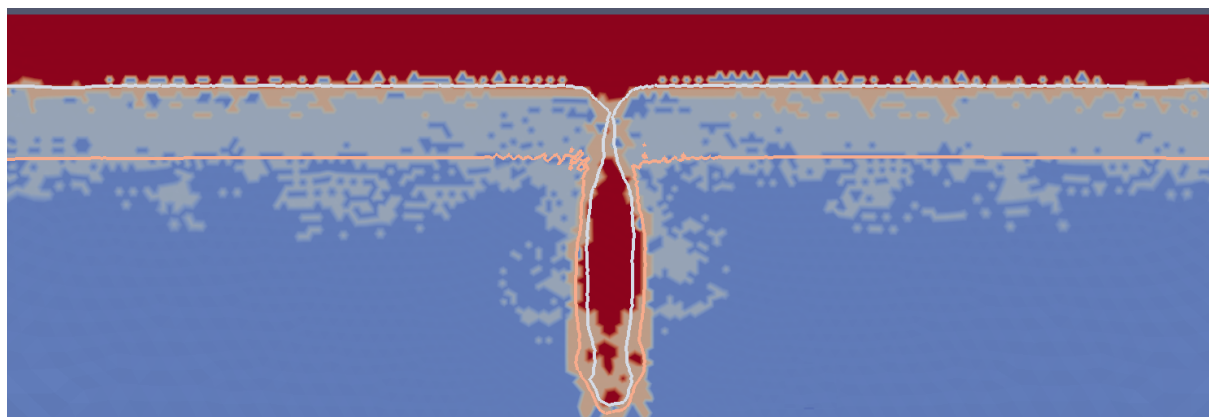
(b) 565 Kyr

(c)

Figure C.10: These plots denote whether diffusion-, dislocation- or Peierls creep dominates rheology in model 14. Isotherms are also plotted for 1073 K and 1473 K.

Appendix D
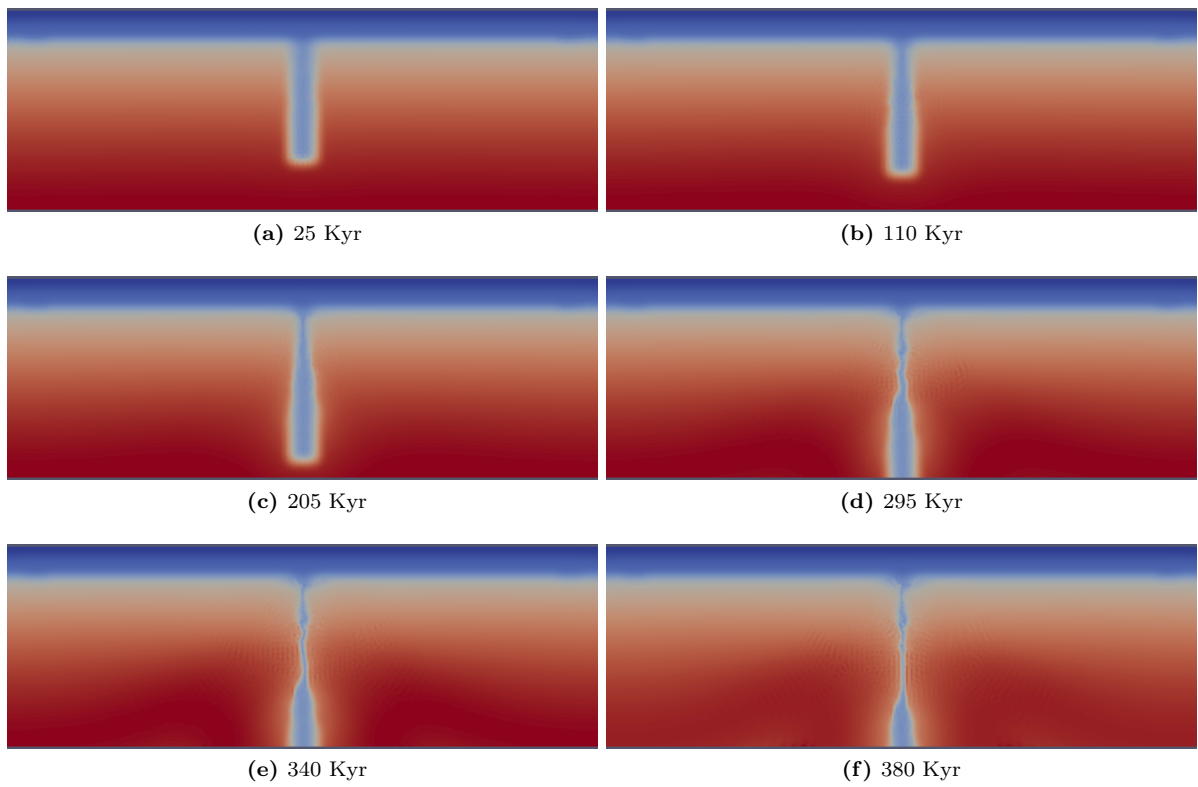
Model 9

D.1 Appendix D1 (Model 9)

(a) 25 Kyr

(b) 110 Kyr

(c) 205 Kyr

(d) 295 Kyr

(e) 340 Kyr

(f) 380 Kyr

Figure D.1: Temperature field, model 9

(a) 205 Kyr   (b) 340 Kyr   (c) 380 Kyr   (d) 430 Kyr
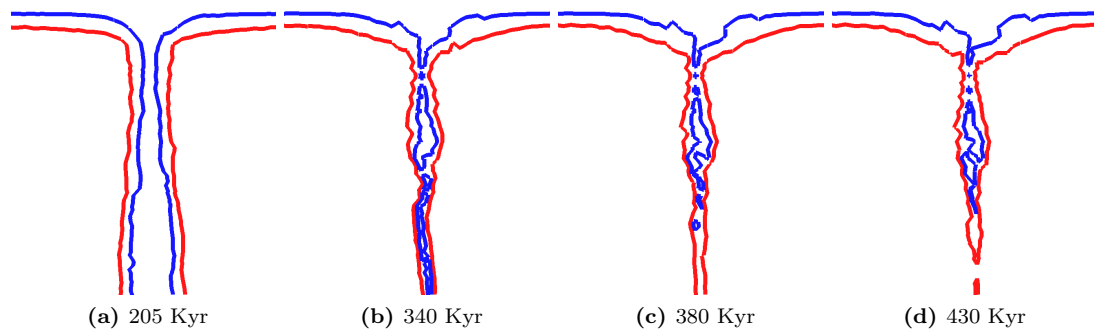
Figure D.2: Temperature contours for 873 K (blue) and 1073 K (red) depicting the slab detachment in detail, model 9
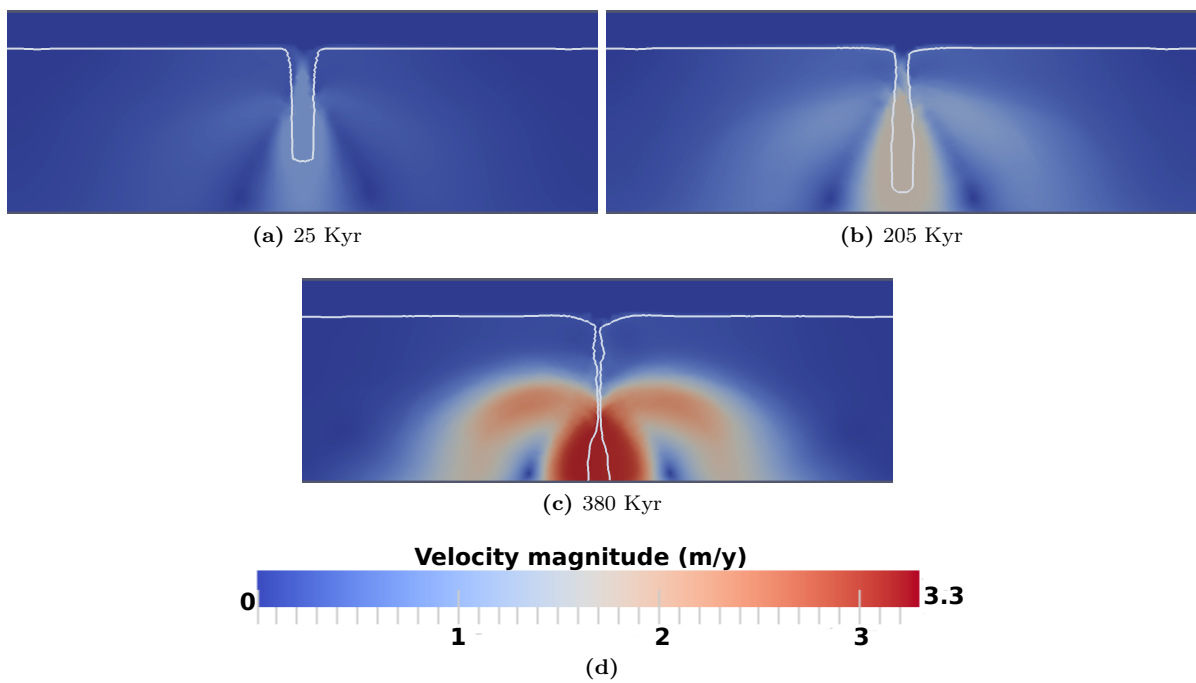

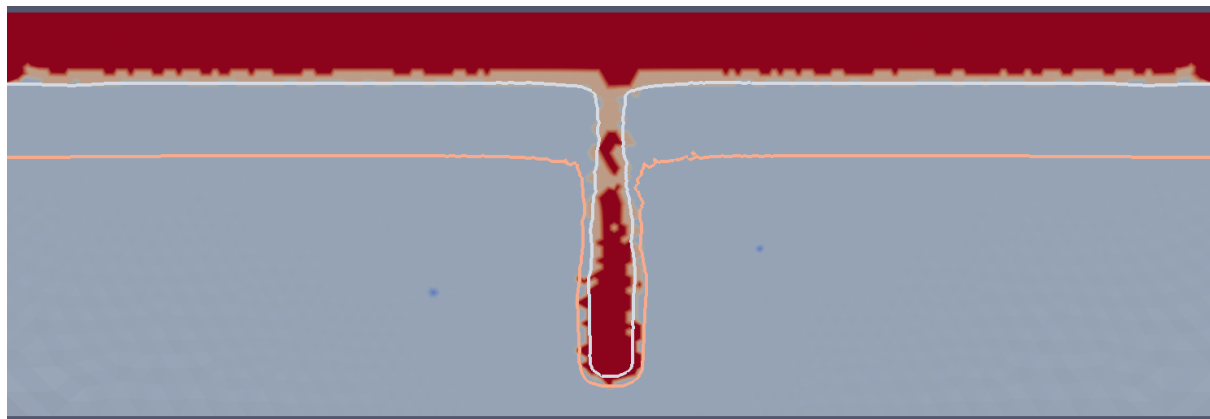(a) 25 Kyr   (b) 205 Kyr

(c) 380 Kyr

(d)
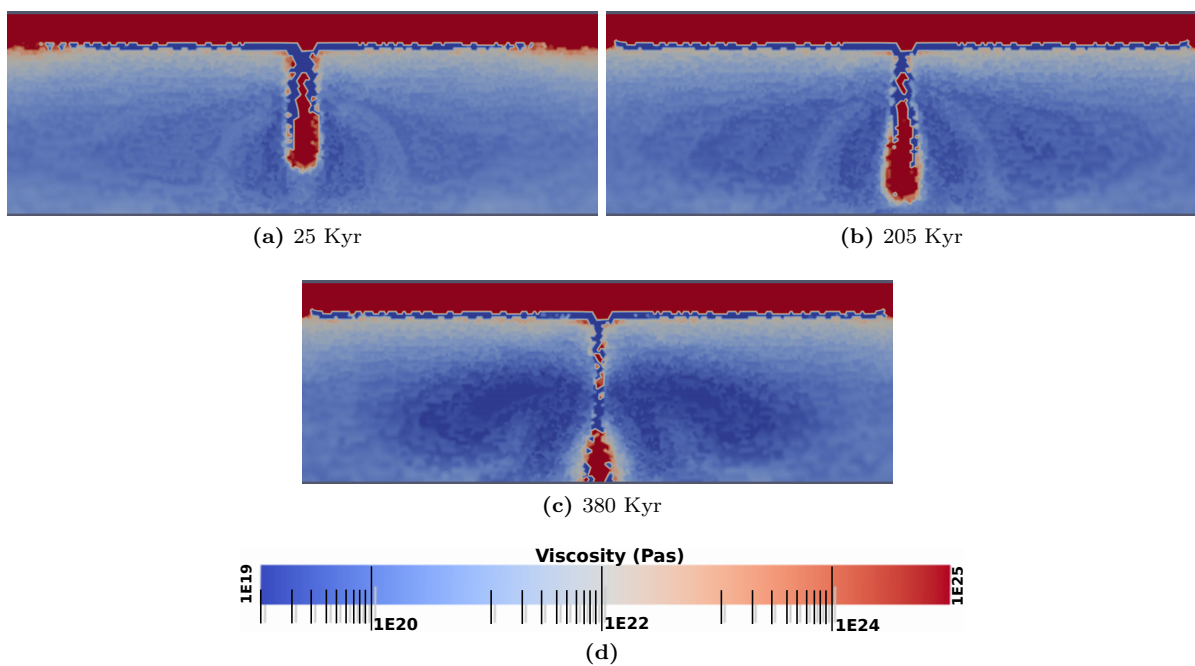
Figure D.3: Viscosity field, model 9

(a) 25 Kyr

(b) 205 Kyr

(c) 380 Kyr

(d)

Figure D.4: Velocity magnitude, model 9. White line is the 1073 K isotherm.

(a) 205 Kyr
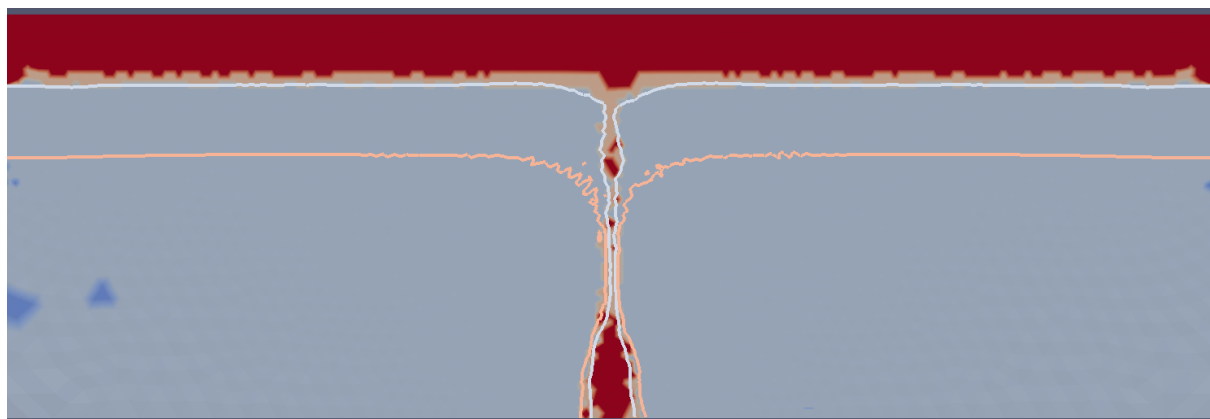
(b) 380 Kyr

(c)

Figure D.5: These plots denote whether diffusion-, dislocation- or Peierls creep dominates rheology in model 9. Isotherms are also plotted for 1073 K and 1473 K.
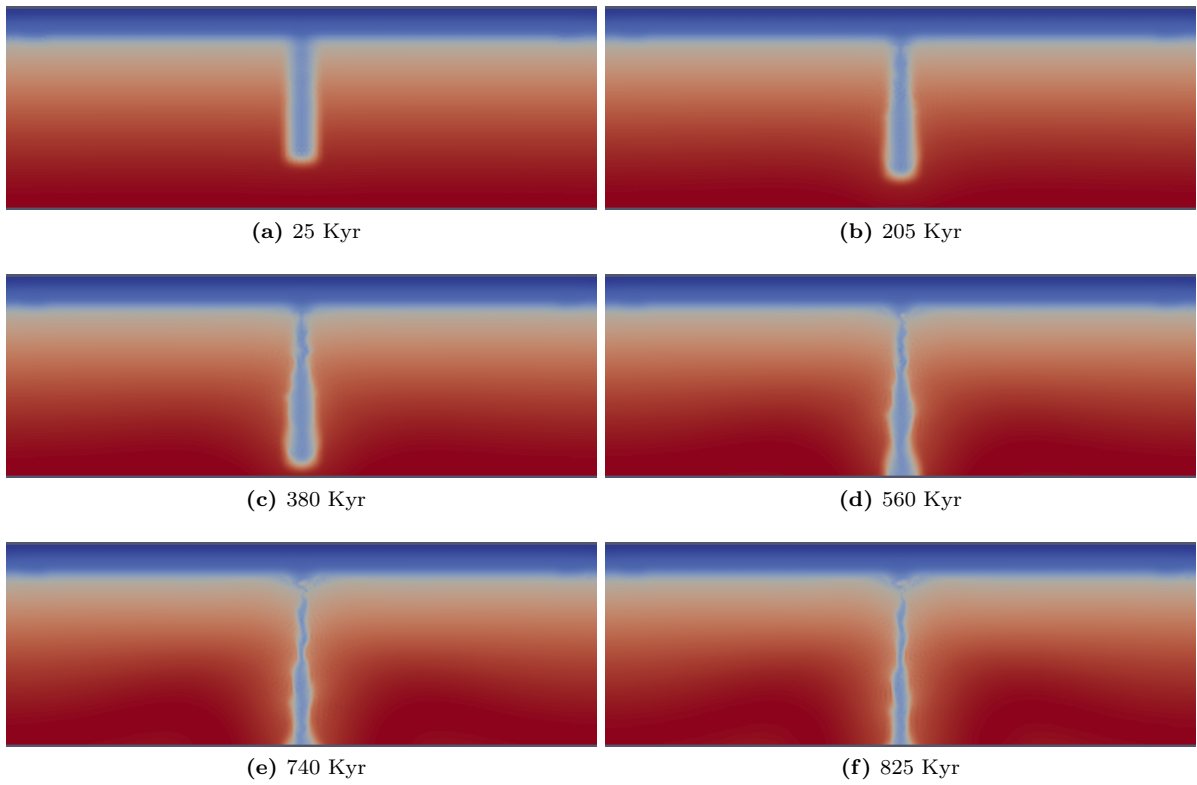
Appendix E

Model 18

E.1 Appendix E1 (Model 18)

(a) 25 Kyr

(b) 205 Kyr

(c) 380 Kyr

(d) 560 Kyr

(e) 740 Kyr

(f) 825 Kyr

Figure E.1: Temperature field, model 18
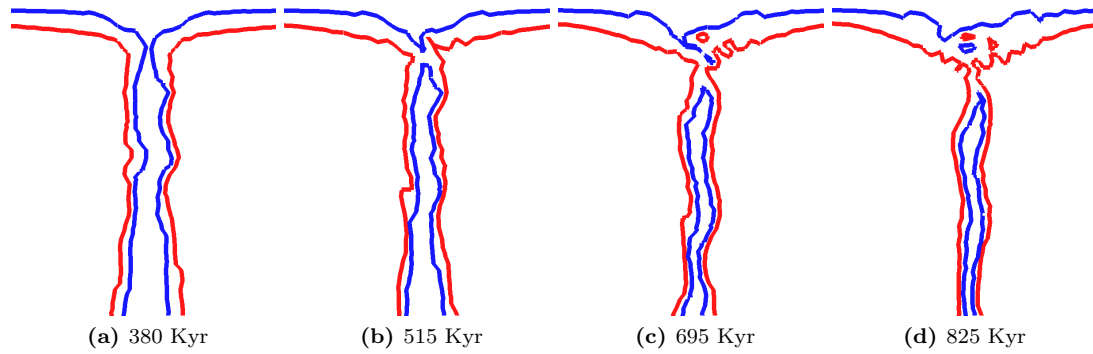
(a) 380 Kyr   **(b)** 515 Kyr   **(c)** 695 Kyr   **(d)** 825 Kyr

Figure E.2: Temperature contours for 873 K (blue) and 1073 K (red) depicting the slab detachment in detail, model 18
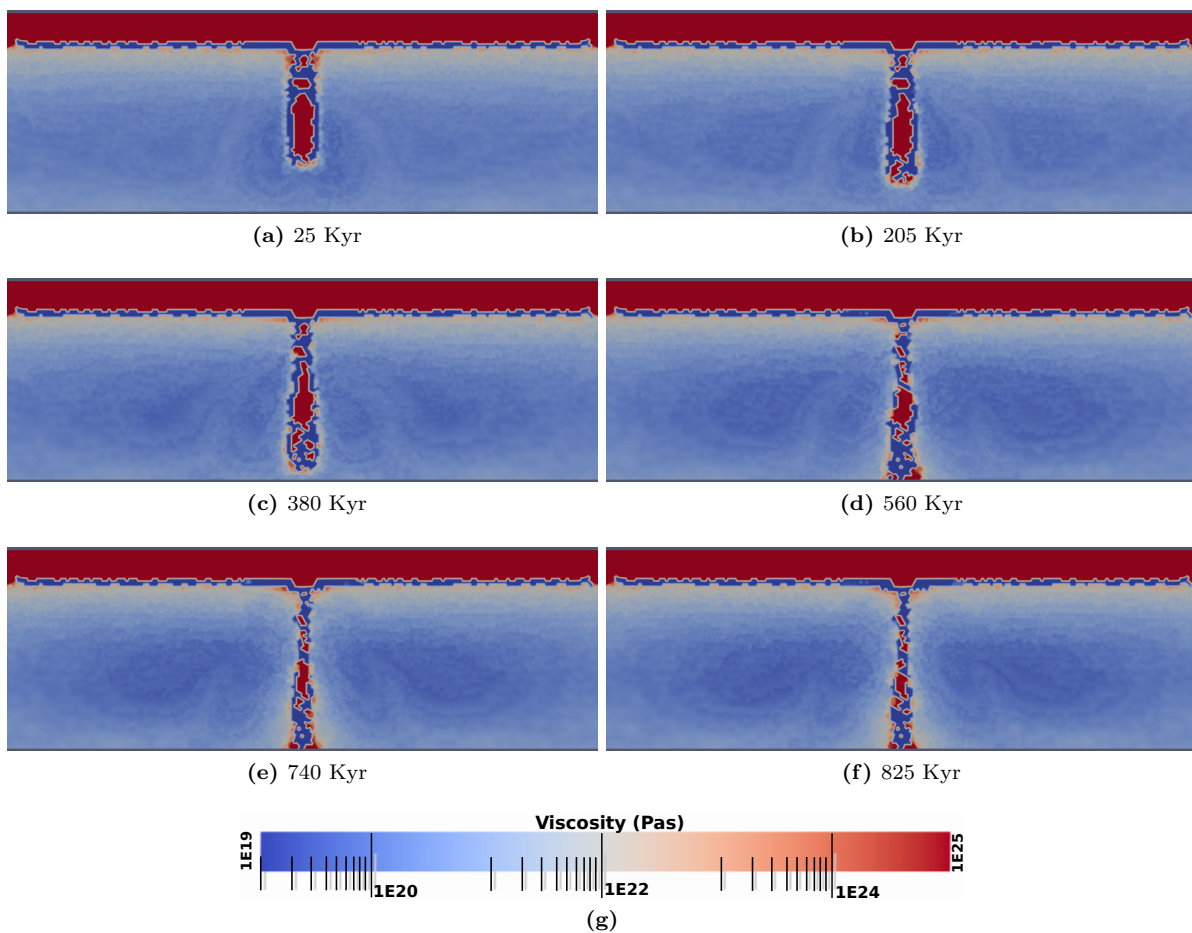

(a) 25 Kyr   **(b)** 205 Kyr

(c) 380 Kyr   **(d)** 560 Kyr

(e) 740 Kyr   **(f)** 825 Kyr

(g)

Figure E.3: Viscosity field, model 18

(a) 25 Kyr

(b) 205 Kyr

(c) 380 Kyr

(d) 560 Kyr

(e) 740 Kyr

(f) 825 Kyr

Velocity magnitude (m/y)

0 0.4 0.8 1.2 1.6 2

(g)
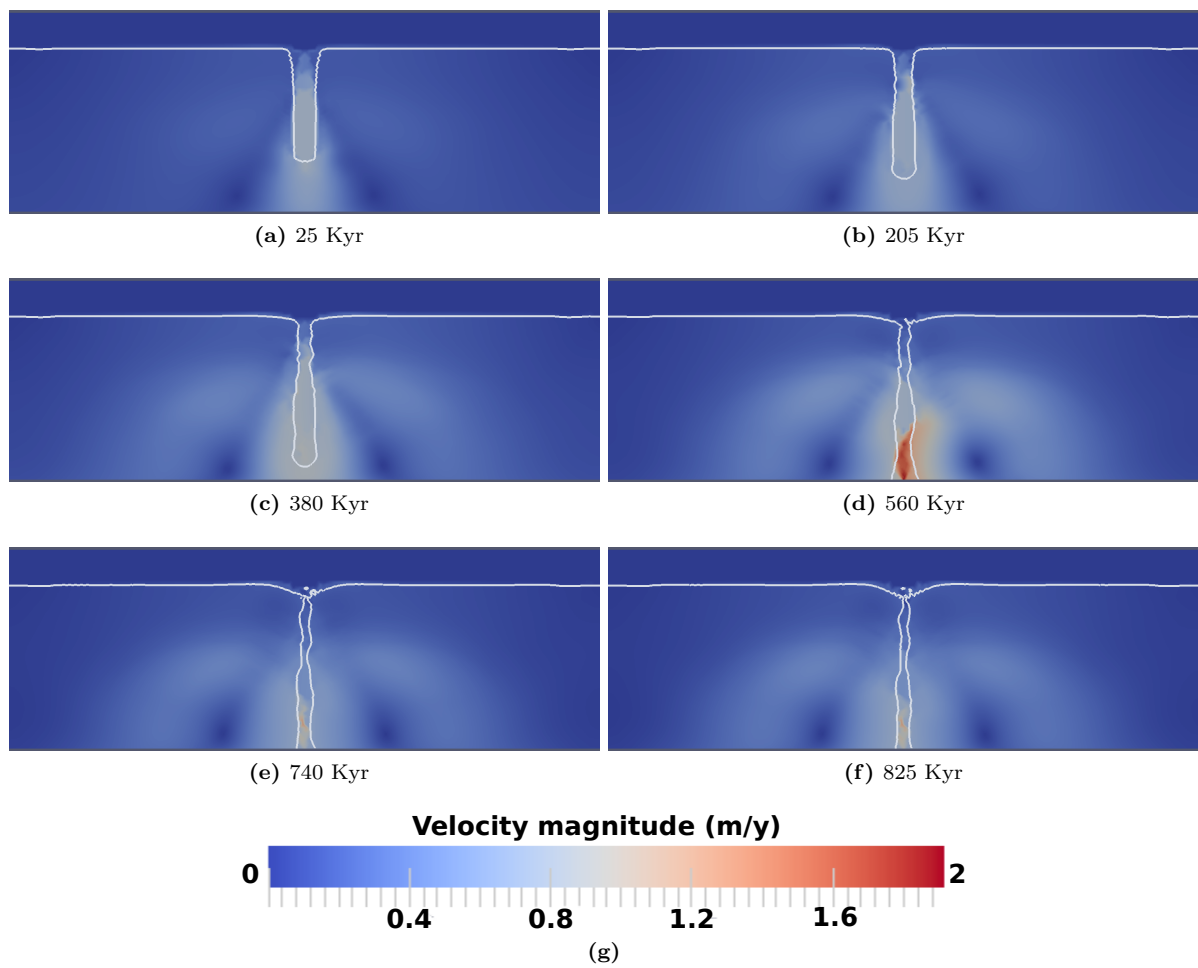
Figure E.4: Velocity magnitude, model 18. White line is the 1073 K isotherm.

(a) 205 Kyr

(b) 560 Kyr

Maximum Allowed Viscosity   **Peierls creep Dominated**   **Dislocation creep Dominated**   **Diffusion creep Dominated**
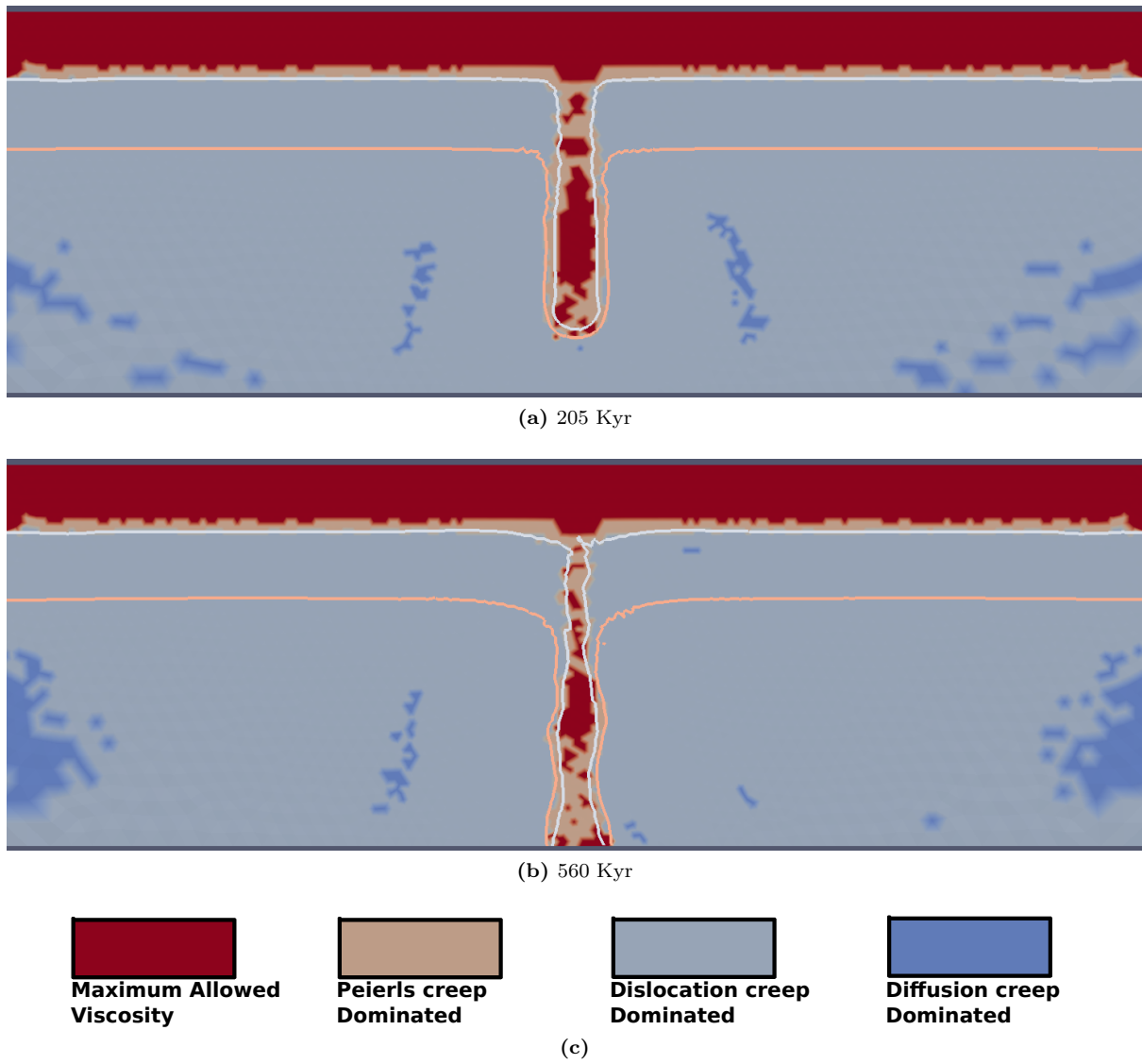
(c)

Figure E.5: These plots denote whether diffusion-, dislocation- or Peierls creep dominates rheology in model 18. Isotherms are also plotted for 1073 K and 1473 K.

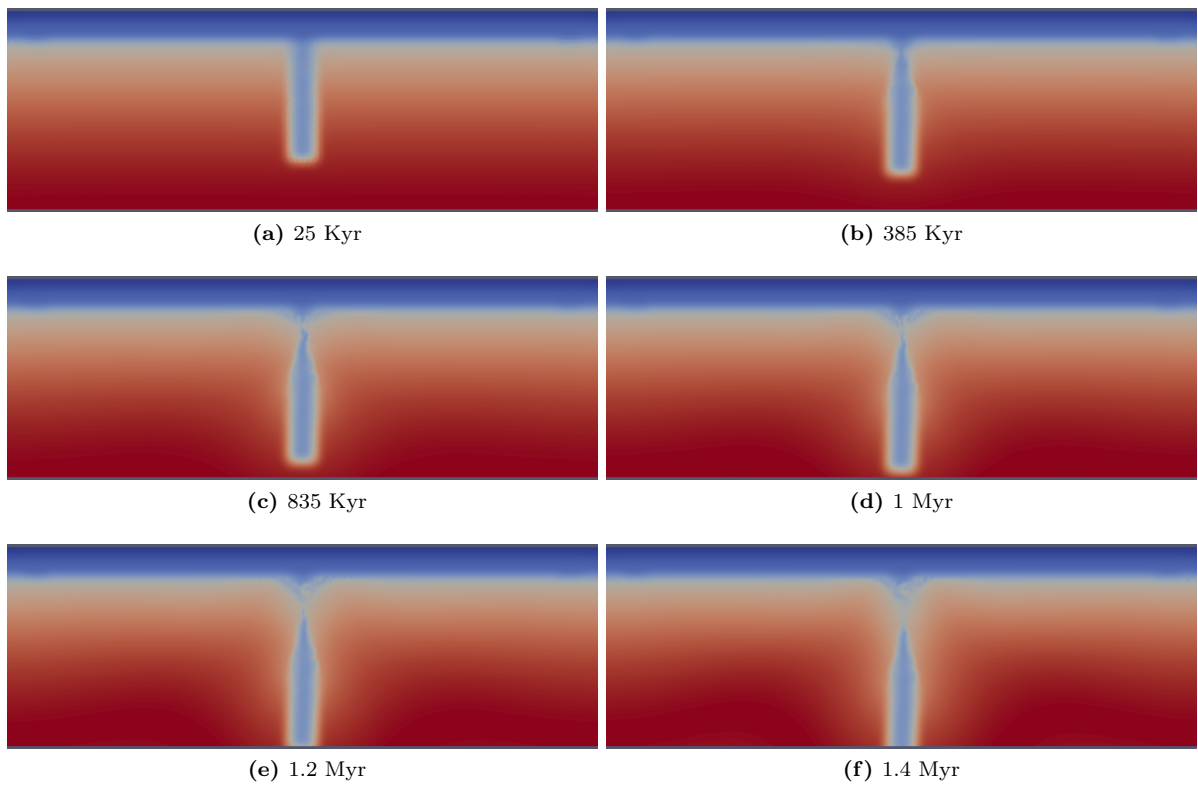# Appendix F

Model 19

F.1 Appendix F1 (Model 19)

(a) 25 Kyr

(b) 385 Kyr

(c) 835 Kyr

(d) 1 Myr

(e) 1.2 Myr

(f) 1.4 Myr

Figure F.1: Temperature field, model 19
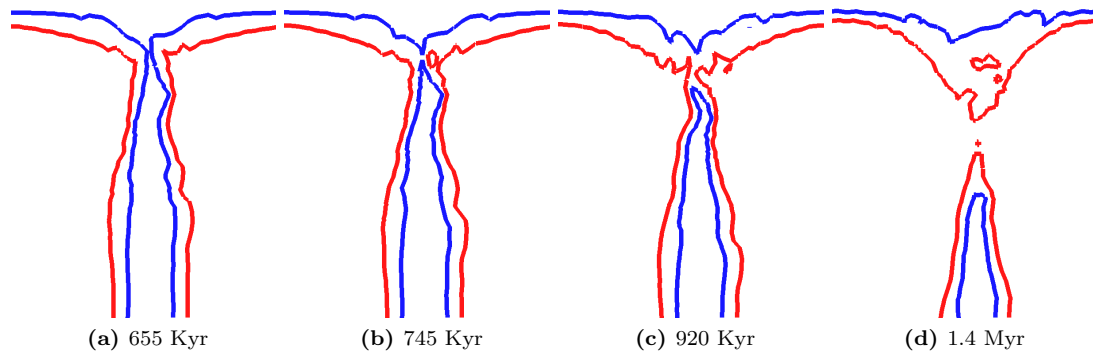
(a) 655 Kyr **(b)** 745 Kyr **(c)** 920 Kyr **(d)** 1.4 Myr

Figure F.2: Temperature contours for 873 K (blue) and 1073 K (red) depicting the slab detachment in detail, model 19

(a) 25 Kyr **(b)** 385 Kyr
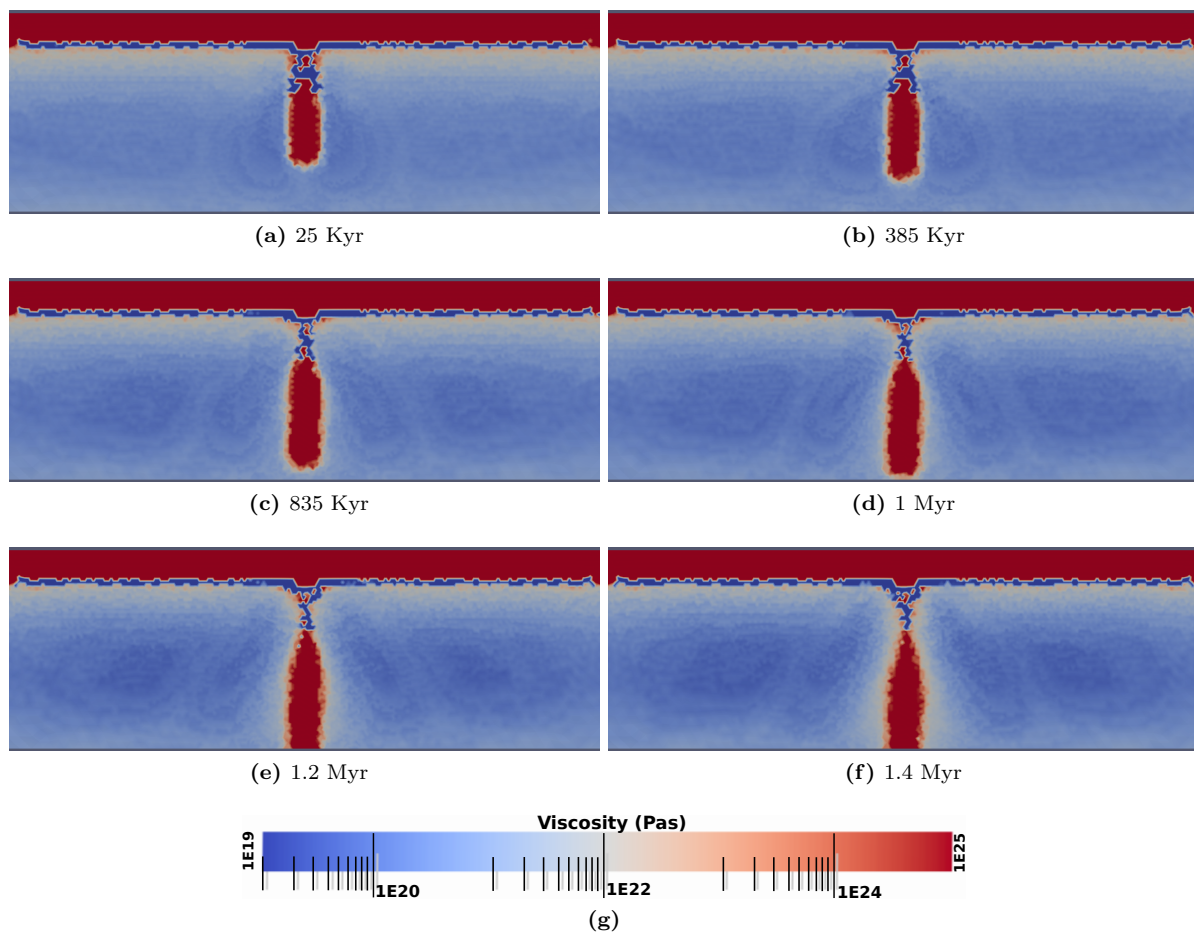
(c) 835 Kyr **(d)** 1 Myr

(e) 1.2 Myr **(f)** 1.4 Myr

(g)

Figure F.3: Viscosity field, model 19

(a) 25 Kyr

(b) 385 Kyr

(c) 835 Kyr

(d) 1 Myr

(e) 1.2 Myr

(f) 1.4 Myr

Velocity magnitude (m/y)

0   0.2   0.4   0.6

(g)
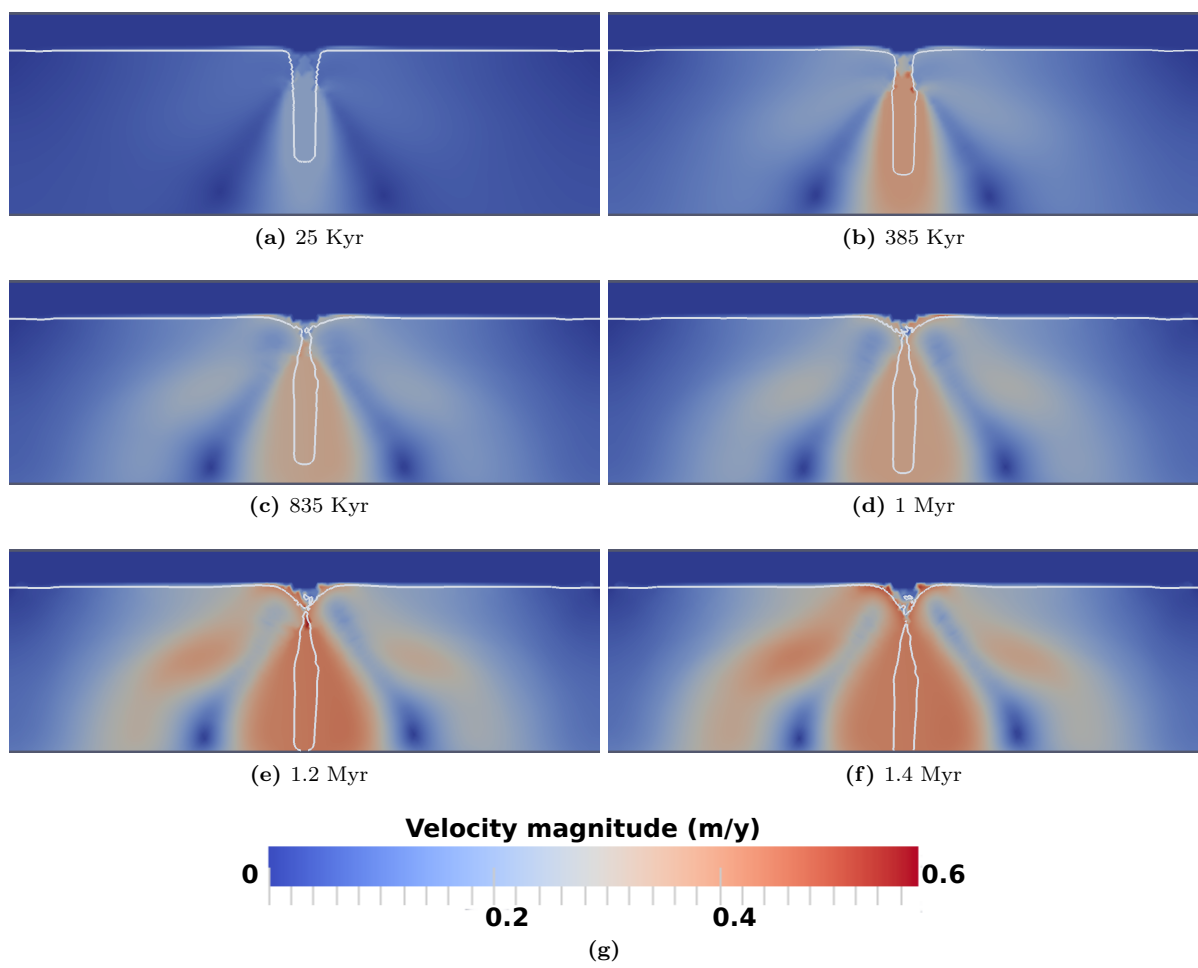
Figure F.4: Velocity magnitude, model 19. White line is the 1073 K isotherm.

(a) 205 Kyr

(b) 565 Kyr

Maximum Allowed Viscosity   **Peierls creep Dominated**   **Dislocation creep Dominated**   **Diffusion creep Dominated**
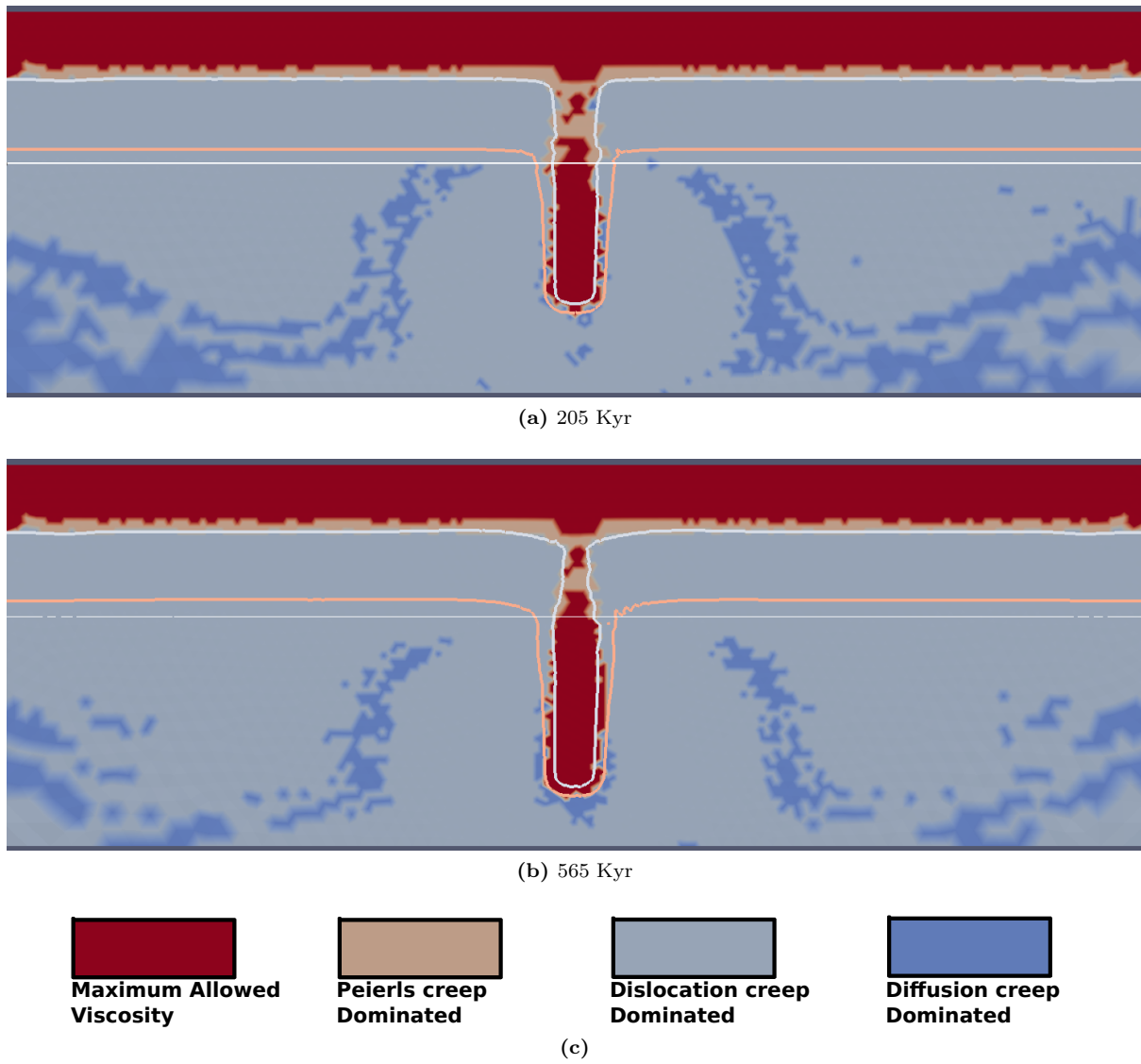
(c)

Figure F.5: These plots denote whether diffusion-, dislocation- or Peierls creep dominates rheology in model 19. Isotherms are also plotted for 1073 K and 1473 K. The white line indicates the depth constraint of 280 km.